INVESTIGATION OF AMYLOID β (12-28) SELF-RECOGNITION BY NMR

INVESTIGATION OF THE AMYLOID β (12-28) PEPTIDE SELF-RECOGNITION BY SATURATION TRANSFER DIFFERENCE AND OFF-RESONANCE RELAXATION NMR

By

HAO HUANG, B. Sc., M .Sc.

A Thesis

Submitted to the School of Graduate Studies in Partial Fulfillment of the Requirements

For the Degree

Master of Science

McMaster University

Master of Science (2005) McMaster University
Hamilton, Ontario

(Chemistry)

TITLE:

Investigation of the Amyloid β (12-28) Peptide Self-Recognition by Saturation Transfer Difference and Off-Resonance Relaxation NMR

AUTHOR: Hao Huang, M.Sc. (Tsinghua University, P.R.China)

SUPERVISOR: Dr. Giuseppe Melacini

NUMBER OF PAGES: xv, 123

ABSTRACT

The formation of soluble amyloid oligomers by polypeptide chains is the main pathogenic mechanism underlying several neurodegenerative disorders including some of the most common debilitating and aging-related illnesses such as Alzheimer's and Parkinson's diseases. However, the molecular basis of polypeptide oligomerization and amyloid formation is currently not fully understood. In this thesis the focus will be on the early steps of oligomer formation that precede the nucleation of amyloid fibrils, that are still reversible. The reversibility of these initial self-association equilibria makes them an attractive target for therapeutic intervention in the treatment of amyloid diseases. Specifically three general questions will be addressed: (a) What are the residues within a given polypeptide chain that mediate self-recognition? (b) What are the driving forces for self-association? (c) Is self-recognition coupled with conformation changes?

The objective of this thesis is to provide initial responses to these key questions using as prototypical system the Aβ (12-28) peptide, which has been previously proposed as a model for the initial self-association events that are linked to Alzheimer's disease. Given the flexibility of this peptide the main tool for its investigation will be Nuclear Magnetic Resonance (NMR) spectroscopy. Specifically, both classical (*i.e.,* TOCSY and NOESY) and more novel (*i.e.* saturation transfer difference and off-resonance relaxation) NMR experiments were used to probe the soluble oligomers through the comparative analysis of samples with different monomer/oligomer distributions. The combined analysis of this integrated set of experiments reveals that while the residues in the central hydrophobic core (CHC) drive self-recognition, stable oligomers require a conformational change towards more folded structures that affects residues well outside the CHC. The conformational change occurring upon self-association thus effectively couples CHC and non-CHC residues. This model may also explain why mutations outside the CHC (*i.e.* E22, D23) can affect significantly the kinetics of self-association.

ACKNOWLEDGEMENT

I would like to extend my sincere appreciation to my supervisor Dr. Melacini, for his support and help in finishing this Aβ project. With his offer, I have this opportunity to come to Canada and enjoy the advanced education at McMaster University. In addition, I truly believe Dr. Melacini's direction and profound suggestions will help me in my future career. I would like to thank Veronica for her contribution on development of the off-resonance relaxation NMR method, Rahul for his suggestions in sample preparation, Julijana for working on a related project and for her helpful discussions, and Dr. Abu-Abed for her help in the urea sample preparation. I greatly appreciate Dr. Bain and Dr. Berti for their suggestions throughout my graduate studies. The Mass Spectrometry Lab staff (Dr. Green and Gina) and the NMR Lab staff (Dr. Hughes et. al) are appreciated for their assistance.

I would also like to thank Christina for teaching me English and Vivien for her encouragement for my study.

TABLE OF CONTENTS

LIST OF TABLES

LIST OF FIGURES AND SCHEMES

ABBREVIATIONS

Aβ- Amyloid beta peptide

AD-Alzheimer's disease

AFM-Atomic Force Microscopy

APP-Aβ Precursor Protein

CD-Circular Dichroism

HIV – Human Immunodeficiency Virus,

IR – Infra Red,

MD – Molecular Dynamics,

HMQC – Heteronuclear Multiple Quantum Coherence spectrum,

HSQC – Heteronuclear Single Quantum Coherence spectrum,

MRD – Magnetic Relaxation Dispersion,

MS – Mass Spectrometry

MW-Molecular Weight

NMR - Nuclear Magnetic Resonance,

NOE – Nuclear Overhauser Effect,

NOESY – 2D-NOE Spectroscopy,

ORR-Off-resonance Relaxation

PDB – Protein Data Bank,

PFG – Pulsed Field Gradient,

ROE – Rotating frame Overhauser Effect,

ROESY – 2D-ROE Spectroscopy,

STD-Saturation Transfer Difference

S/N-Signal to Noise

TOCSY- TOotal Correlation SpectroscopY

TROSY – Transverse Relaxation Optimized SpectroscopY

WG-WATERGATE

XH – Proton exchangeable with water

Chapter 1

Introduction

1.1 Amyloid-Related Diseases and Peptides

Amyloid diseases are characterized by the accumulation of extra cellular amyloid protein deposits in the brains of animals or humans. While all amyloid diseases are related to the oligomerization and fibrillization of a misfolded or unstructured protein, different amyloid disorders are associated with different proteins. For instance, Alzheimer's disease (AD) is linked to the amyloid beta peptide (Aβ), Parkinson's disease to synuclein, prion diseases to prions, Huntington's disease to huntingtin, tauopathies to the tau protein and type II diabetes to the islet amyloid polypeptide (IAPP).

1.2 The Amyloid Beta Peptide & Aβ (12-28)

The amyloid β (Aβ) peptide was the protein associated with Alzheimer's disease, which is an adult-onset cortical neurodegenerative disease characterized by progressive memory and intellectual deficits [1]. The amyloid plaques and the neurofibrillary tangles are the two main abnormal structures in the brain of patients affected by AD. Aβ is the dominant component of the core of the senile plaque. Aβ is a peptide of 39-43 residues derived from the Aβ precursor protein (APP), which is a transmembrane protein of 695 residues.

The current consensus mechanism for the aggregation of the Aβ is based on a "seeding" model [1-3], in which two phases are clearly separated: nucleation and extension (Figure 1.1). The Aβ monomers first form the nucleus (seed), which is the rate limiting step of the Aβ aggregation. After the nucleus is formed, the growth of the oligomers to form the Aβ fibrils becomes thermodynamically and kinetically favorable. The focus of this study is on the pre-nuclear soluble oligomers. The reasons are two fold: (1) the pre-nuclear oligomers are critical for the amyloid fibril formation and (2) the understanding of this state is an attractive target for drug design and screening, since the nucleation phase (from monomer to oligomers) is more easily reversed than the extension phase (from oligomers to fibrils).

The Aβ fragment 12-28 is chosen as model system for this thesis, as it contains the central hydrophobic core (17-21: LVFFA), which is considered in the major determinant for the Aβ aggregation. This Aβ (12-28) also includes the flanking residues such as E22 and D23, which are also reported to be important in the Aβ aggregation since mutations at these sites are found in patients affected by familial forms of AD [4, 5]. Considering that Aβ is highly flexible, solution NMR is an excellent tool to characterize this system. Specifically, we have relied on a comparative NMR strategy based not only on well established experiments such as TOCSY and NOESY but also on more recent methods such as saturation transfer difference (STD), hydration and off-resonance relaxation.

1.3 General STD Overview

The application of the STD NMR method to the Aβ peptide is systematically investigated in this thesis. In the past STD has been successfully applied to drug screening [6-8]. Recently preliminary experiments proving the usefulness of STD to map self-recognition in amyloidogenic peptides have been published [9]. In this thesis, the limitations of the strengths and limitations of the STD experiments for probing self-association will be evaluated (Chapter 3) and a new STD method based on hydration NMR techniques will be proposed to overcome these limitations (Chapter 5). Therefore we will review here the general background of hydration NMR experiments.

1.4 General Overview of Hydration NMR Experiments [10]

Water is ubiquitous in biological systems and it has a profound influence on the structure and dynamics of biomolecules as well as on the affinity and specificity of their non-covalent interactions. The biomolecule-binding water molecules can be classified according to their location and residence time into surface and buried waters [11, 12]. Buried water may stabilize protein structure by bridging protein hydrogen bonds and/or salt bridges, whereas the most functionally relevant surface water molecules are usually located at binding and/or active sites playing a crucial role in ligand recognition and enzyme catalysis [13, 14]. Surface water molecules that are released upon binding provide a mainly entropic driving force as is often the case in protein-DNA complexes

[14]. Similarly, the displacement of water molecules from the apo form of the heat shock 70 chaperone protein caused by a hydrophobic ligand was suggested to provide a favorable contribution to the binding free energy [15]. Surface water molecules that are preserved upon binding provide a mainly enthalpic interaction driving force because of their ability to screen electrostatic repulsion, to fill cavities and to act as linkers/bridges between the interacting biomolecules. From a survey of protein-protein interfaces in homo-dimeric proteins and protein-protein complexes available in the PDB, interfacial water molecules were reported to form hydrogen bonds with protein residues mainly involving backbone carbonyls and the charged side chains of Glu, Asp and Arg [16]. It is therefore clear that interfacial water molecules are key determinants not only of affinity but also of specificity in the non-covalent interactions between biomolecules. Interfacial water molecules play a critical role also in the understanding of molecular mimicry and in rational drug design [17, 18, 19]. For instance, Lam et al. [18] designed a series of highly effective inhibitors against the human immunodeficiency virus (HIV) protease HIV-1 by using the carbonyl oxygen of a cyclic urea to mimic the hydrogen-bonding features of a key structural water molecule within the binding site.

The increasing appreciation of the importance of hydrating water molecules in protein function and drug design has motivated a multitude of investigations on water-protein interactions [11, 14, 20-29]. Multiple experimental techniques are available to characterize water molecules that interact

with proteins, including X-ray and neutron diffraction, Brillouin and neutron scattering, volumetric measurements, Raman, IR and NMR spectroscopies [20, 23-25]. High resolution solution NMR is particularly informative because it probes at atomic resolution both the location and the residence-time of hydrating water molecules. In addition, solution NMR can be applied to samples under physiological conditions [26-29].

The high resolution solution NMR experiments designed to investigate macromolecule–water interactions are generally composed of three major building blocks (Scheme 1). First, the water magnetization is selected while the biomolecule magnetization is suppressed; second, magnetization is transferred through dipole-dipole cross-relaxation and/or chemical exchange from water to macromolecular protons that serve as hydration probes; third, these macromolecular probe protons are properly frequency labeled in one or two homo- or hetero-nuclear dimensions for the purpose of facilitating their assignment. While the third block essentially relies on very well established 1D and 2D experiments such as the 1D-WATERGATE [30] and the 2D-TOCSY or the 2D-HSQC [11, 26, 27, 31, 32], the first two blocks have been recently modified to address technical challenges that are specific of hydration NMR pulse sequences.

High-resolution hydration NMR experiments are based on the transfer of magnetization from water to nearby probe protein protons through dipole-dipole cross-relaxation. Cross-relaxation can occur either in the laboratory frame (NOEs)

or in the rotating frame (ROEs). The assignment and the relative sign of the protein-water NOEs and ROEs provide information on the position and on the dynamics of the hydrating water molecules. NMR investigations on the hydration of both globular [11, 12, 41] and fibrous [42] proteins have clearly differentiated between the two main types of hydration sites in solution: (a) Tightly bound water molecules usually observed in the interior of proteins with residence times typically in the 0.1 – 10 μs range (in this case NOEs and ROEs have opposite signs); (b) Loosely bound water molecules usually detected on the protein surface with sub-nanosecond residence times (in this case NOEs and ROEs have the same sign) [29, 43].

While NOE/ROE-based high-resolution hydration NMR experiments have provided the first detailed view of hydration in solution, these methods still suffer from several limitations. One of the major drawbacks is caused by undesired alternative pathways that can transfer polarization from the water to the protein protons, effectively competing with the desired direct dipole-dipole cross-relaxation (*i.e.* NOE or ROE). The alternative pathways originate either from proton/proton exchange between water and polar groups of the protein and/or from exchange-relayed NOE/ROEs. The latter is a two-step transfer in which polarization is first transferred from water to the XH groups [X = N, O, S] through chemical exchange and then from the XH protons to nearby protein protons through intra-molecular dipole-dipole cross-relaxation [11, 44]. Typical relaying labile protons (XH) include carboxyl, amino, hydroxyl, imidazole,

guanidinium and amide protons, depending on the pH [26, 45, 46]. Direct cross-relaxation and direct exchange contributions result in ROESY cross-peaks with opposite signs, and therefore they can be efficiently separated. However, the signals originating from exchange relayed cross-relaxation are not easily distinguished from those generated by direct cross-relaxation because these two pathways result in very similar NOESY/ROESY patterns. This is a major drawback since both proton exchange and intra-molecular cross-relaxation are often very efficient processes and therefore the indirect exchange-relayed peaks are frequently more intense than the direct intermolecular NOE/ROE peaks. As a result, the exchange-relayed peaks usually obscure the more informative signals originating from the direct transfer. The only case in which direct and exchange-relayed cross-relaxation contributions can be easily separated is when the protein protons used to probe the hydration events are far enough from exchangeable groups that the exchange-relayed effects are negligible. The generally accepted cutoff distance from XH protons beyond which exchange relay effects become insignificant has been recently increased to ~6 Å based on non-uniform model, with the result of excluding more than ~80 % of non-labile protons as possible probes of hydration water molecules [29]. Furthermore, this conservative approach to the exchange-relay problem is reliably applicable only to systems with well defined three-dimensional structures. The ambiguity between direct and exchange-relayed cross-relaxation has therefore severely hampered the extensive application of high resolution NMR hydration experiments to molecular

systems that are highly dynamic and/or are rich in polar groups. These include for instance: (a) the surface of proteins where polar side chains are usually abundant and quite flexible, (b) intrinsically unstructured proteins, (c) amyloid forming polypeptides, (d) carbohydrates, (e) RNA. In some cases, the effect of exchange-relay artifacts in experiments designed to probe surface hydration can be minimized by extensive mutations of exchange-relaying residues without significantly perturbing the overall structure [47]. However, when exchange-relay artifacts must be eliminated from the hydration spectra of wild type proteins, spectroscopic exchange network editing methods can provide a useful alternative.

As discussed above, one of the major unsolved problems in the field of high resolution NMR hydration is the separation of direct and exchange-relayed cross-relaxation effects. A possible initial route to the solution of this problem lies in the use of exchange network editing techniques [48-50] that select only for the desired direct polarization transfer pathway from the water to the protein protons [42, 51-54]. The selective suppression of the exchange-relayed cross-relaxation transfer can be achieved through two main strategies: NOE/ROE compensation (Figure 1.2a) or selective repeated inversions of the relaying labile protons (Figure 1.2b). The NOE/ROE compensation can be implemented using, for instance, off-resonance ROESY methods at a ~35.5^{o} angle or tailored pulse trains such as the CLEANEX sequence [42, 55, 56].

Exchange network editing methods based on NOE/ROE compensation, such as the Off-Resonance ROESY [56] or the CLEANEX experiments [55] have

the advantage of not being limited to the slow regime for the exchange between water and the relaying labile protons. However, these methods suppress not only exchange-relayed artifacts but also the peaks arising from cross-relaxation between long-lived interior water molecules and protein protons. As a result the NOE/ROE compensation strategy is best suited for probing surface water molecules that are highly dynamic and usually give rise to cross-relaxation well outside the spin-diffusion limit where NOE/ROE compensation applies. However, even when investigating surface hydration by methods based on NOE/ROE compensation, care should be taken to account for potential exchange-relay leakages caused by solvent-exposed polar side chains in rapid local motion. Ideally, the best experimental strategy is to combine, when possible, both the selective saturation and the NOE/ROE compensation complementary exchange network editing methods through a controlled selection of the experimental conditions. This combined exchange network editing approach, in conjunction with PHOGSY-like hydration experiments [57] approach, was essential to probe the dynamics of water molecules hydrating the collagen triple helix, which represents a challenging application because collagen is very rich in hydroxyproline hydroxyls [42]. In general, the modified mixing blocks that implement exchange network editing as described above can be employed in conjunction with several water selection schemes and protein detection pulse sequence blocks (*i.e.* 1D, HSQC, HMQC, TROSY [11, 12]).

1.5 Thesis Objectives

The objectives of this thesis are to address the following fundamental questions:

(a) What are the residues within a given polypeptide chain that mediate self-recognition?

(b) What are the driving forces for self-association?

(c) Is self-recognition coupled with conformation changes?

The first question will be addressed by using STD experiments, first in their original version (Chapter 3) and then in a modified version based on hydration NMR experiments (Chapters 4 and 5). This set of STD experiments provides preliminary evidence that not only hydrophobic residues are involved in the self-association but also more polar side chains have to be taken into account. Further evidence of the dual hydrophobic/hydrophilic nature of the interactions driving self-recognition (*i.e.* question (b)) is provided by the urea induced denaturation of the soluble Aβ (12-28) oligomers, which is discussed in Chapter 6. Chapter 6 also includes the comparative analysis of NOEs in samples with and without soluble oligomers showing that self-recognition is most likely coupled to conformational changes from extended to more folded structures. We anticipate that the investigations outlined in this thesis will be relevant not only for Aβ but for amyloidogenic peptides and proteins in general.

References

1. Y. Xing, K. Higuchi, Mechanisms of Ageing and Development 2002 (123) 1625-1636
2. P. M. Gorman, A. Chakrabartty, Biopolymers 2001 (60) 381-394
3. J. T. Jarrett and P. T. Lansbury, Cell, 73 (1993) 1055-1058
4. J.P. Melchor, L.McVoy, and W.E. Van Nostrand, J. Neurochem., 75 (2000) 2209-2212
5. A. Päiviö, J. Jarvet, A. Gräslund, L. Lannfelt and A. Westlind-Danielsson, J. Mol. Biol., 339 (2004) 145-159
6. M. Mayer and B. Meyer, J. Am. Chem. Soc., 123 (2001) 6108-6117
7. M. Mayer and T.L. James, J. Am. Chem. Soc., 124 (2002) 13376-13377
8. H. Takahashi, T. Nakanishim, K. Kami, Y. Arata and I. Shimada, Nat. Struct. Biol. 7 (2000) 220-223
9. S. Narayanan and B. Reif, Biochemistry, 44 (2005) 1444-1452
10. H. Huang and G. Melacini, Analytica Chimica Acta, *In press*
11. G. Otting, Progr. NMR Spectrosc. 31 (1997) 259
12. K. Wüthrich, Angew. Chem. Int. Ed. 42 (2003) 3340
13. J.A. Ernst, R.T. Clubb, H.X. Zhou, A.M. Gronenborn, G.M. Clore, Science 267 (1995) 1813
14. B. Jayaram, T. Jain, Annu. Rev. Biophys. Biomol. Struct. 33 (2004) 343
15. S. Cai, S.Y. Stevens, A.P. Budor, E.R. Zuiderweg, Biochemistry. 42 (2003) 11100

16. F. Rodier, R.P. Bahadur, P. Chakrabarti, J. Janin, Proteins. 60 (2005) 36
17. A. Wlodawer, J. Vondrasek, Annu. Rev. Biophys. Biomol. Struct. 27 (1998) 249
18. P.Y. Lam, P.K. Jadhav, C.J. Eyermann, C.N. Hodge, Y. Ru, L.T. Bacheler, J.L. Meek, M.J. Otto, M.M. Rayner, Y.N. Wong, et al., Science. 263 (1994) 380
19. M. Fornabaio, F. Spyrakis, A. Mozzarelli; P. Cozzini; D.J. Abraham, G.E. Kellogg, J. Med. Chem. 47(2004) 4507
20. T.V. Chalikian, Annu. Rev. Biophys. Biomol. Struct. 32 (2003) 207
21. G.D. Noudeh, N. Taulier, T.V Chalikian, Biopolymers. 70 (2003) 563
22. T.V. Chalikian, J. Phys. Chem. B 105 (2001) 12566
23. N. Taulier, T.V. Chalikian, Biochim. Biophys. Acta. 1595 (2002) 48
24. F. Massi and J.E. Straub, J. Comp. Chem. 24 (2003) 143
25. T.V. Chalikian, A.P. Sarvazyan, K.J. Breslauer, Biophys. Chem. 51(1994) 89
26. G. Otting, E. Liepinsh, Acc. Chem. Res. 28 (1995) 171
27. Wider G., Progr. NMR Spectrosc. 32 (1998) 193
28. G. Otting, E. Liepinsh, B. Halle, U. Frey, Nat. Struct. Biol. 4 (1997) 396
29. B. Halle, Phil. Trans. R. Soc. Lond. B 359 (2004) 1207
30. M. Piotto, V. Saudek, V. Sklenář, J. Biomol. NMR 2 (1992) 661
31. L. Braunschweiler and R.R. Ernst, J. Magn. Reson. 53 (1983) 521
32. G. Bodenhausen and D.J. Ruben, Chem. Phys. Lett., 69 (1980) 185

33. G. Melacini, R. Boelens, R. Kaptein, J. Biomol. NMR, 15 (1999) 189

34. S. Mori, M.O. Johnson, J.M. Berg, P.C.M. van Zijl, J. Am. Chem. Soc. 116 (1994) 11982

35. S. Mori, C. Abeygunawardana, P.C.M. van Zijl, and J.M. Berg, J. Magn. Reson. B110 (1996) 96

36. B. Cutting, JH. Chen, D. Moskau, J. Biomol. NMR 17 (2000) 323

37. G. Otting, E. Liepinsh, J. Biomol. NMR 5 (1995) 420

38. E. Liepinsh, P. Sodano, S. Tassin, D. Marion, F. Vovelle, G. Otting J. Biomol. NMR 15 (1999) 213

39. I. Bertini, C. Dalvit, J.G. Huber, C. Luchinat, M. Piccioli, FEBS Lett. 415 (1997) 45

40. J.C. Rodriguez, P.A. Jennings, G. Melacini, J. Am. Chem. Soc. 124 (2002) 6240

41. G. Otting, E. Liepinsh, K. Wüthrich, Science 254 (1991) 974

42. G. Melacini, A. Bonvin, M. Goodman, R. Boelens, R. Kaptein, J. Mol. Biol. 300 (2000), 1041

43. K. Modig, E. Liepinsh, G. Otting, B. Halle, J. Am. Chem. Soc. 126 (2004) 102

44. E. Liepinsh, G. Otting, K. Wüthrich, J. Biomol. NMR, 2 (1992) 447

45. K. Wüthrich, NMR of Proteins and Nucleic Acids, Wiley, New York, 1986

46. B.J. Stockman, C. Dalvit, Progr. NMR Spectrosc. 41 (2002) 187

47. H. Iwai, G. Wider, K. Wüthrich, J. Biomol. NMR 29 (2004) 395

48. N. Juranic, Z. Zolnai, S. Macura, J. Biomol. NMR 9 (1997) 317

49. Z. Zolnai, N. Juranic, J.L. Markley, J.L. Markley, S. Macura Chem. Phys. 200 (1995) 161

50. C.G. Hoogstraten, W.M. Westler, S. Macura, and J.L. Markley J. Magn. Reson. B102 (1993) 232

51. J. Fejzo, W.M. Westler, S. Macura, J.L. Markley, J. Magn. Res. 92 (1991) 195

52. G. Melacini, R. Boelens, R. Kaptein, J. Magn. Res., 136 (1999) 214

53. G. Melacini, R. Boelens, R. Kaptein, J. Biomol. NMR 13 (1999) 67

54. A.T. Phan, J.L. Leroy, M. Gueron, J. Mol. Biol. 286 (1999) 505

55. TL. Hwang, PC. van Zijl, S. Mori, J Biomol NMR.11(1998) 221

56. N. Birlirakis, R. Cerdan, E. Guittet J Biomol NMR.8 (1996) 487

57. C. Dalvit, U. Hommel, J. Biomol. NMR 5 (1995), 306

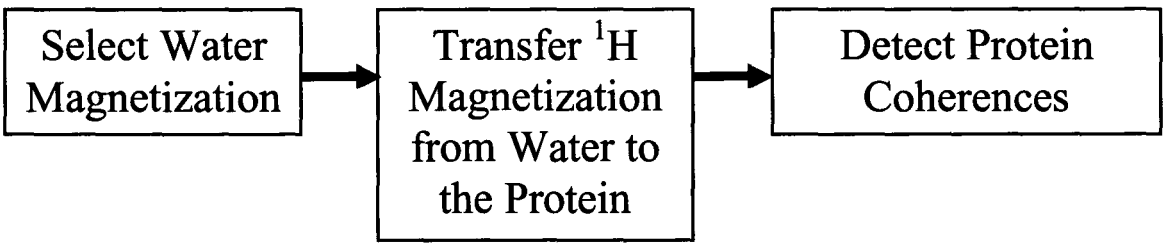

Scheme 1.1: General architecture of high-resolution solution NMR experiments.

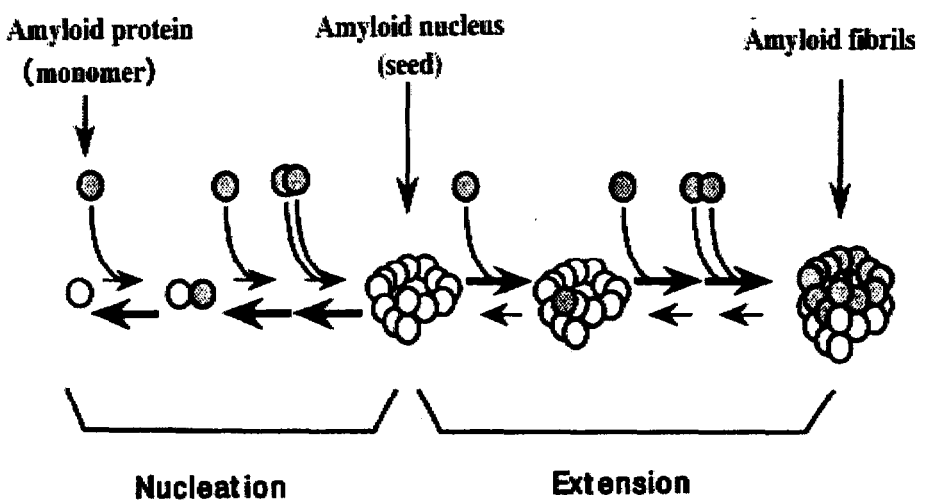

Figure 1.1: Nucleation-dependent polymerization model of amyloid fibril formation [1].

a. Editing of Exchange-Relayed Transfer Using NOE/ROE Compensation:

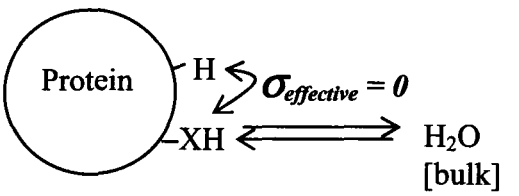

b. Editing of Exchange-Relayed Transfer Using Selective Saturation:

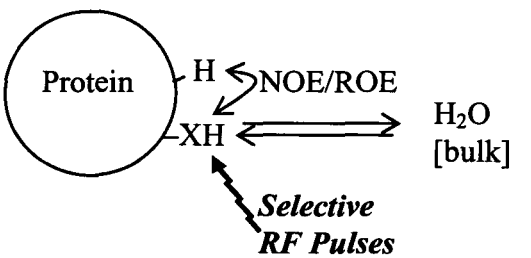

Figure 1.2: Two independent strategies to edit exchange-relayed cross-relaxation in high-resolution hydration NMR experiments.

Chapter 2

Sample Preparation and Initial Spectroscopic Investigation of Aβ (12-28)

2.1 HPLC Purification

Crude synthetic peptide was purchased from the Genscript Corporation., NJ, USA. In this study, the WATERS Atlantis™ reverse phase HPLC columns (C18) are employed to separate and collect the fractions of peptide Aβ (12-28). The analytical column was C_{18}, 4.6×150mm, 5μm particle size; the semi-preparative column is C_{18}, 10×150mm, 10μm particle size.

Table 2.1 Analytical HPLC Gradient for Aβ 12-28

Time	ACN%	H_2O%	Flow rate
0	10	90	1 ml/min
17	30	70	1 ml/min
17.1	100	0	1 ml/min
23.9	100	0	2.4 ml/min
24	10	90	2.4 ml/min
35	10	90	2.4 ml/min

The above gradient condition (Table 2.1) is used in the analytical HPLC. H_2O and ACN (Acetonitrile) are the two solvents used to separate the desired peptide and other impurities. Although TFA (Trifluoroacetic acid) is the most commonly acidic modifier used in peptide /HPLC separation, 0.1% formic acid was added into both H_2O and ACN, because that the HPLC is shared with another Mass Spec group and TFA would interfere with the mass spectra quality. As ACN is less polar than H_2O, we can increase the ACN percentage to elute the peptide binding to the reverse HPLC column. From 0 min to 17 min, the ACN linearly increases from 10 % to 30 %; from 17.1 min to 23.9min, the 100% ACN (Table 2.1) was used to wash out all the peptide remaining in the column; from 24 min to 35 min, the initial condition was employed again to equilibrate the column for the next injection. During the elution time 0 min to 17 min, the flow rate is 1 ml/min, and then the flow rate is changed to 2.4 ml/min to achieve the necessary volume for equilibration of the column.

The side chains of aromatic amino acids absorb at 280nm (Tyr and Trp, ~280nm; Phe, ~260nm), while the backbone peptide bonds absorb at 220 nm. Thus the 220 nm is frequently chosen for concentration measurement in HPLC-peptide separation. The wavelength of 220 nm is also used here to monitor and quantify the fractions of peptide in the crude product. As shown in Figure 2.1 the analytical column results in a good separation of the components in the crude peptide mixture. The most abundant fraction at 12.03 min was considered as the target product and collected with the automatic fraction collector. To verify this

assumption, the major fraction at 12.03 min was submitted for ESI-MS (Figure 2.2).

This mass spectrum (Figure 2.2) is quite clean: the strong peak is the monomer of this peptide (MW=1955), the peak at 1977 is considered as the (peptide+Na^+). The peak at 2931.5 is consistent with the hexamer (6-mer) with +4 charges or trimer (3-mer) with +2 charges. However, the peak at 2692.5 cannot be unambiguously interpreted. Regardless of this ambiguity, this mass spectrum still helps us to confirm that this major fraction at 12.03 min is indeed the target peptide.

With the semi prep HPLC column, the fractions were collected using the gradient of Table 2.2. Due to differences between the two columns, the major fraction eluted in the semi-prep column at 10.2 min [Figure 2.3], which is slightly different from the elution time observed in the analytical HPLC trace when the injection sample is 1mg/ml. Since the semi-prep HPLC column has larger particle size than the analytical column, these changes in the HPLC trace are expected. As the volume of the semi-prep column is 4 times of the analytical column, a flow rate of 4 times of the one for analytical column was employed. The gradient condition (Table 2.2) was the same as the analytical.

Table 2.2 Semi-Preparative HPLC Gradient			
Time	ACN%	H_2O%	Flow rate
0	10	90	4 ml/min
17	30	70	4 ml/min
17.1	100	0	4 ml/min
23.9	100	0	10 ml/min
24	10	90	10 ml/min
35	10	90	10 ml/min

As shown in Figure 2.3, the small injection mass (1mg/ml) will lead to better separation. However, the sample of 10mg/ml is still used for separation considering the time and elution solvents needed for the separation. After HPLC collection of the major fraction, the liquid fractions were lyophilized by a lyophilizer equipped with a centrifuge. The yield (17%) (Figure 2.4) seems too low compared to what expected based on the HPLC trace. This could be due to some aggregates (e.g. the peak at 11.02 min) which were missed in the collection or to same salt compositions in the crude peptide. The salt would not be detected because of no UV absorption. As the collection has to be split into several tubes to fit the rotor, some loss could also be due to the transfer between tubes.

In an attempt to understand the low yield problem and to try to separate the aggregates of Aβ (12-28) though HPLC, LC-ESI MS was carried out to see

the composition of the peaks in the HPLC trace. A 2.3×150mm C_{18} column, gradient condition (ACN 10%-30% in 25 min) and flow rate 0.2 ml/min were employed. In the HPLC trace (Figure 2.5), the peak at 13.63 min was identified as the major product. Several other peaks were also chosen to see if they contain oligomers of the Aβ peptide.

The fractions of 10.35min, 13.63min, 15.09min and 16.68min (Figure 2.5) were checked with ESI-MS. The processed mass spectra are reported here (Figure 2.6). The spectra of the fractions at 10.35 min and 13.63 min are relatively clean, with major peaks at 1809 and 1956 respectively; while the spectra of the 15.09 min and 16.68 min fractions reveal a multitude of impurities. The oligomers with bigger molecular weight are expected to elute later than the monomer. In this LC-MS study, we learned that the effluent sequence is determined by the combined effect of molecular weight (MW), charge and shape of molecules. At present, the oligomers have not yet been separated by HPLC.

2.2 Preliminary MS and NMR Studies

The mass spectrometry (MS) techniques ESI (electron spray ionization) and MALDI have been employed to study the aggregation state of the Aβ (12-28) peptide. The ESI spectrum (Figure 2.7) shows different charge states for the monomer, with the +4, +3 and +2 charge states being predominant. Please notice the different sample conditions between Figure 2.2 and Figure 2.7, the Figure 2.2 is the ESI-MS of the HPLC collection, which contains ca. 10~30% ACN, and no

buffer; while the sample used here to observe the aggregation state with ESI-MS contains 50 mM d_3-acetate buffer, 10% D_2O and no ACN. Undoubtedly, the peptide should have different aggregation states under these two conditions. In Figure 2.7, the small peak at 1304.5 m/z could be the triply charged dimer ((1955*2+3)/3=1304.3), which is consistent with the aggregation state of the Aβ (12-28) peptide under the experimental conditions used (1 mM peptide, 50 mM d_3-acetate buffer and 10% D_2O).

MALDI TOF Mass spectrometry has been employed to investigate the existence of soluble oligomers in solution (1mM Aβ (12-28), 50 mM d_3-acetate buffer and 10% D_2O) (Figure 2.8 (a)). Figure 2.8 (a) shows that the major state in the solution is the monomer; high molecular weight (HMW) oligomers represent only a minor population in solution. If we focus on the high molecular weight region, the 2mer, 3mer, 4mer, 5mer, 6mer ..... series is detected. However this result could be an artifact caused by oligomerization on the matrix rather than in solution. It is therefore critical to continue our investigation of the soluble oliogomers of Aβ (12-28) by NMR to probe directly the solution behavior of this system (see section 2.3).

The sequence specific assignment [2] of the Hα-NH region was obtained using TOCSY and NOESY spectra (Figure 2.8 (b)) and confirms the sequence identity of the peptide. Unless otherwise specified, all NMR spectra in thesis were processed using either an exponential decay or a squared cosine bell window function prior to zero filling, Fourier transform and phase correction. All

processing and data analysis was carried using the software XWINNMR and Sparky (UCSF), respectively.

2.3 A Comparative NMR Approach to the Investigation of Soluble Peptide Oligomers

Our approach to the characterization of the oligomerization equilibria in solution was based on comparative NMR studies aimed at measuring the variations in the NMR properties between samples with different 'perturbed' molecular weight (MW) distributions of oligomers (Figure 2.9). Mutation, dilution, filtration [1] and manipulation of the solution conditions are some of the most common perturbation methods available. However mutations can possibly change also the native conformation of the peptide, and the applicability of the dilution method is limited due to poor S/N (signal to noise). Thus we investigated further filtration and solution condition manipulations as effective methods to perturb the oligomer distribution in solution (Figure 2.9) which were then probed by NMR experiments.

The effect of filtration on the oligomer distribution was monitored by NMR spectra. For instance, Figure 2.10 shows how 1D spectra of Aβ (12-28) change upon 30 kDa cut-off filtration. Figure 2.10 confirms that filtration preserves a good signal-to-noise ratio in the NMR spectra. Indeed the peaks for which the line-width is not significant affected by filtration (*e.g.* peaks at ~7.8 ppm and ~8.35 ppm in Figure 2.10) have similar intensities before and after

filtration (Figure 2.10). This observation indicates that only a very small fraction of the peptide has been filtered out, *i.e.* the high molecular weight oligomers. The low population of the oligomers suggested by filtration-NMR confirms the previous MS results (Figure 2.8). Despite the fact that the oligomers represent only a minor fraction in solution, their effect on the line-width, and in general on the self-/cross-relaxation properties of the monomeric peptide, is quite dramatic (Figure 2.10). Relaxation NMR measurements on the monomeric peptide are therefore a valuable source of information about the soluble oligomers and the comparative analysis of relaxation rates before and after filtration is an effective method to extract this information.

The filtered samples were stable in the time scale of weeks before oligomers start to spontaneously re-appear. The stability of the filtered samples despite the mM concentration of the peptide is attributed to the absence of seeds that can nucleate oligomerization. In other words, filtered samples are kinetically stabilized against oligomerization. This in marked contrast with diluted samples where self-association is thermodynamically unfavorable

As mentioned above, an alternative method to perturb the oligomer distribution focuses on the manipulation of solution conditions. For instance, the population of soluble oligomers of Aβ (12-28) can be increased by adding salt. Therefore the higher the salt concentration, the broader the NMR line widths (Figure 2.11). This effect has been used in the hydration analysis of Aβ (12-28)

to ensure similar oligomer populations in wild type (wt) and mutant peptides (Chapter 3).

2.4 Conclusions

In conclusion, the HPLC has been used for the purification of the Aβ (12-28) peptide starting from the crude peptide and the yield was 17%. Mass Spectrometry (MS) and NMR have been used in the preliminary investigation of the Aβ peptide. Both MS and NMR confirm the identity of the peptide and show that the oligomers exist in the solution of Aβ (12-28) 1mM, pH 4.7, 50mM d_3-acetate buffer and 10% D_2O. The filtration and addition of salt have been demonstrated to have significant effects on the aggregation state of the sample, and they will be extensively employed for the comparative NMR investigations outlined in the following chapters.

References

1. J. Jarvet, P. Damberg, K. Bodell, L.E.G. Eriksson and A. Gräslund, J. Am. Chem. Soc., 122 (2002) 4261-4268
2. K. Wuthrich, "NMR of Proteins and Nucleic Acids," John Wiley & Sons, New York, (1986).

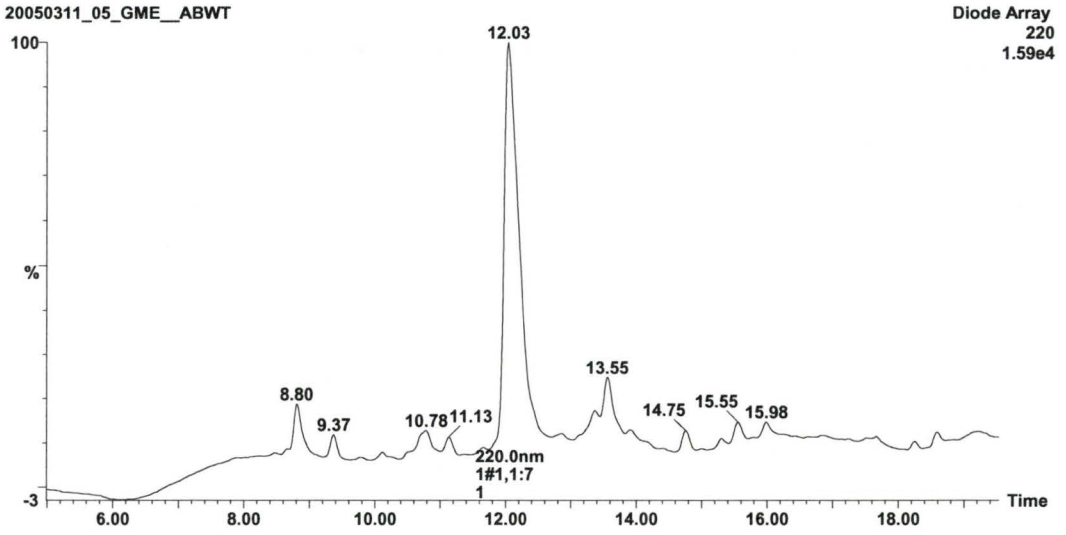

Figure 2.1: The HPLC trace of Aβ (12-28) under the gradient condition in Table 2.1. UV detection at 220nm, analytical column C_{18}, 4.6×150mm, 5μm as particle size.

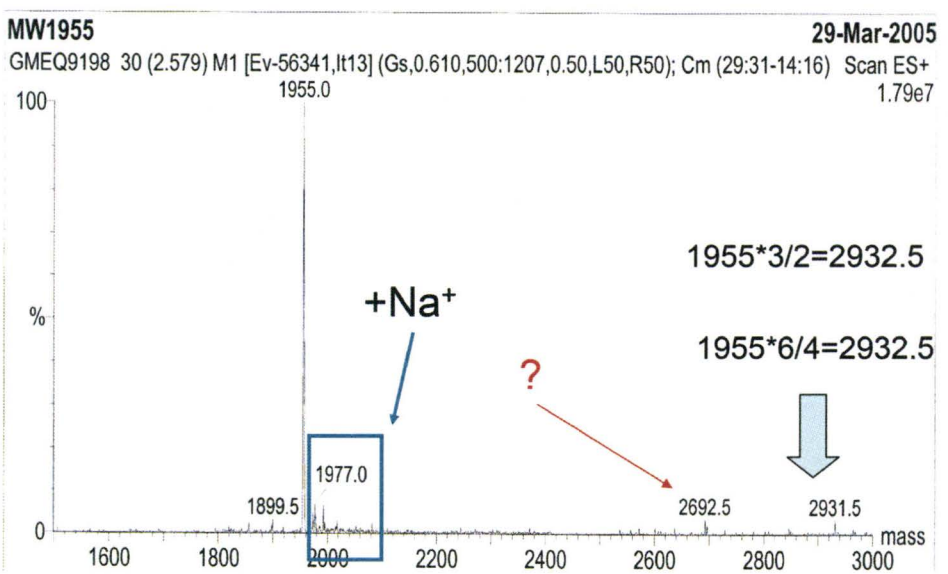

Figure 2.2: ESI-MS of HPLC collection of fraction at 12.03 min with analytical column. This spectrum has been processed to report the mass of the molecules instead of m/z.

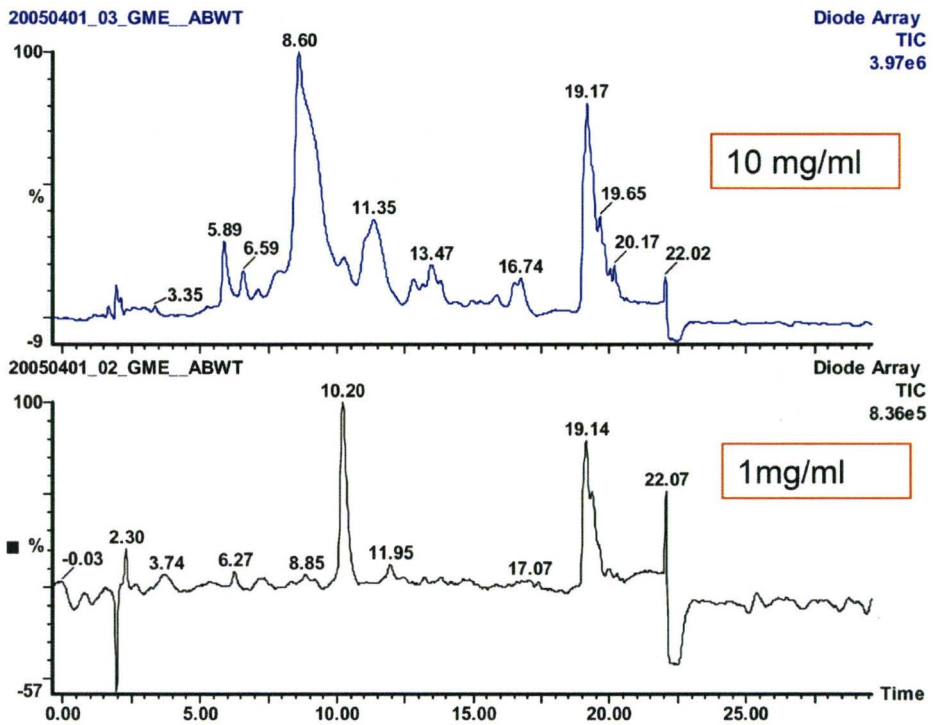

Figure 2.3: The HPLC trace of Aβ (12-28) under the gradient condition in Table 2.2. UV detection at 220nm, semi-prep column C18, 10×150mm, 10μm as particle size. 10mg/ml and 1mg/ml sample concentrations were injected for each separation.

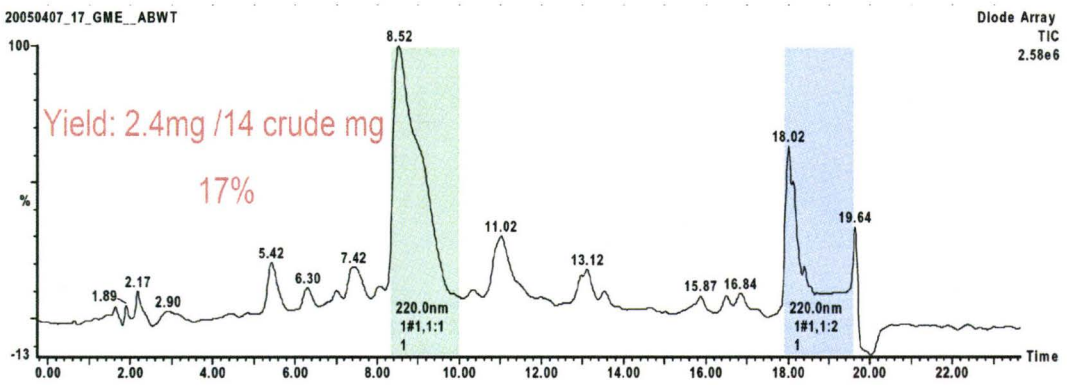

Figure 2.4: The semi-prep HPLC trace of Aβ (12-28). 10mg/ml sample concentration was injected for separation. A yield of 17% was achieved.

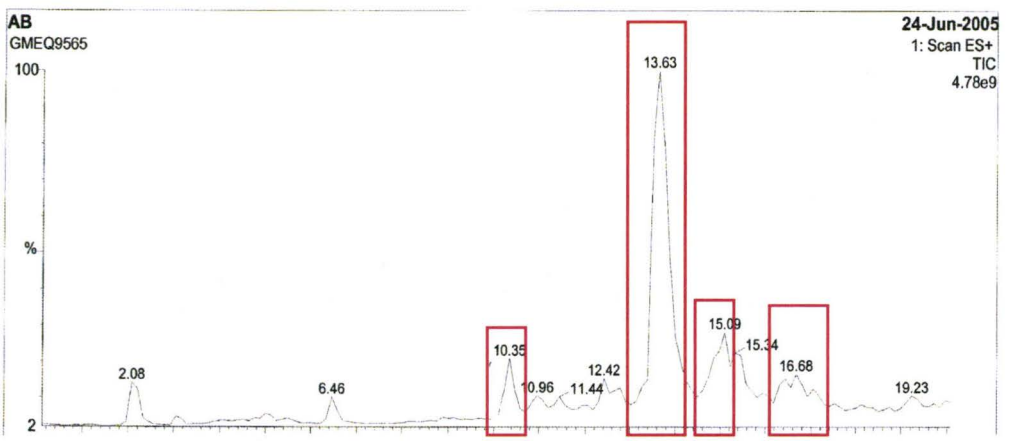

Figure 2.5: The HPLC trace of Aβ (12-28) in LC-MS. A 2.3×150mm C_{18} column, gradient condition (ACN 10%-30% in 25 min) and flow rate 0.2 ml/min were employed.

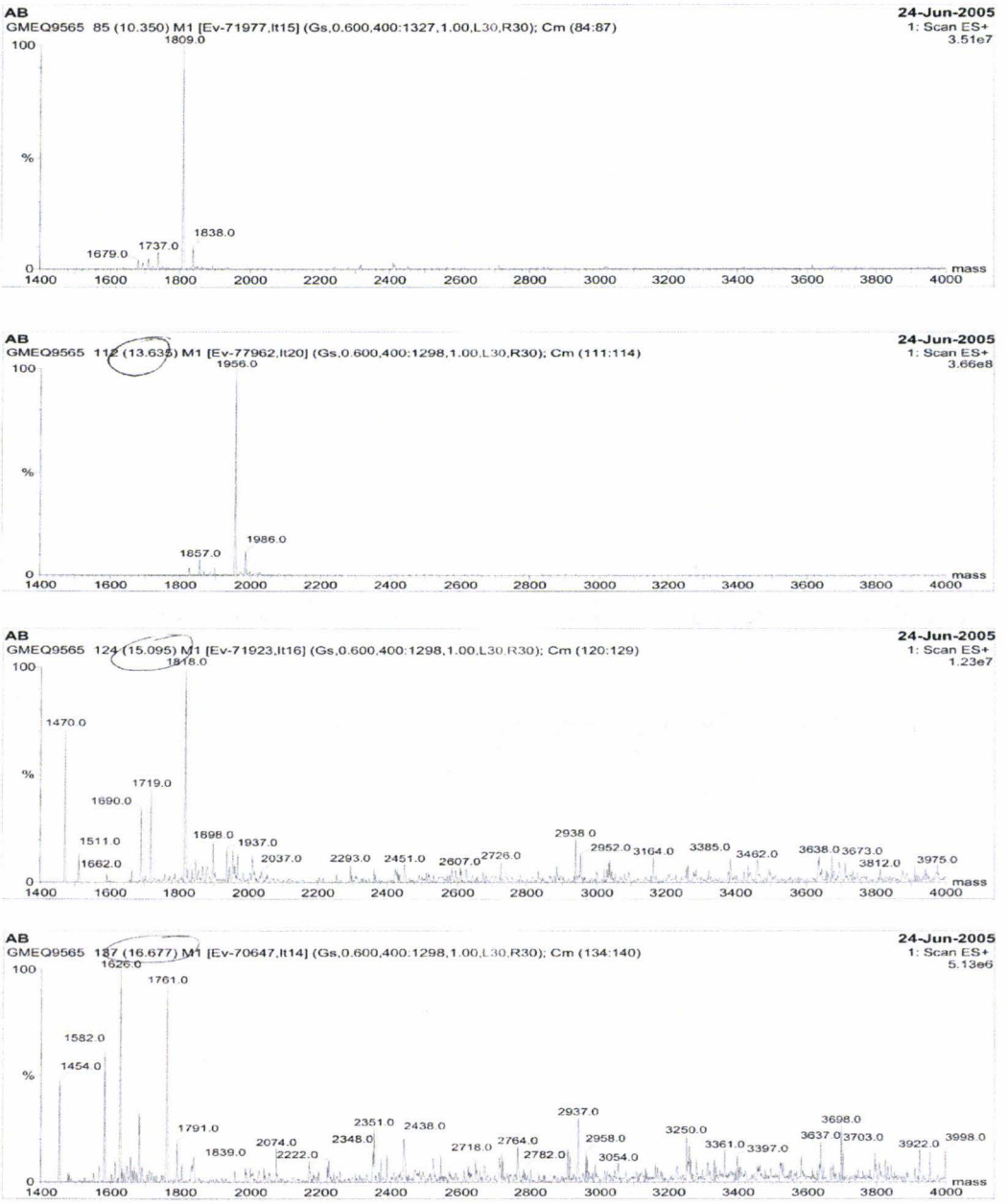

Figure 2.6: Processed Mass spectra after separation by reversed phase HPLC: fractions at 10.35, 13.63, 15.09 and 16.67min.

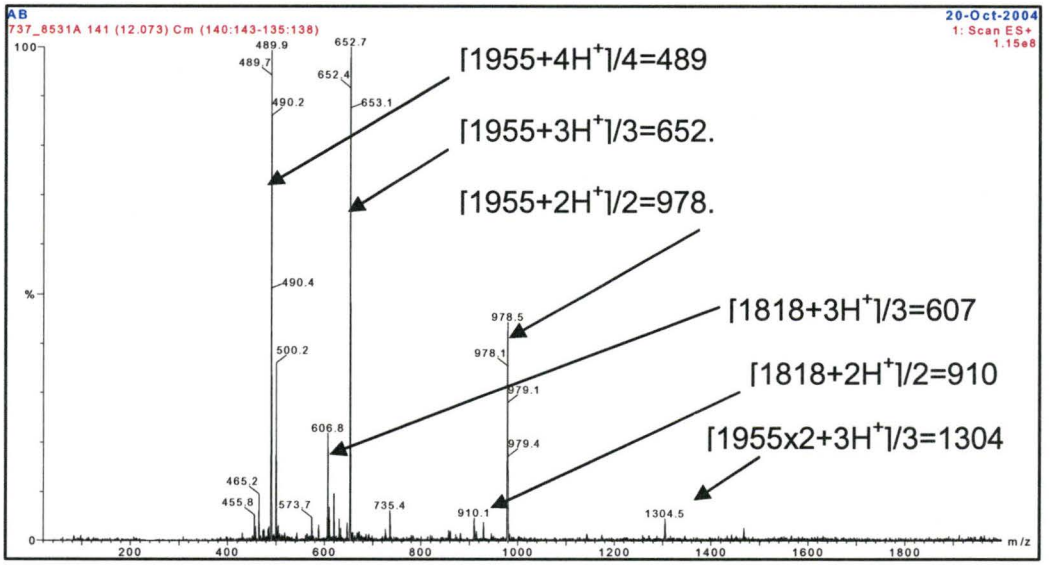

Figure 2.7: ESI MS of Aβ (12-28): two components were detected with MW=1955 and MW=1818. For the molecule with MW 1955, three charged states +4, +3 and +2 have been identified; for the molecule with MW 1818, the charged states of +3 and +2 have been identified. The Aβ dimer with +3 charges is also detected.

a

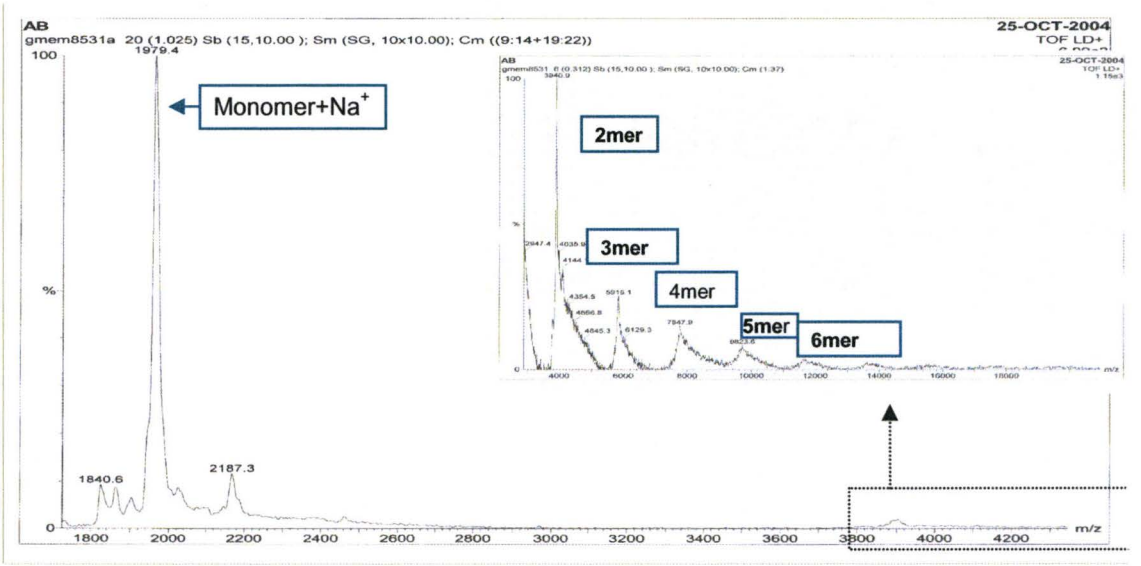

b

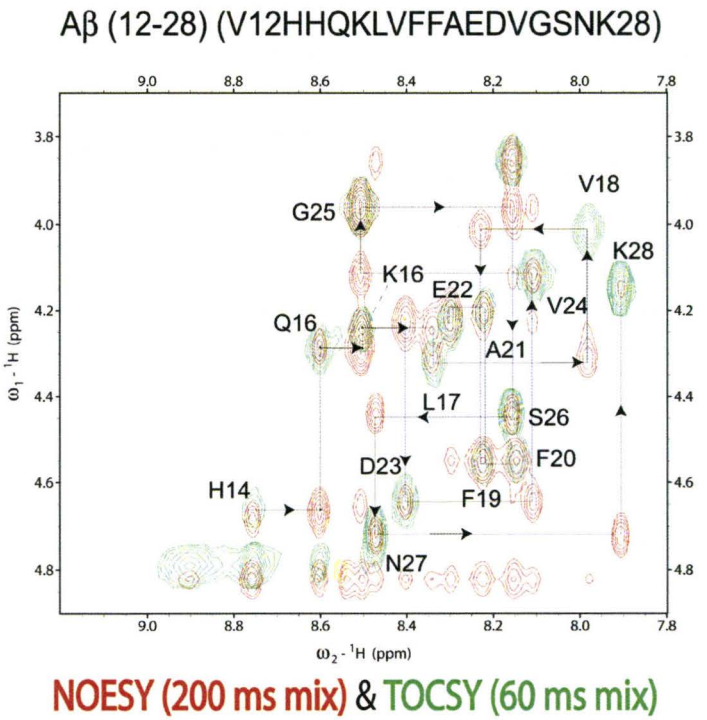

Figure 2.8: Identity of Aβ (12-28) with MALDI TOF mass spectrum (a) and NMR Sequence specific assignment (b).

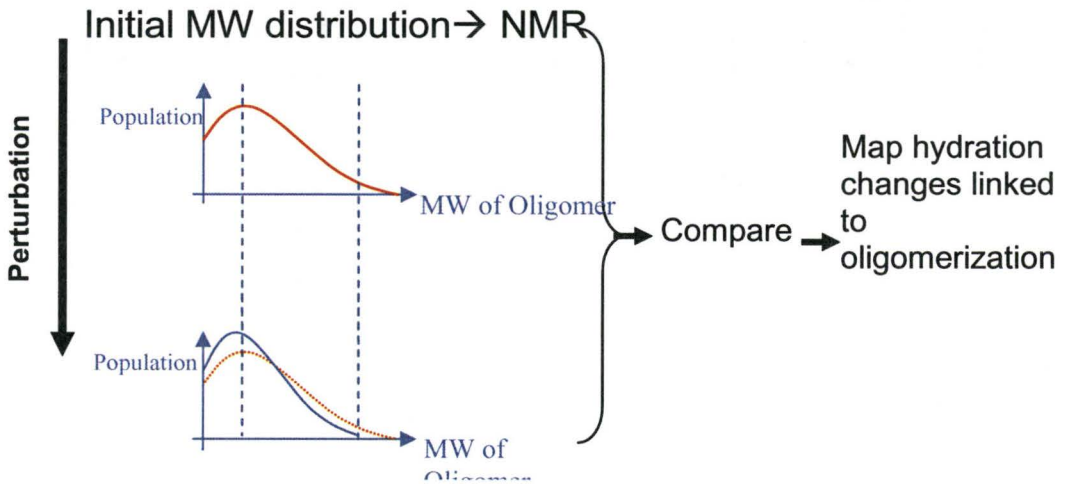

Figure 2.9: Scheme for filtration comparative NMR studies. The filtration shifts the oligomer distribution towards low molecular weights (MW).

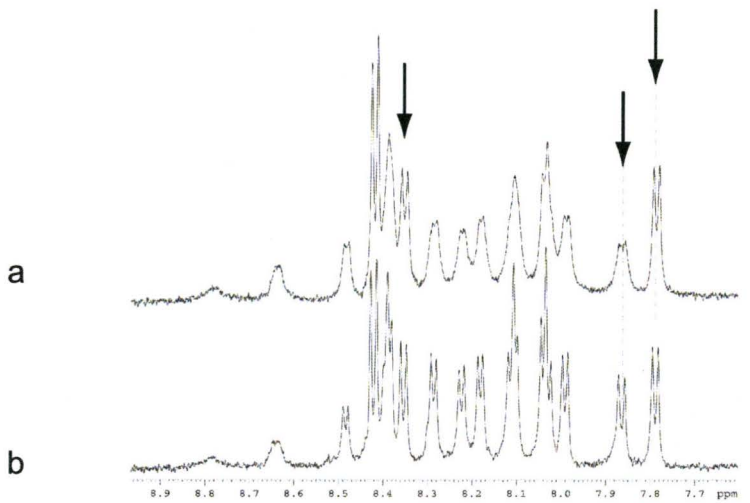

Figure 2.10: 1-D spectra showing the effect of filtration. **(a)** 1 mM Aβ (12-28), 50 mM d_3-Acetate. Buffer, pH 4.7, 293 K **(b)** same as **(a)** but after 30 K Da-filtration. The arrows indicate representative peptide amide proton signals.

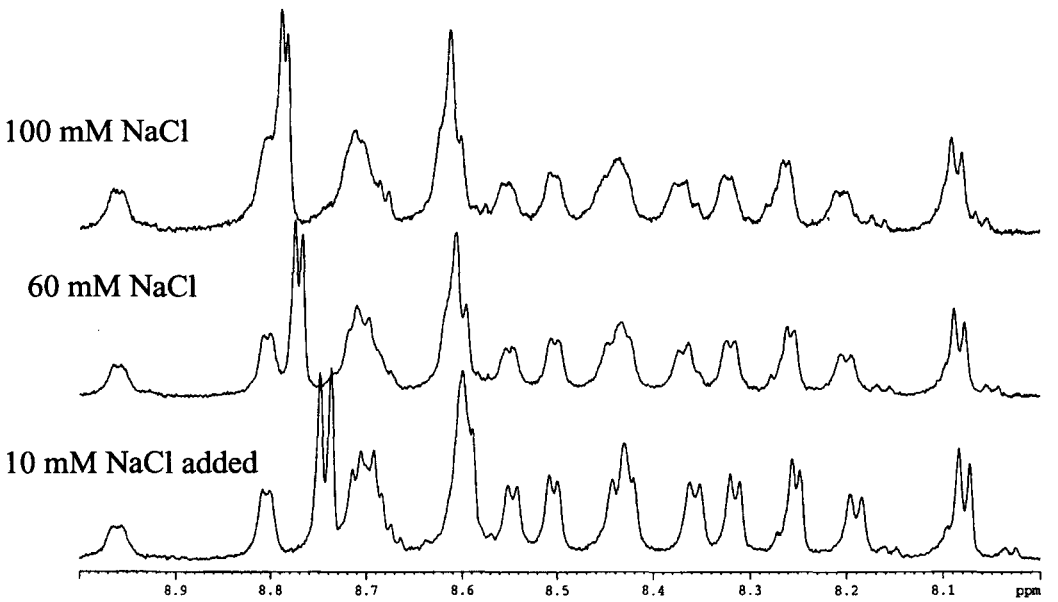

Figure 2.11: Effect of NaCl on the aggregation of Aβ (12-28) monitored by 1D-WG NMR spectra: 10 mM, 60 mM and 100 mM NaCl were added to 1 mM Aβ (12-28), 50 mM d_3-Acetate Buffer, pH 4.7, 293K.

Chapter 3

STD Analysis of Amyloid-Forming Polypeptides

3. 1 Introduction

3.1.1 Background

The Saturation Transfer Difference (STD)-NMR method was initially proposed [1, 2] to investigate the binding of small ligands to biological macromolecules, including proteins [3] and nucleic acids [4]. One of the strengths of the STD method is its ability to detect weak binding with great sensitivity: STD is suitable for interactions with dissociation constants within the range of ca. 10^{-3}-10^{-8} M [3] and 1 nmol of receptor is often enough to achieve good signal-to-noise ratios with commercial NMR spectrometers [3]. In addition, the binding epitope can be mapped based on the intensity of the ligand STD signal.

Recently the application of the STD-NMR methods has been extended to self-recognition mapping in oligomerizing peptide systems [5]. While this pioneering use of STD experiments opens new opportunities for investigating the molecular determinants of self-association, it is important to assess to what extent the STD experiments traditionally used to map protein-ligand interactions can be extended without modifications to self-associating amyloidogenic peptides. Here, we systematically investigate the strengths and limitations of the traditional STD-

NMR methods as applied to oligomer/monomer interactions of the amyloid beta peptide 12-28, Aβ (12-28), which has been used throughout this thesis as model system for the early steps of fibrillization.

3.1.2 Mechanism of STD Experiments

Figure 3.1 illustrates the principles underlying the traditional STD-NMR experiments. STD-NMR depends on the transfer of saturation from the protein to the ligand or in our case, from the oligomers to monomers. In the original version of the STD experiments (Figure 3. 1 (a)), the protein is irradiated at a resonance where no ligand signal is present, thus a selective saturation of the protein is achieved and then this selective saturation can be transferred to the entire protein due to spin diffusion. The saturation can also be transferred to the binding site of the ligand by intermolecular saturation transfer. The larger protons in Figure 3.1 (a) represent the hydrogen of the ligand in close contact with the protein, while the medium-sized H atoms indicate groups with less and/or more remote contacts. The smallest Hs symbolize the protons with minimal or no interaction with the protein receptor. Considering that the STD-signal intensity reflects the average distance of a ligand proton from the receptor, it is possible to map the proximity of these protons to the protein receptor surface using the degree of saturation.

In our new STD-NMR experiment (Figure 3.1 (b)), we study the Amyloid beta peptide oligomer/monomer interaction. In this case, considering that the exact resonance frequencies of the oligomers are unknown, we actually mainly

saturate the monomer in solution (*e.g.* selective RF irradiation on the methyl or aromatic signals). Then the saturation is transferred to the oligomer from the monomer in tight contact with the oligomer, and then transferred back from the oligomer to monomer through chemical exchange between the oligomers and monomers. The saturated ^{1}H spins of the monomer will result in the detected STD signals.

3.1.3 Potential Artifacts of STD Experiments

The STD measurement applied to self-associated polypeptides is potentially affected by other mechanisms such as saturation frequency offset effects, intra-molecular magnetization transfer within the monomer, partial spin diffusion within the macromolecule and water competition as well. For the purpose of critically evaluating the effects of these potential biases, here we report on the investigation of the dependence of peptide STD signal on the saturation time and frequency at different peptide oligomerization states. We also compared the 2D-STD results with previous OR-Relaxation measurements which provide an independent map of self-recognition. The artifact analysis presented here will be useful to assess the reliability of STD data on oligomerizing systems in general.

3. 2 Material and Methods

The 1-D STD NMR pulse sequence (Figure 3.2) has been previously described [3] and we used a similar pulse sequence with WATERGATE for water

suppression of the H_2O signal through a binomial 3-9-19 pulse sandwich, resulting in inversion of all signals except the H_2O signal at the carrier frequency. The subtraction between spectra with and without monomer saturation is performed after every scan via phase cycling. The on- and off-frequency of the selective pulse is therefore switched between 30 ppm and our selectively irradiated resonance (*e.g.* 0.57 ppm for methyl group saturation) after each scan. The length of each Gaussian saturation pulse is 50ms, and the strength is 120 Hz. The delay δ between the saturation pulses is 1ms. The total saturation time is determined by the number of saturation pulses n. The delay d1 is an additional short relaxation delay: 100 ms in this experiment to minimize sample heating effects. The data points are 4096 for the 1D experiments. For the TOCSY experiments shown in this chapter, the mixing time is 45 ms, the carrier frequency is 3291.081 Hz; the acquisition time of the directly detected *F2* dimension is 91.8452 ms; the number of points are 1024 and 512 for the F2 and F1 dimensions, respectively. For the off-resonance relaxation experiment, further details are available in reference [12]. The sample preparation protocol was the same as that discussed in the hydration Chapter 4.

3. 3 Results and Discussion

Saturation time dependence: The STD effect is known to reach an asymptotic behavior for increasing saturation times [4]. It is important to determine the saturation time at which the asymptotic regime starts and this

saturation time can be then used in STD experiments where other parameters (*i.e.* saturation frequency, oligomeric state etc.) are probed. Figure 3.3 shows that the STD signals reach a plateau after T_{sat} ~2s. Thus the T_{sat} = 2s is chosen for the subsequent 2D STD spectra.

3.3.1 Evaluation of Offset Effects

Figure 3.4 a shows that there are other relatively intense methyl peaks at 1.0~0.8 ppm beside the irradiated V18 methyl groups for the 0.1mM Aβ sample. Considering that the monomeric form of this peptide is known to be quite unstructured, and the poor ppm dispersion of the methyl region, these additional methyl peaks are identified as caused by the offset effect. Similarly, for the aromatic saturation (Figure 3.4 (b)), those peaks in 7.2~6.9 ppm are identified as caused by the offset effect. From these 1D spectra, it is clear that offset effects are more intense than the effect of monomer cross-relaxation. However the offset effect is easily identified as these peaks have close chemical shifts to the irradiated frequency and the selectivity of the saturating RF field can be reliably modeled using simple simulations based on the Bloch equations. For instance, Figure 3.5 shows the results of simulations carried out at a field of 700.23 MHz for a 50ms Gaussian pulse with 1% truncation and maximum strength of 116.1 Hz, which was used in the selectively saturating pulse train. The initial magnetization is assumed to be aligned along the z-axis and have a magnitude of 1 arbitrary unit. While the inversion profile describing the z-component of the magnetization

after the Gaussian pulse is limited to a relatively narrow frequency range (Figure 3.5, black line), the use of a train of Gaussian pulses means that selectively is also determined by the trajectory of the magnetization *during* the repeated Gaussian pulses. Considering that at frequencies outside the inversion bandwidth of the Gaussian pulse the trajectories for the evolution of magnetization are essentially adiabatic, the selectivity of the train of Gaussian pulses can be appreciated by reporting the z-component of the effect (Figure 3.5, red line), showing that offset-effect can extend up to 0.5 ppm from the saturating frequency. Indeed, in the study of 0.1mM Aβ, the aromatic saturation was at ~7.2 ppm and offset effect peaks are observed even at 7.65 ppm (Figure 3.4 (b)).

3.3.2 Evaluation of Monomer Contributions

Possible contribution from intra-molecular cross-relaxation of the monomeric peptide was evaluated by the comparative analysis of 1D-STD spectra acquired at different peptide dilutions. At 0.1 mM the Aβ (12-28) is know to be mainly in the monomeric state under the conditions used [12, 13], while at 1 mM the Aβ (12-28) solution contains detectable amount of soluble oligomers. If we selectively saturate at the methyl group (401Hz), the 1mM Aβ (12-28) solution shows significant STD signals (Figure 3.4 (a)) as expected for the oligomers in the solution. When the same experiment is repeated for the 0.1mM Aβ (12-28) solution some weak STD signals are still observed (Figure 3.4 (a)). These residual peaks observed at 0.1 mM Aβ (12-28) cannot be accounted for by offset-

effects (Figure 3.4 (a)) and they are likely the result of the intra-molecular monomer cross-relaxation. The V18 Hα (~ 4 ppm) and V18Hβ (~ 1.8 ppm) are caused by the monomer cross relaxation as the selective saturation is at the methyl groups of V18 (401Hz). Similarly, the same monomer cross relaxation is identified for the aromatic saturation (Figure 3.4 (b)). Both the offset effects and the monomer contributions interfere with the measurement of the real STD contributions arising from self-recognition. It is therefore important to consider both artifacts when analyzing STD NMR data for oligomer/monomer equilibria.

3.3.3 Evaluation of Partial Diffusion

STD experiments can be used to map self recognition at residue resolution by measuring the STD effect for different Hα protons. This requires 2D STD NMR experiments which were acquired for the sample of 1mM Aβ (12-28) in 50 mM acetate buffer, pH 4.7 and 10% D_2O. In Figure 3.6, the normalized I_{sat}/I_{unsat} is used to evaluate the importance of the specific residues involved in the self-recognition of the Aβ peptide. In methyl STD, the hydrophobic residues L17 and V18 had the highest values; while in aromatic STD, the 2 aromatic residues F19 and F20 have highest values. The reason for the discrepancy caused by different saturating frequency (methyl and aromatic) could be the partial spin diffusion within the oligomer of Aβ. If the saturation transfers to the whole oligomer, the I_{sat}/I_{unsat} in the Hα-NH region should not depend on the saturation frequency. However the Methyl (green) and Aromatic (brown) STDs show saturation

dependence here (Figure 3.6), suggesting that the spin diffusion within the oligomer may be only partial.

3.3.4 Possible Strategies to Experimentaliy Overcome the STD Limitations

A possible solution to the partial diffusion problem is to combine STD information at different saturation frequencies. For instance, the normalized STD data acquired at the two saturation frequencies of methyl and aromatic protons can be averaged and then normalized again to the highest average STD value. The normalized Me-Ar average STD (black) maps well the central hydrophobic core Aβ (17-21) (LVFFA), which was independently shown by mutational analysis to be a key determinant of self-recognition [7].

3.3.5 Comparison with OR-Relaxation

The STD and the OR-Relaxation (Off-resonance relaxation) measurements provide two independent experiments to probe self-recognition and therefore the comparison between the STD and OR-R results is a good approach to investigate possible artifacts and cross-validate these methods. The 35.5° non-selective off-resonance relaxation rates measured earlier [12] are reported (Figure 3.6). In the Me-Ar average STD, the acidic residues E22 and D23 have lower values than expected based on the Off-resonance relaxation rates. The different mechanisms underlying the STD and OR-R effects could explain this discrepancy

observed between the STD and off-resonance measurements. While the OR-R probes how the flexibility of a given residue is affected by self-recognition, the STD probes also additional relaxation pathways that effectively compete with cross-saturation. For instance, when methyl or aromatic protons are saturated, the bulk water magnetization remains largely unaffected and therefore protons in close proximity to exchanging labile protons will be less saturated than other protons in less polar regions of the system. In other words, water competition introduces a bias in methyl- and aromatic-STD experiments towards hydrophobic residues, which should be considered when analyzing STD data in term of self-recognition patterns. Therefore the fact that E22 and D23 display STD vaules that are lower than what is expected based on the OR-R rates may just reflect a limitation of the traditional STD approach rather than a limited involvement of these residues in self-recognition. This interpretation is consistent with mutation data showing that E22 and D23 are indeed involved in self-associations [14-16]. The limitations caused by water competition will be effectively overcome though the proposed WSTD method (see Chapter 5).

3.4 Conclusions

The limitations arising from the offset effects, the monomer contributions and the partial spin diffusion within the oligomers including the water competition have been investigated in this chapter. The assessment of these limitations will facilitate a reliable analysis of STD spectra in terms of

polypeptide self-recognition maps. An initial solution to overcome these limitations has been proposed based on the acquisition of spectra at multiple saturating frequencies. However, this approach represents only a partial solution and alternative STD methods need to be developed to probe at residue resolution and more directly the self association epitopes of Aβ and other amyloidogenic peptides.

References

1. M. Mayer, B. Meyer, Angewandte Chemie-International Edition 38 (1999): 1784-1788
2. J. Klein, R. Meinecke, M. Mayer, B. Meyer, J. Am. Chem. Soc. 121 (1999): 5336-5337
3. M. Mayer and B. Meyer, J. Am. Chem. Soc., 123 (2001) 6108-6117
4. M. Mayer and T.L. James, J. Am. Chem. Soc., 124 (2002) 13376-13377
5. S. Narayanan and B. Reif, Biochemistry, 44 (2005) 1444-1452
6. JL Yan, A. D. Kline, et al, J. Magnetic Reson., 163 (2003) 270-276
7. J. Jarvet, P. Damberg, et al., J. Am. Chem. Soc., 122 (2002) 4261-4268
8. K. Wuthrich, NMR of Proteins and Nucleic Acids, John Wiley & Sons Inc., 1986
9. A.D. Ferrao-Gonzales et al. J. Mol. Biol. 328 (2003) 963–974
10. G. Otting, J. Am. Chem. Soc., 1994, 116, 9670-9674
11. A. Paivio, J. Jarvet, J. Mol. Biol. 339, (2004), 145

12. V. Esposito, R. Das, G. Melacini, J. Am. Chem. Soc. 127 (2005): 9358-9359

13. S.L. Mansfield, D.A. Jayawickrama, J.S. Timmons and C.K. Larive, Biochimica et Biophysica Acta 1382 (1998) 257–265

14. J.P. Melchor, L.McVoy, and W.E. Van Nostrand, J. Neurochem., 75 (2000) 2209-2212

15. A. Päiviö, J. Jarvet, A. Gräslund, L. Lannfelt and A. Westlind-Danielsson, J. Mol. Biol., 339 (2004) 145-159

16. A.T. Petkova, Y. Ishii, J.J. Balbach, O.N. Antzutkin, R.D. Leapman, F. Delaglio, R. Tycko, Proc. Natl. Acad. Sci. 99 (2002): 16742-16747

(a)

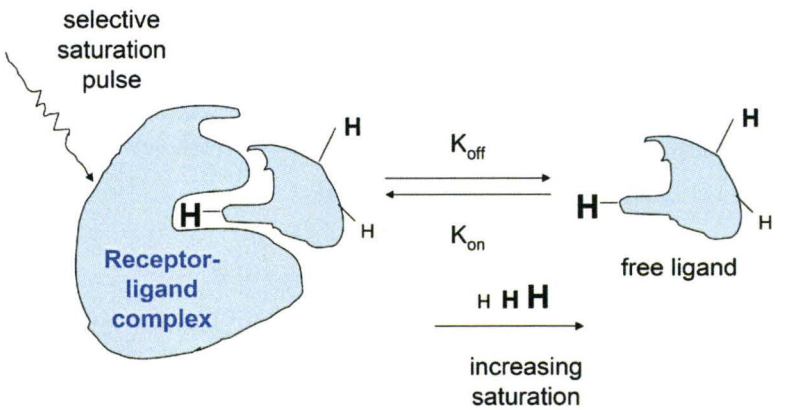

(b)

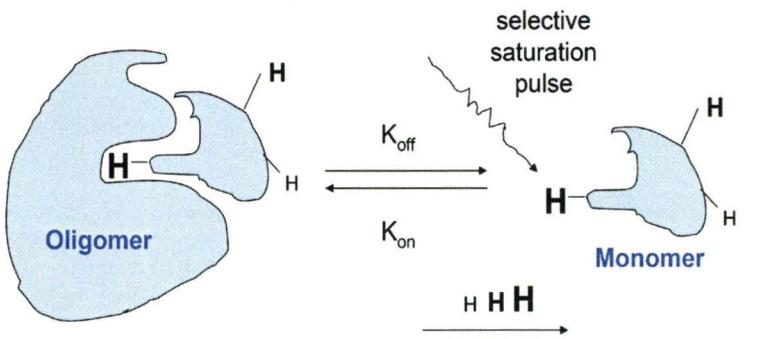

Figure 3.1: STD-NMR saturation transfer mechanisms. (a) Original version of the STD-NMR experiment. [3]; (b) The STD-NMR mechanism employed in studying the Amyloid beta peptide oligomer/monomer equilibria.

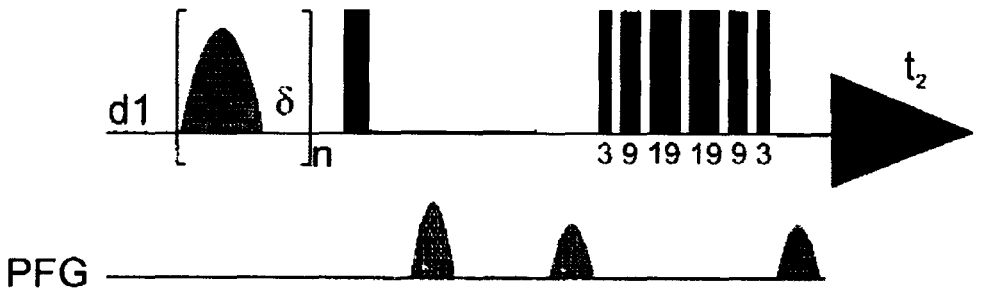

Figure 3.2: 1-D STD-NMR pulse sequence [3]. PFG: pulsed field gradient; d1: the relaxation delay.

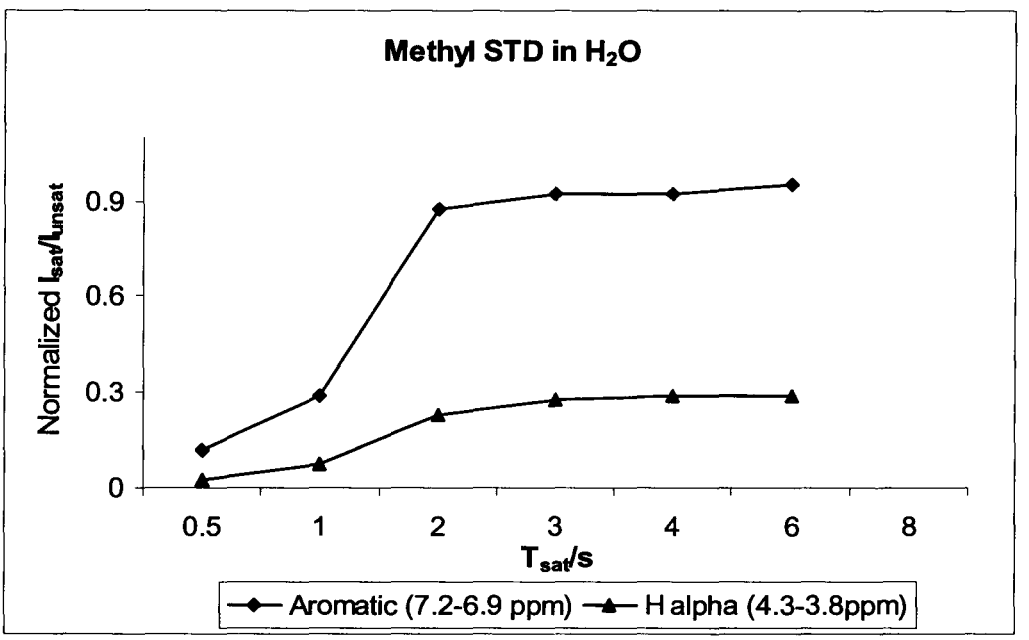

Figure 3.3: The 1D-STD intensity reaches a plateau after Tsat ~ 2s, therefore Tsat = 2s is employed in the above 2D-STD experiments.

(a)

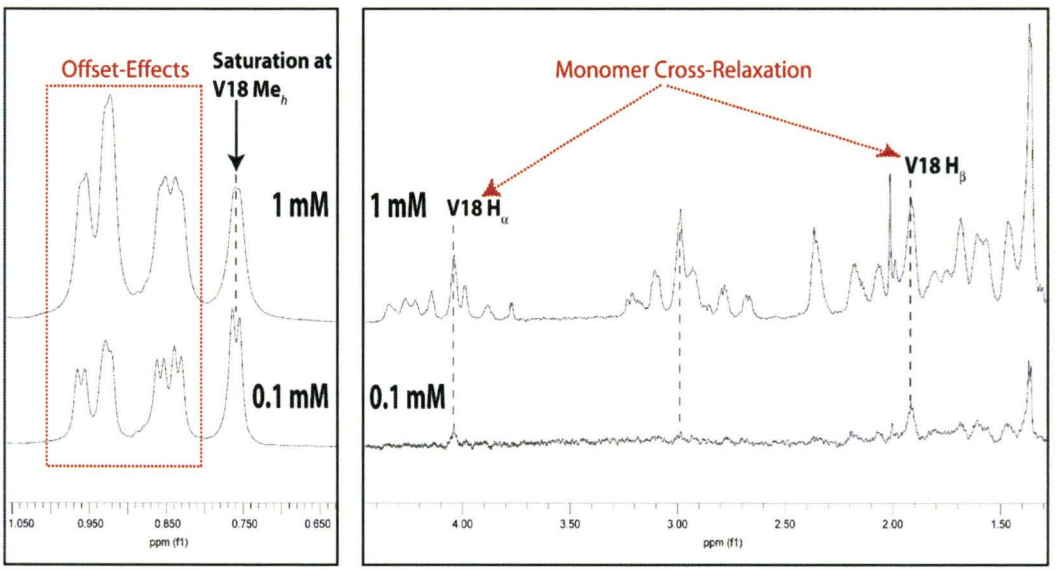

(b)

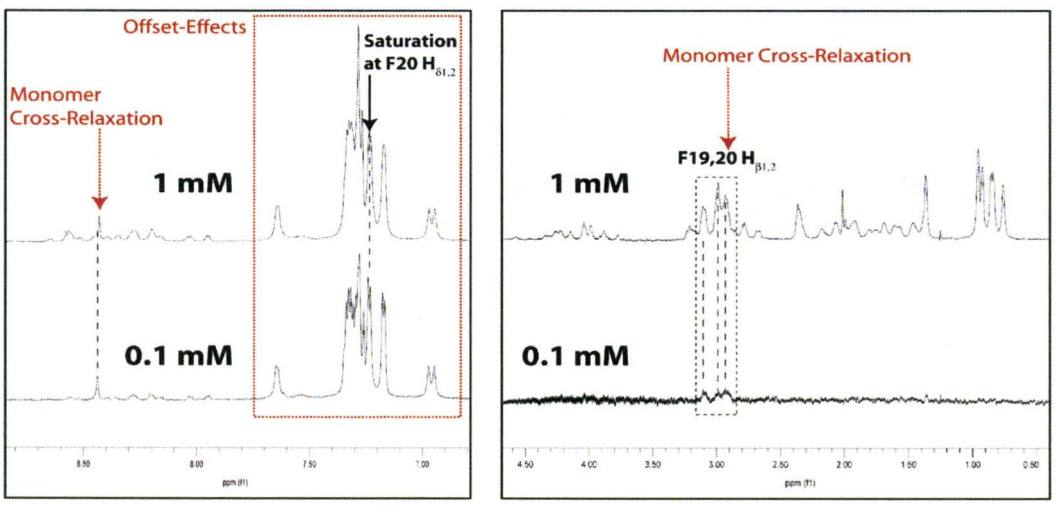

Figure 3.4: The 1D STD of 1mM Aβ and 0.1mM. Here the limitations of offset effects and monomer cross-relaxation have been shown. Please see the text for interpretation. (a) methyl saturation STD; (b) aromatic saturation STD.

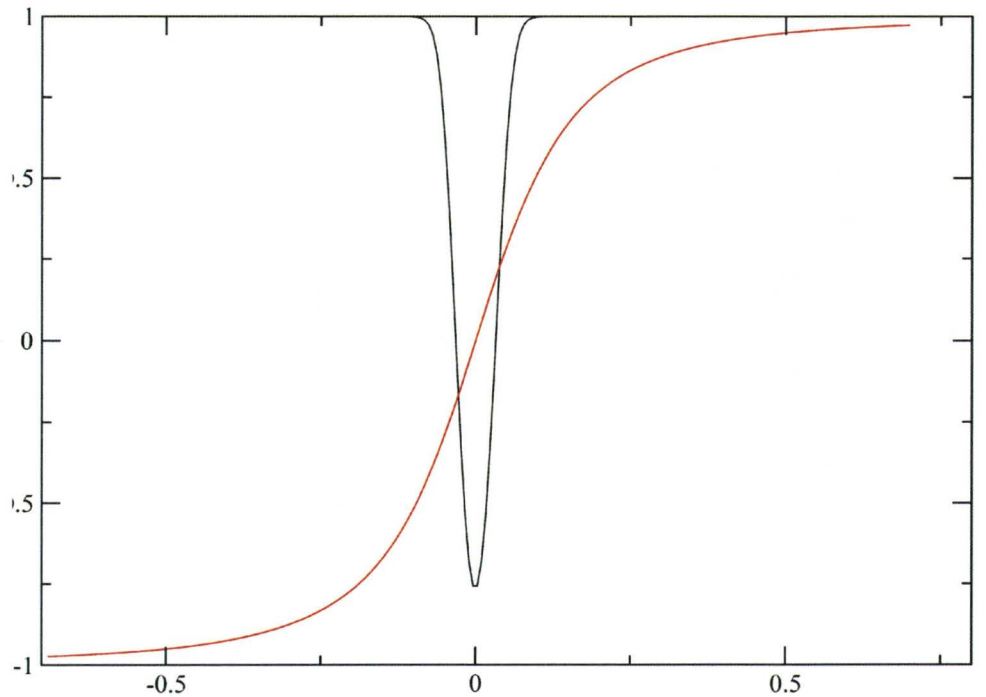

Figure 3.5: Black: z component of the magnetization after the selective Gaussian pulse at different offsets in ppm. Red: z projection of the maximum effective field (normalized to unity) at different offsets in ppm.

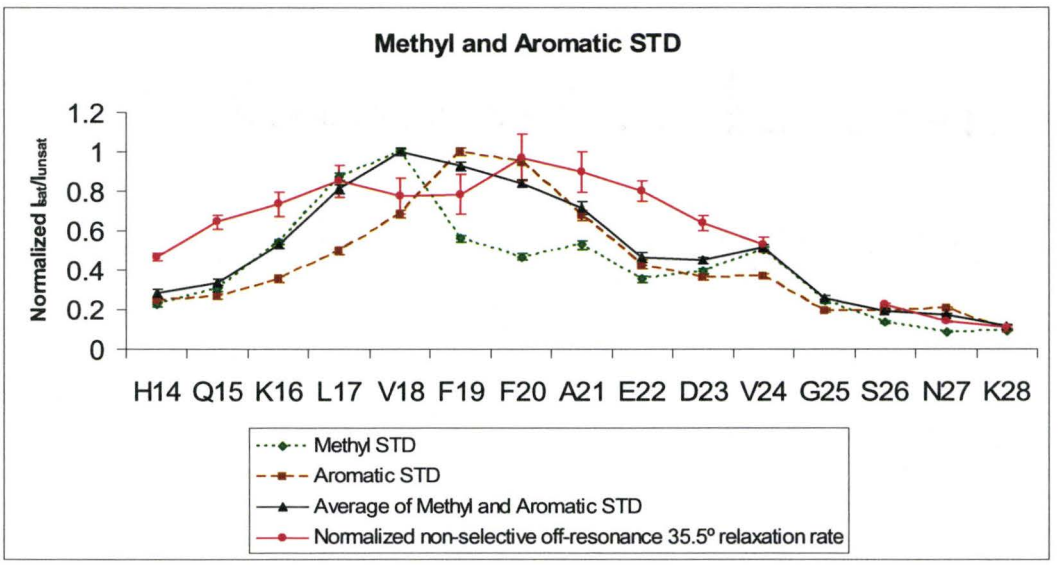

Figure 3.6: The 2D STD of 1mM Aβ (50mM acetate buffer, pH 4.7 and 10% D_2O). Green, methyl saturation STD, normalized to the highest; brown, aromatic saturation STD, normalized to the highest; black, the average of methyl and aromatic saturation STD, normalized to the highest; red, the non-selective off-resonance 35.5˚ relaxation rate, normalized to the highest [12].

Chapter 4

Hydration Studies of the Aβ (12-28) Peptide

4.1 Introduction

The formation of soluble oligomers is mainly driven by hydrophobic and electrostatic interactions between amyloid forming peptide molecules [1-3]. In addition, recent evidence suggests that hydration and packing are crucial to amyloidogenesis [4], and that solvation changes correlate with fibrillization-enhancing mutations [5]. These findings are also consistent with the correlation between aggregation sites and water exposure of atoms involved in intra-molecular H-bonds [6, 7]. Our goal here is to further probe the role that water molecules play in amyloidogenesis, focusing on the early stages of oligomerization that precede nucleation. Specifically we are interested in testing the hypothesis that hydration dynamics and self-recognition are coupled processes. This speculation is reasonable if the early oligomers formed by self-assembly behave similarly to protein folding intermediates, in which water cavities exist [8]. We will use a combined strategy based on NMR hydration experiments as well as mutant design to test our hypothesis.

The system we are studying is the amyloid β (Aβ) peptide (12-28) with the sequence $VHHQ_{15}KLVFF_{20}AEDVG_{25}SNK_{28}$. This is a fragment of the full length Aβ (1-42) known as the full length peptide is Alzheimer disease related peptide.

The Aβ (12-28) peptide contains a central hydrophobic core (CHC) Aβ (17-20) (LVFFA), which is the major determinant of aggregation, as well as the flanking charged residues. The Aβ (12-28) peptide is characterized by a very flexible structure and therefore NMR is an ideal tool to investigate this system. The lack of significant structure in this peptide implies poor chemical shift dispersion and therefore high field NMR (*i.e.* 700 MHz) is required to obtain atomic resolution.

4.2 Material and Methods

A 50mM d_3-acetate buffer at pH 4.7 was prepared starting from 99.5% d_3-acetic acid (Aldrich). The volume of 57.4 μL concentrated acetic acid was used to prepare 20 mL of 50 mM acetate buffer. We then diluted this amount of acetic acid with 10 mL double distilled H_2O (Type I, 18 MΩ cm^{-1}). The pH was 2.7~2.8 and 1M NaOH (NaOH powder is from Sigma) was added in 10 μL increments to reach pH 4.7. Additional double distilled H_2O was added again to reach the total volume of 20 mL and the final pH was 4.7.

Our NMR studies were carried out at 50 mM d_3-acetate buffer, pH 4.7, 293 K, 10% D_2O (Cambridge Isotope Laboratories, Inc., MA, USA) and 1 mM Aβ (12-28). Under these experimental conditions the samples were stable for months. The filtration with 30 kDa cut-off filter (Ultrafree®-MC centrifugal filter device for volumes less than 0.5mL from Milipore Corporation, MA, USA) was carried out after washing the filter 6 times (4500 g×3 min) with the above buffer to remove the glycerol. The filtration of a 400 μL peptide solution was carried

out at 5700 g for 20 min. Additional peptide solutions of 100~150 μL were added and filtered again at 5700 g for 20 min to obtain ca. 500 μL for NMR experiment. The temperature during filtration was maintained at 4 °C.

Echo anti echo NOESY (EA NOESY) (Figure 4.1 and 4.2) has been used in this study to observe the interaction between the protons of water molecules and the protons in the peptide oligomers. The 180° pulse is used here for re-focusing the chemical shift evolution. The WATERGATE (WG) 3-9-19 is used for water suppression. In Figure 4.2, the selective saturation is achieved by applying the soft pulse (the solid rectangle) in the mixing time. The soft pulse is 130Hz and 150ms long. For the TOCSY experiments conducted in this chapter, the mixing time is 45 ms, the carrier frequency is 3291.081 Hz; repetition delay of 1s; acquisition time of the F2 dimension was 0.122 s; 2048 points and 512 points for the F2 and F1 dimensions were acquired.

To understand the roles played by different driving forces and different residues in the self recognition, several important mutants have been studied. These mutants were synthesized through solid state methods (Fmoc peptide synthesis) and purified by Peptron Inc. (Korea). The mutants are listed below, the underlined letters are the mutated amino acids. The details of rationale of the mutant design will be addressed in Section 4.3.1.

Table 4.1 The Sequences of wt Aβ (12-28) and Related Mutants

WT	V_{12}HHQKLVFFAEDVGSNK_{28}
Mutant1 (S26A)	V_{12}HHQKLVFFAEDVG<u>A</u>NK_{28}
Mutant2 (triple mutant)	<u>Ac</u>V_{12}<u>KK</u>QKLVFFAEDVG<u>A</u>NK_{28}
Mutant3 (E22Q)	V_{12}HHQKLVFFA<u>Q</u>DVGSNK_{28}

4.3 Results and Discussion

Our first goal was to establish how sensitive the hydration spectra are to the presence of soluble oligomers. For this purpose we acquired NMR hydration spectra applying the pulse sequence of Figure 4.1 on two samples: a 1 mM Aβ (12-28) unfiltered sample simply obtained by dissolving the lyophilized peptide in acetate buffer and another sample differing filtered through a 30 kDa cut-off filter. The first sample is known to contain small populations of soluble oligomers [3, 13] while the second solution represents mainly the monomeric state of the peptide which is kinetically stabilized by the absence of nucleation seeds that are removed through the filtration step. The peptide concentration in the two samples is not significantly different as seen by comparing the signal for the amide proton of K28 in the respective 1D-WG spectra (Figure 2.10). The line-width of the amide proton of K28 is not significantly perturbed by the soluble oligomers as the C-terminal K28 is not directly involved in oligomerization. The K28 signal is therefore a good reporter of the peptide concentration. The similarly between the

K28 signals in the 1D spectra of Figure 2.10 is consistent with the low population of soluble oligomers in the unfiltered sample. Figure 2.10 also shows that filtrations cause a major sharpening of most peaks involved in self recognition [13] confirming the effectiveness of the filtration step in removing the majority of the soluble oligomers. The comparison of the hydration spectra of the unfiltered *vs.* filtered samples provides therefore valuable information on the effect of oligomerization on hydration. Figure 4.3 shows that the hydration NMR spectra change dramatically upon filtration. It has been previously shown [3] that viscosity does not change significantly upon filtration and therefore viscosity variations cannot account for the observed dramatic hydration spectra change (Figure 4.3). So this change must arise from the oligomers which affect the magnetization transfer from water to oligomerizing peptide molecules.

There are three kinds of mechanisms for the magnetization transfer between water molecules and the peptide aggregates. They are direct NOE, chemical exchange and chemical exchange relayed NOE (Figure 4.4) [9]. Direct NOE refers to the NOE (Nuclear Overhauser Effect) between water molecules and peptide protons within a distance of ~5 Å. Chemical exchange denotes the H/H exchange between water and the labile protons of the peptide (*e.g.*, O-H, N-H and S-H). If chemical exchange occurs, and some other non-exchangeable protein protons are within 5 Å, the magnetization transferred by chemical exchange could be further transferred to these nearby protons by intra-molecular cross-relaxation. This two step pathways is commonly referred to "chemical

exchange relay". As indicated in Table 4.2, the water-peptide cross peaks caused by different mechanisms have different signs in different NMR spectra according to the nature of the mixing period and the residence time of the hydration water molecules (e.g. NOESY, TOCSY, Off-Resonance ROESY (OR ROESY)). The summary of the signs of the peaks and of their dependence on the residence time of water molecules (Table 4.1) is extremely useful to find which mechanisms accounts for the observed dramatic change in the hydration spectra before and after filtration (Figure 4.3).

With the TOCSY spectrum (Figure 4.5), we detect the signal caused by chemical exchange, as only chemical exchange can account for these positive peaks on the water row in TOCSY. The spectra before and after 30 kDa filtration show basically the same chemical exchange properties as H/H exchange senses mainly the monomeric state of the peptide (Figure 4.5). Thus we rule out the chemical exchange as the mechanism causing the hydration spectra to change. The only remaining possible mechanisms accounting for the hydration spectra change are therefore the direct NOE or the exchange-relayed NOE or both.

Table 4.2 Dissecting the Contributions to the Hydration Spectrum Arising From Different Polarization Transfer Pathways

Water → Solute Polarization Transfer Pathways	Coherence Transfer in Pulse Sequence			
	NOESY	54.7° OR ROESY	35.5° OR ROESY	TOCSY
Direct Cross-Relaxation	+/-[1]	-	0/-[2]	0
Chemical Exchange	+	+	+	+
Chemical Exchange Relay	+/-[3]	-	0/-	0

'0' means no signal, '+' means positive signal, '-' means negative signal

1. The sign is '-' for surface water with short residence time (less than 1ns), while it is '+' for internal water with relative long residence time (>1 ns);
2. The sign is '-' for surface water with short residence time (less than 1ns), while it is '0' for internal water with relative long residence time (>1 ns);
3. The sign is '-' for flexible side chain with short residence time (less than 1ns), while it is '+' for rigid side chain with relative long residence time (>1 ns).

4.3.1 Editing of NMR Hydration Spectra

In order to further dissect the direct NOE and exchange-relayed NOE contributions to the hydration spectra it is important to inspect more carefully the H/H exchange rates. Based on the pH dependence of H/H exchange rates of amino acids in water (Figure 4.6) [10], we know that some protons are in fast exchange with water while others are in slow exchange with water at the selected pH of 4.7. Thus we developed spectroscopic editing and chemical editing strategies (Figure 4.7) for slow and fast chemical exchange, respectively. For slow exchange protons (H13, H14 back bone NH and K16, K28 side chain NH_3^+), we can observe the exchange peaks in the spectrum, thus we can suppress them with a selective continuous wave (CW) irradiation in the mixing time with our pulse sequence. The exchanging protons are saturated by CW, so there is no net magnetization transfer and the corresponding exchange relay path ways are also suppressed. For fast exchange protons (*i.e.* N-terminal -NH_3^+, His 13, 14 side chain NHs, and the S26 side chain OH), the hydration peaks may be covered by water peaks, thus it is hard to be selectively suppressed spectroscopically without compromising the hydration spectrum. We therefore have to mutate them to slow exchange amino acids (Figure 4.7).

As indicated in Table 4.1, we created Mutant 1 (S26A), Mutant 2 (triple mutant: N-terminal acetylated H14K, H15K, and S26A) and Mutant 3 (E22Q). These mutations are unlikely to perturb the structural integrity of the central hydrophobic core (CHC), which is known not to depend on the charged flanking

residues [11]. In addition, it is possible to validate the hypothesis that these mutants are good models to study the WT Aβ (12-28) by using control experiments aimed at detecting chemical shift signatures for the CHC.

For instance, the finger print and CHC methyl regions of the TOCSY spectra as well as the αH secondary chemical shifts shown in Figure 4.8 suggest that Mutant 1 (S26A) maintains the main structural features of the wild type peptide (WT). In addition, the chemical shift changes of all amino acids but the mutated amino acids S26 and the adjacent amino acid N27 are within 0.06 ppm. Based on the observation that the chemical shift changes of the amino acids in CHC are insignificant and that the CHC methyl signature remains intact (Figure 4.10) in mutant S26A, we conclude that S26A preserved an intact CHC. The mutant S26A is therefore a good model for the WT. Similarly, we can demonstrate that mutant 2 (Table 4.1) is also a good model to study WT (Figure 4.8).

4.3.2 Coupling Mechanisms between Peptide Oligomerization and Water-to-Peptide Transfer Efficiency

The comparison of the hydration spectra of the WT Aβ (12-28) peptide and the S26A mutant (Figure 4.10) indicates that the hydration peaks are not significantly affected by the mutation. This observation rules out the possibility that the S26-OH relay pathway contributes to the CHC hydration of the oligomers. If we apply the selective continuous wave irradiation to the slow exchange

protons of S26A with the purpose of specifically suppressing the chemical exchange signals and the exchange relay pathways thereof, we can see that the hydration peaks remain intact (Figure 4.11). Thus the CHC hydration peaks are likely caused either by real long-lived water or by exchange relayed NOEs from other labile protons, such as those of the histidine side chains and/or the N-terminal NH_3^+. However the comparison between hydration spectra of WT and Mutant 2 (triple mutant) (Figure 4.12) suggests that the His side chains and the N-terminal NH_3^+ relay pathways do not contribute to the CHC hydration in the oligomers. Even after using CW to selectively suppress the K side chain NH_3^+, no significant change of hydration peaks in the CHC is observed (Figure 4.13), indicating that the source for these hydration peaks is the direct NOE created by real long-lived water or the exchange relay by other labile protons such as those of the acidic amino acids E22 and D23. The carboxylic protons of E22 and D23 are in fast exchange with water (the exchange peak overlaps with water resonance). Therefore we designed a new mutant E22Q which was tested for hydration signal with the EA NOESY (Figure 4.14). Since a cryo probe was installed on the 700MHz NMR spectrometer during this project, the third mutant E22Q was tested with the cryo probe resulting in better sensitivity in the spectrum than for the wt and the other mutants (Figure 4.14). The hydration peaks of mutant E22Q suggests E22 would not be the only source contributing to hydration properties of Aβ.

4.3.3 Open Problems

While our data unambiguously indicate that the hydration properties of Aβ (12-28) are exquisitely sensitive to the presence of even small amounts (<< mM) of soluble oligomers, it is presently still unknown which mechanism accounts for the observed dramatic change in the hydration properties upon oligomer formation. The existing data is consistent with a synergetic effect of both direct NOE and chemical exchange relay. It is difficult to dissect the hydration mechanisms further using spectroscopic and/or chemical NMR hydration editing methods. The spectroscopic methods are limited to the slow exchanging labile protons, while the effectiveness of the chemical editing approach is compromised by the different amounts of oligomers in different mutants. Thus different experimental conditions (*i.e.* salt concentration and/or pH) are required to introduce significant biases in the comparative analysis of the hydration spectra of wt *vs.* mutant peptides. A better avenue to test the presence of long lived water molecule in Aβ soluble oligomers is the magnetic relaxation dispersion (NMRD) of ^{17}O, which is not affected by exchange relay artifacts. Through ^{17}O NMRD it will be possible to assess the relative contributions of each of the possible mechanisms to hydration of Aβ. If NMRD experiments confirm the presence of long lived water molecules, several hypotheses on the nature of the soluble oligomers will be tested. For instance, according to the model of Figure 4.16 long lived water molecules with residence time >1ns can be accounted for through water-filled cavities formed by the CHC upon self-recognition. If this cavity

model is confirmed, it will provide important insight on the nature of the soluble oligomers. For instance, water-filled cavities indicate that the oligomers are likely to adopt a non-compact structure, suggesting that plasticity is required for further progression in the fibrillization pathway. However, presently the cavity model (Figure 4.16) is only a speculation and further supporting data is required.

4.4 Conclusions

The existing ^{1}H NMR data clearly show that the Aβ (12-28) hydration transfer efficiency is tightly coupled to peptide oligomerization. While further experiments are required to dissect the exact mechanism of this coupling in terms of direct *vs.* exchange relayed cross-relaxation, just the observation of this tight coupling has several implications. First, this coupling alone provides the basis for designing saturation transfer difference (STD) experiments aimed at probing self-recognition in amyloidogenic peptides as explained in greater detail in Chapter 3 and 5. Second, the efficient magnetization transfer mechanism existing between the soluble oligomers and bulk water implies that hydration-like methods could be used to improve contrast in the MRI monitoring of the early steps of fibrillization processes. Third, similar NMR methods could be used to probe the interactions between the peptide oligomers and other molecules different from water. This means that binding sites for other ligands different from water could be revealed using similar NMR approaches and that new drug leads for the early prevention of fibrillization could be screened by NMR.

References

1. Y.Xing and K. Higuchi, Mechanisms of Ageing and Development 123 (2002) 1625-1636
2.
3. P. M. Gorman and A. Chakrabartty, Biopolymers 60 (2001) 381-394
4. J. Jarvet, P. Damberg, K. Bodell, L.E. Göran Eriksson and Astrid Gräslund, J. Am. Chem. Soc., 122 (2000) 4261-4268
5. A.D. Ferrao-Gonzales, L. Palmieri, M. Valory, J. Mol. Biol. 328 (2003) 963–974
6. F. Massi J.E. Straub, J Comput Chem (2003) 24, 143–153
7. D. Grasso, D. Milardi, V. Guantieri, New J. Chem., 27, (2003) 359–364
8. A. Fernández, J. Kardos, L. R. Scott, Y. Goto, and R. S. Berry, Proc Natl Acad Sci 100 (2003) 6446–6451
9. M. S. Cheung, A. E. García, and J. N. Onuchic, Proc Natl Acad Sci USA 99 (2002) 685–690
10. G. Otting, Progress NMR Spectroscopy 31 (1997) 259-289
11. Kurt Wuthrich, NMR of Proteins and Nucleic Acids, 24
12. S.S. Zhang, N. Casey, J.P. Lee Folding & Design 3 (1998) 413–422
13. V. J. McParland, A. P. Kalverda, S.W.Homans, S.E. Radford, Nature Struct. Biol. 9 (2002) 326-331
14. V. Esposito, R. Das, G. Melacini, J. Am. Chem. Soc., 127 (2005): 9358-9359

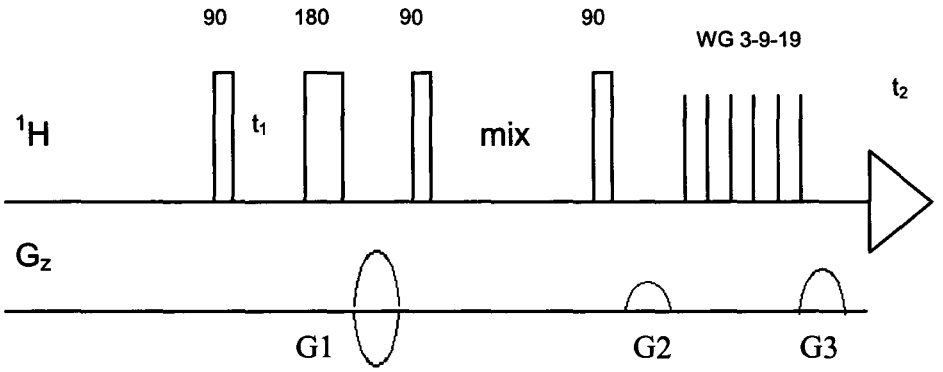

Figure 4.1: Echo anti echo NOESY NMR pulse sequence. This experiment was employed to probe the interactions between water and solutes. The WATERGATE (WG) 3-9-19 is used for water suppression. The carrier frequency is 3291.081 Hz; mixing time is 150 ms; d1=2s; acquisition time of *F2* dimention= 91.8452 ms; TD (*F2*)= 1024, TD (*F1*)=400; The G1, G2, G3 pulsed field gradients are sine-bell shaped and have a duration of 1ms. The relative ratios for the G1, G2, and G3 strengths are 57, 20, 23, respectively.

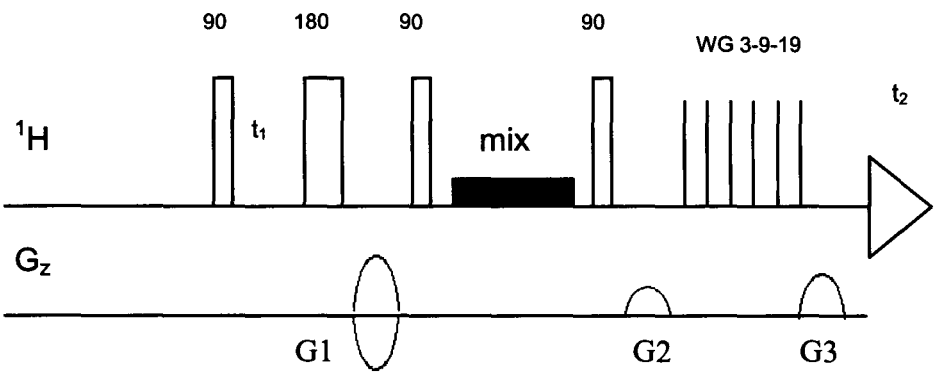

Figure 4.2: Echo anti echo NMR pulse sequence with selective saturation: based on Figure 4.1, the selective saturation is achieved by applying the soft pulse (the filled rectangle) in the mixing time. The WATERGATE (WG) 3-9-19 is used for water suppression. The carrier frequency is 3291.081 Hz; mixing time is 150 ms; d1=2s; acquisition time of *F2* dimention= 91.8452 ms; TD (*F2*)= 1024, TD (*F1*)=400; The G1, G2, G3 pulsed field gradients are sine-bell shaped and have a duration of 1ms. The relative ratios for the G1, G2, and G3 strengths are 57, 20, 23, respectively.

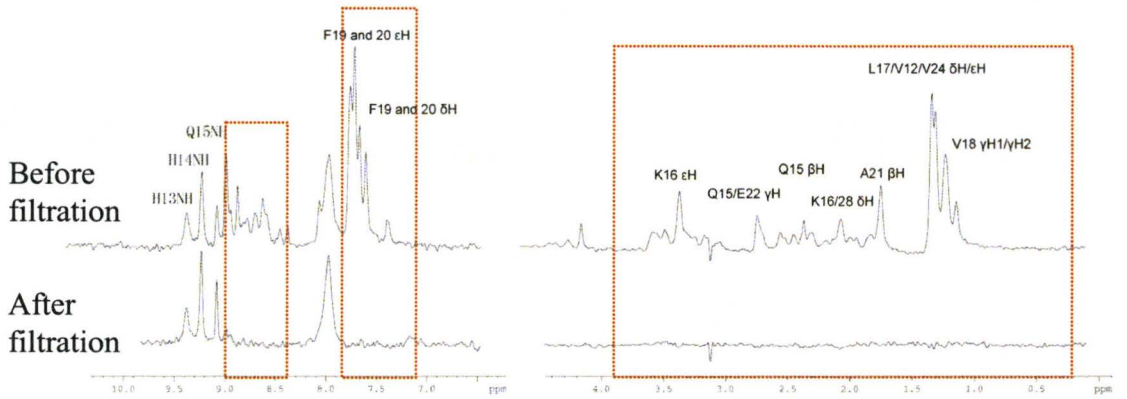

Figure 4.3: Hydration spectra before and after filtration, Water-Row from EA-NOESY, tmix = 150 ms, 700 MHz, showing the cross relaxation between water and protons in the Aβ (12-28).

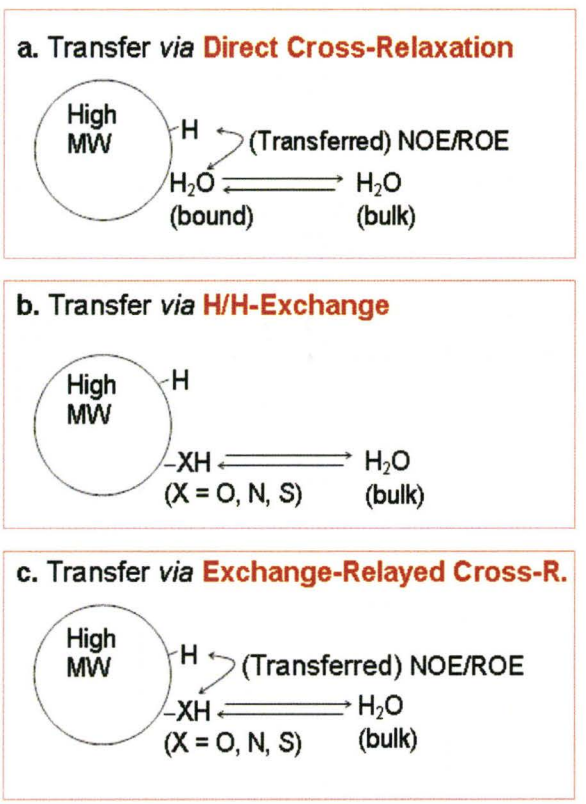

Figure 4.4: Hydration Mechanisms [9]

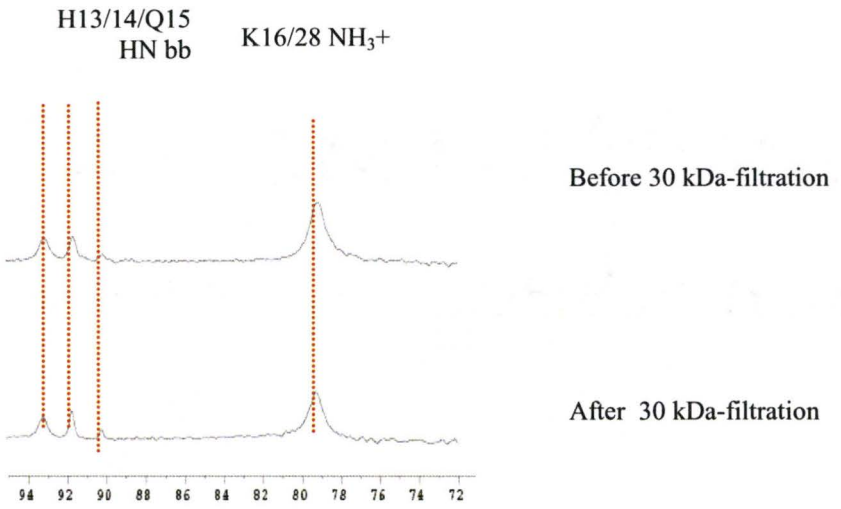

Figure 4.5: Water row in TOCSY spectra before and after filtration showing the exchange between protons in Aβ (12-28) and water. With it we can identify those hydration peaks caused by chemical exchange. The HN bb means the HN on back bone of the peptide.

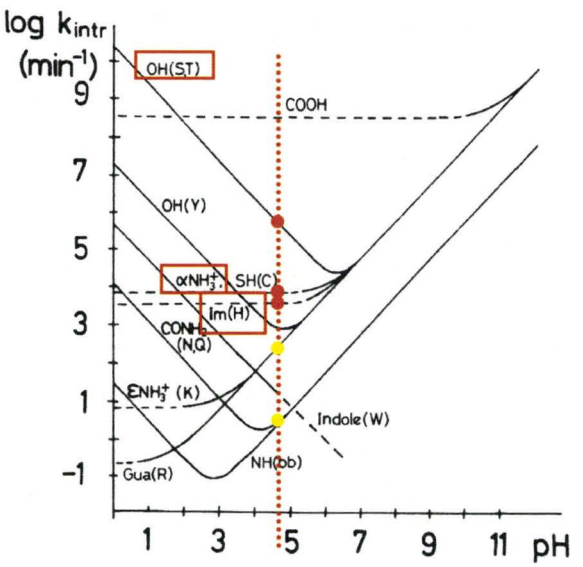

Figure 4.6: Exchange rates of labile protons in amino acids in water solution adapted from [10]. A vertical line shows the exchange rate at pH 4.7, which is the pH employed in experiments in this chapter: the COOH has the highest rate, the OH of Ser or Thr has the second highest rate, the SH of Cys has the third highest, and so on.

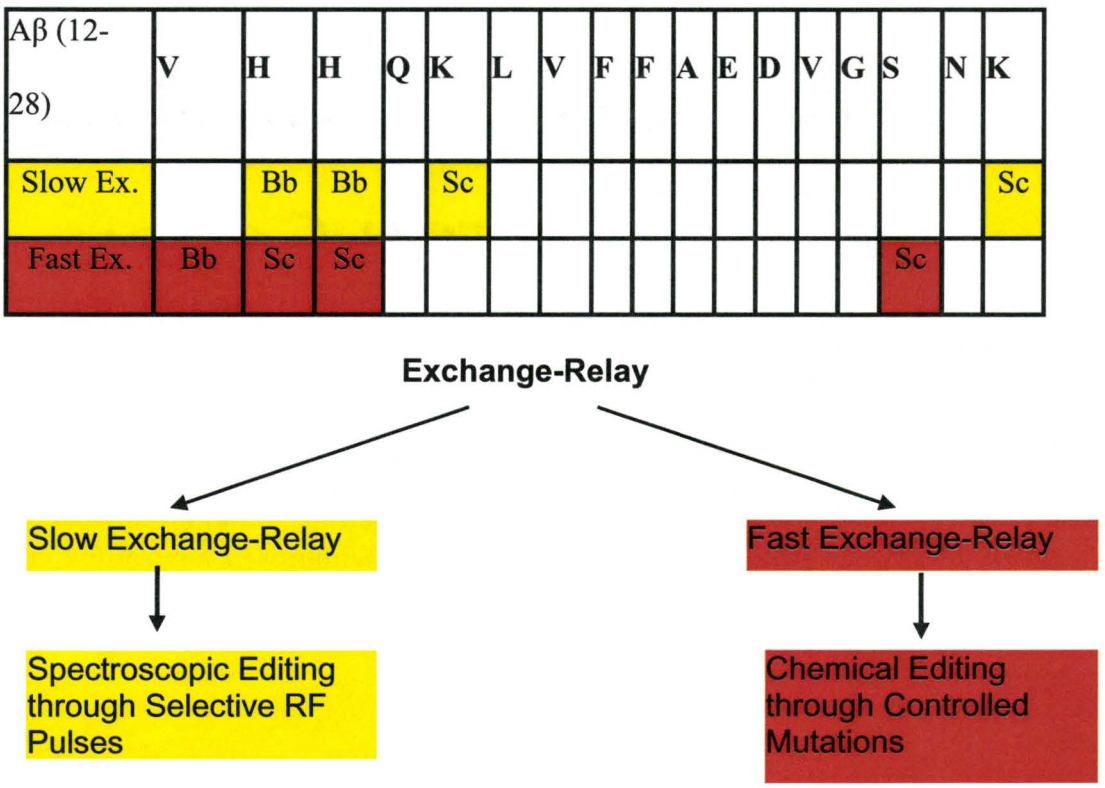

Figure 4.7: Spectroscopic editing and chemical editing strategies for slow and fast chemical exchange protons, respectively. Sc: side chain; Bb: backbone. For slow exchange relay protons, spectroscopic editing is applied; for fast exchange-relay protons, chemical editing (mutation) was applied.

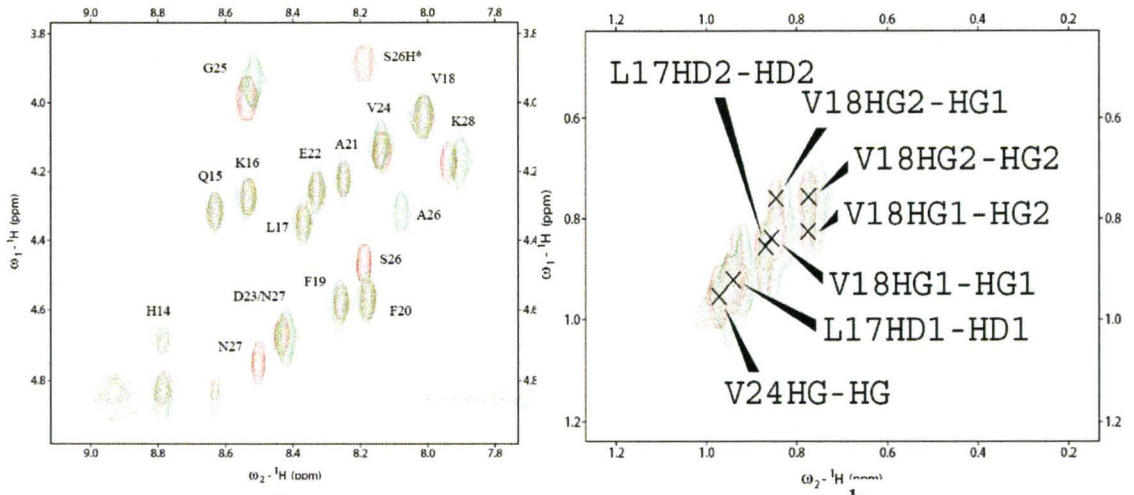

a. b.

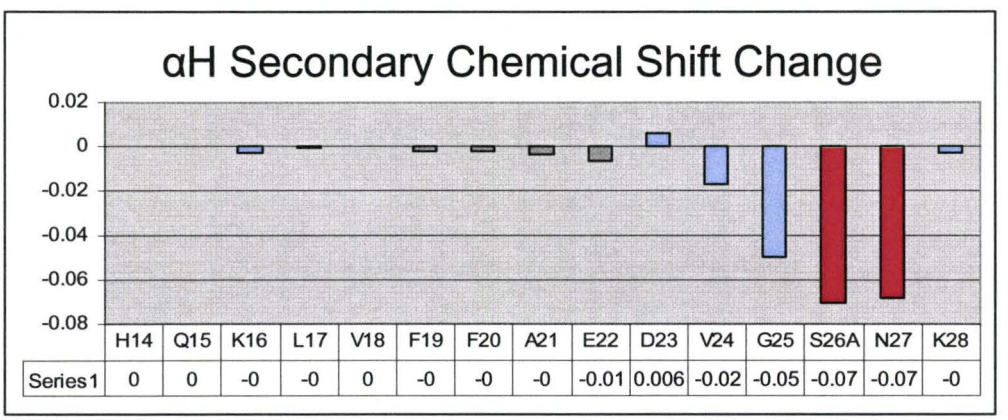

	H14	Q15	K16	L17	V18	F19	F20	A21	E22	D23	V24	G25	S26A	N27	K28
Series1	0	0	-0	-0	0	-0	-0	-0	-0.01	0.006	-0.02	-0.05	-0.07	-0.07	-0

c.

Figure 4.8: TOCSY finger print region overlay (a), CHC (L17-A21) methyl region overlay (b) and αH secondary chemical shift change (c). In (a) and (b), red peaks are WT and green peaks are S26A. The random coil chemical shifts were considered only for the mutated residue.

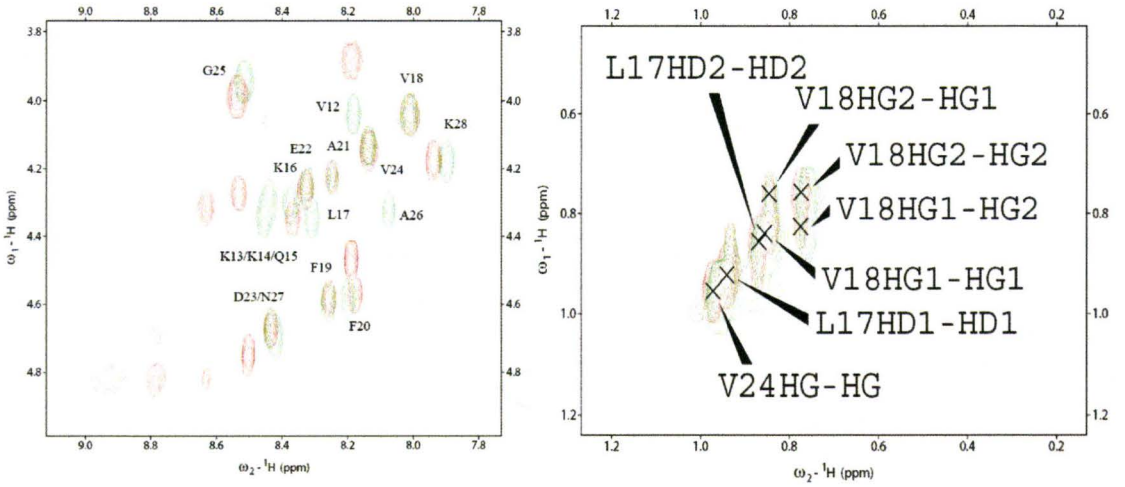

a. b.

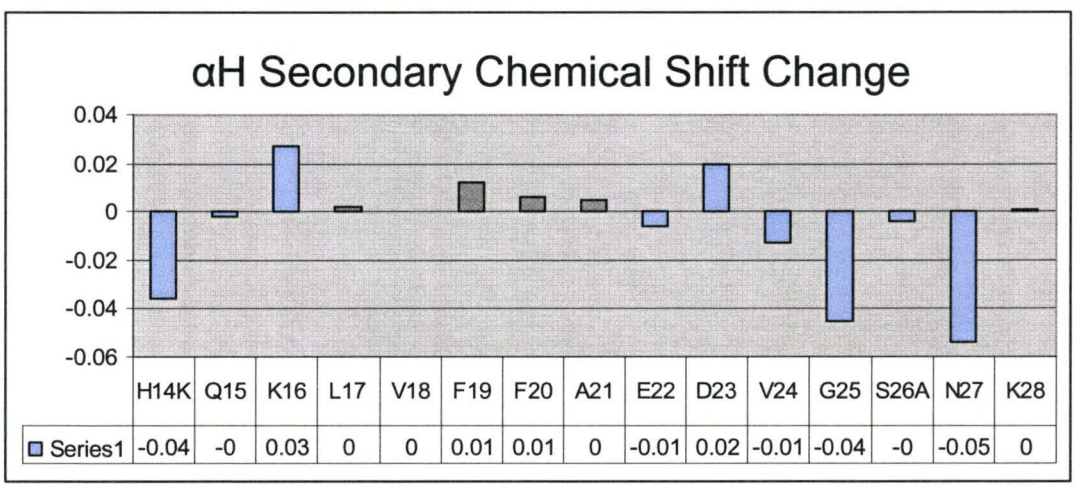

c.

Figure 4.9: TOCSY finger print region overlay (a), CHC (L17-A21) methyl region overlay (b) and αH secondary chemical shift change (c). In (a) and (b), red peaks are WT and green peaks are triple mutant.

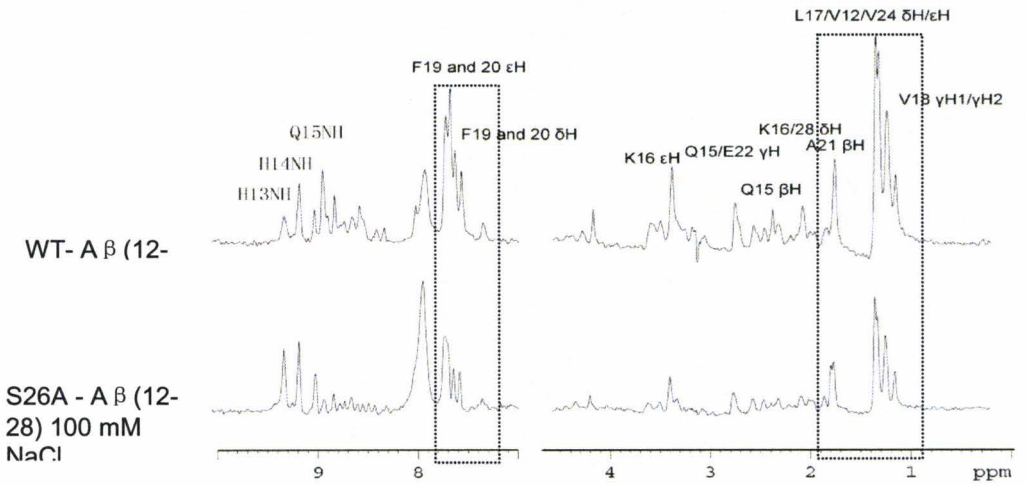

Figure 4.10: Water-Row from EA-NOESY, t_{mix} = 150 ms, 700 MHz, showing the cross relaxation between water and protons in the Aβ (12-28) and mutant S26A. To induce aggregates of S26A, 100mM NaCl has been added.

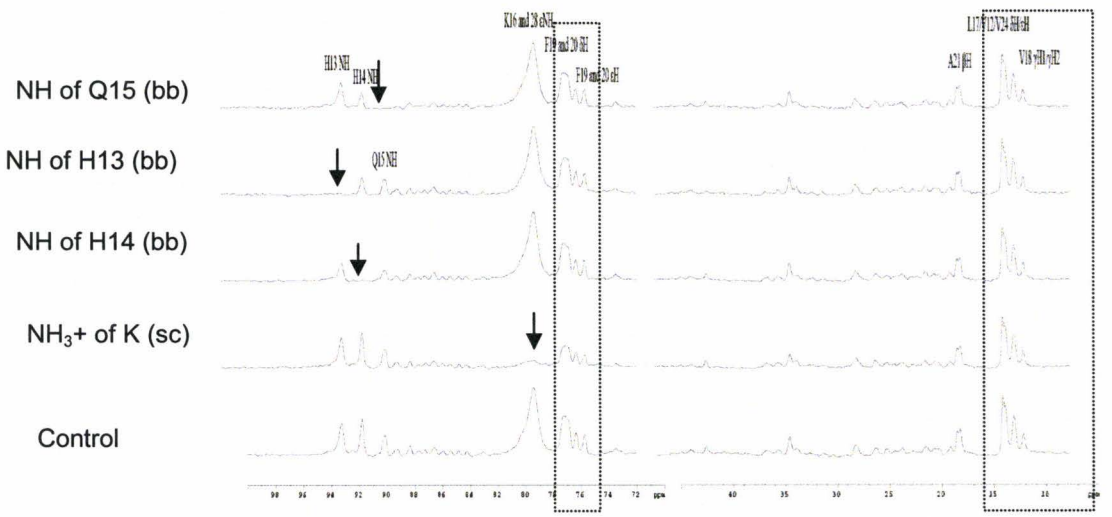

Figure 4.11: Water-Row from EA-NOESY for S26A, tmix = 150 ms, 700 MHz , Continuous wave (CW) is employed to selectively suppress the exchange protons

(NH of H13, H14, Q15 back bone, and NH_3^+ of K side chain), and the exchange relay pathways of corresponding protons are suppressed as well.

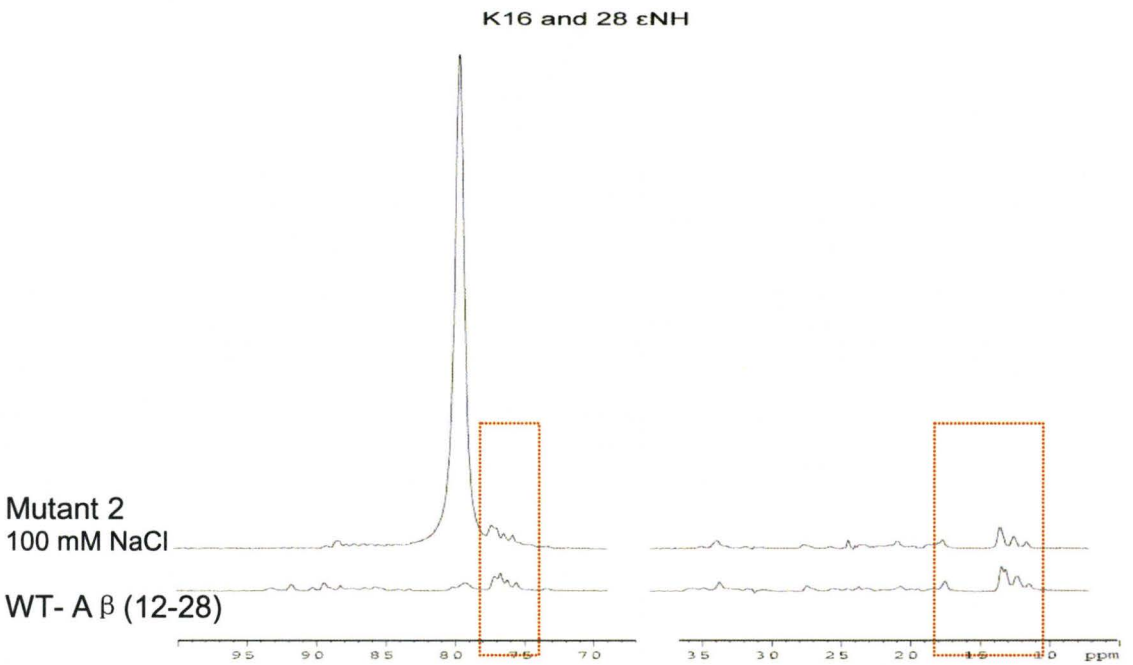

Figure 4.12: Water-Row from EA-NOESY of Mutant 2, tmix = 150 ms, 700 MHz, showing the cross relaxation between water and protons in the Aβ (12-28) and mutant 2. 100 mM NaCl was added into the mutant 2 to induce aggregates.

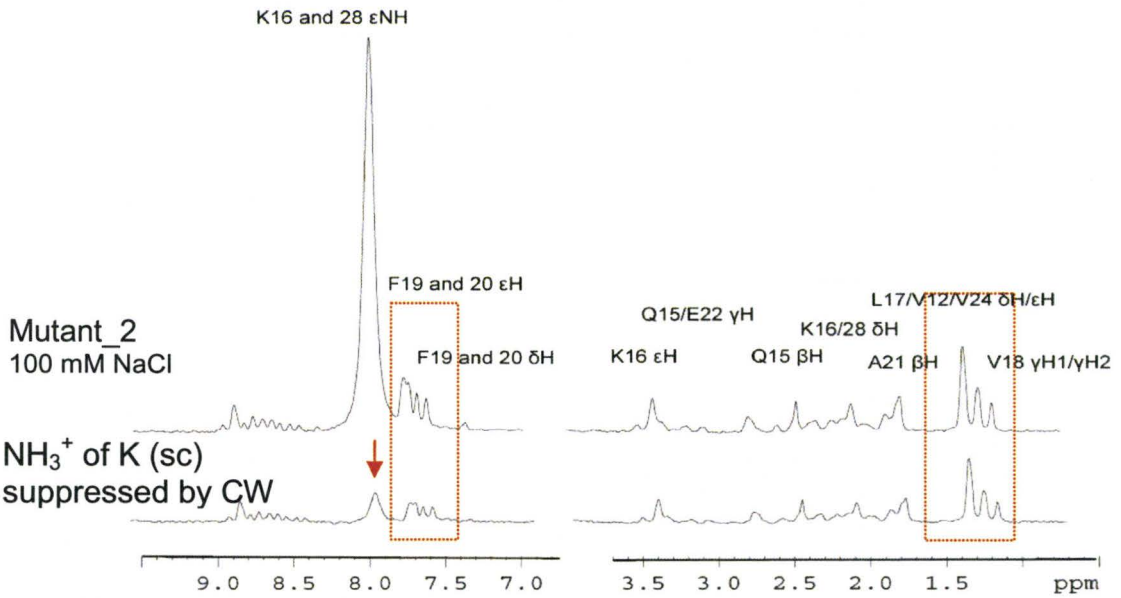

Figure 4.13: Water-Row from EA-NOESY of Mutant 2, tmix = 150 ms. Continuous wave (CW) is employed to selectively suppress the exchange protons (NH_3^+ of K side chain), and the exchange relay pathways of corresponding protons are suppressed as well. 100mM NaCl was added into the Mutant 2 to induce the oligomers of Mutant 2.

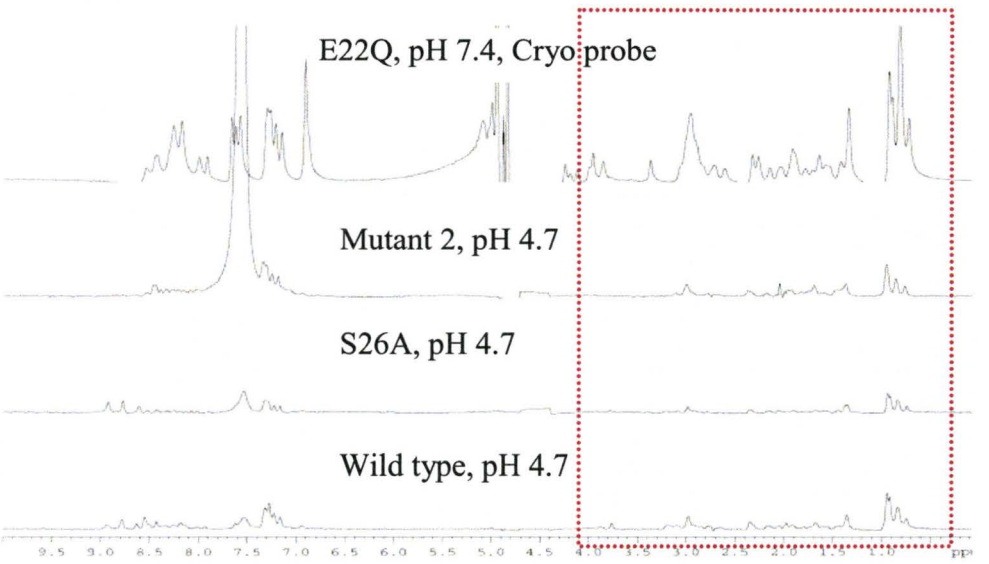

Figure 4.14: The hydration NMR (Echo anti Echo) of wt Aβ sample, Mutant 1, Mutant 2, and Mutant 3. All are at the concentration of 1mM and 50 mM Acetate buffer, except that the Mutant 3 is in the 20 mM Phosphate buffer. 100mM NaCl was employed to Mutant 1 and 2 to induce aggregation. The pH 7.4 was employed to Mutant 3 to induce aggregation as salt was not effective in inducing aggregation. Because of the installation of cryo probe, the Mutant 3 sample was tested with the cryo probe which provided stronger signal.

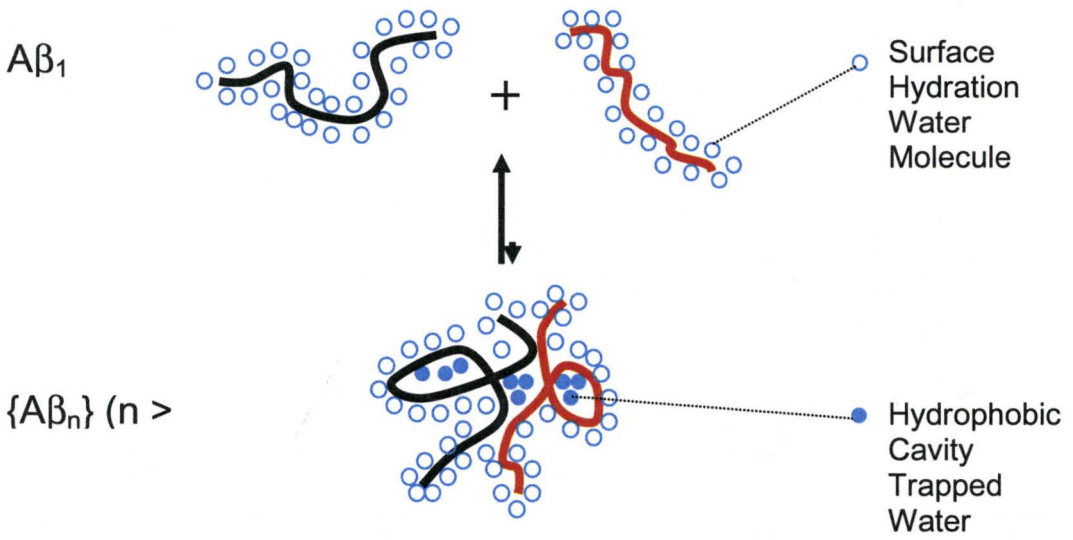

Figure 4.15: Schematic representation of the speculated cavities that trap water molecules

Chapter 5

The Development of the WSTD (Water Saturation Transfer Difference) Experiment

5.1 Introduction

As we have already discussed in the previous chapter (chapter 3), that the established STD methods rely on the oligomer saturation introduced through the monomer. Thus the limitations of monomer contribution, offset effect and partial diffusion seem to be inevitable. A new approach needs to be developed to overcome the above limitations.

Based on the STD NMR experiment and amyloid peptide hydration results discussed in the previous chapters, we developed the Water Saturation Transfer Difference NMR (WSTD) method to saturate the sample peptide via the H/H exchange and possibly hydration water molecules. In this experiment, the water spin polarization is selectively perturbed through the constructive use of radiation damping. The perturbed polarization of water spins is transferred to the peptide spins through chemical (*i.e.* H/H) exchange and/or potential tightly bound water molecules and then it is propagated to the rest of the oligomers via spin diffusion. In other words, magnetization is "injected" into the monomers at multiple sites (*e.g.* polar side chains of amino acids such as Ser, Lys, His) thus ensuring a more complete diffusion throughout the oligomers than obtained through classical

methyl or aromatic STD experiments. In addition, as the magnetization is introduced through water, offset-effects and monomer contributions are greatly minimized.

5.2 Materials and Methods

The 1-D WSTD NMR pulse sequences used are shown in Figure 5.1 where the pulse sequence cluster of WATERGATE is required for the effective water suppression through a binomial 3-9-19 pulse sandwich, resulting in inversion of all signals except that of H_2O set at the carrier frequency. Radiation damping is triggered by an initial 170° pulse. Bipolar gradients were employed to control radiation damping and therefore the selective water inversion without causing excessive lock perturbation thus ensuring the stability of the spectrometer. The length of each bipolar gradient segment (Figure 5.1) was experimentally optimized at 12.5ms (total length of a bipolar gradient = 25 ms), and the strength of these gradients is reduced to zero in alternate scans. The total saturation time is adjusted by the number of bipolar gradients. Twenty bipolar gradients were used in both 1-D and 2D WSTD experiments, leading to a total saturation time of 0.5 s. The subtraction between spectra with and without water inversion is performed after every scan via phase cycling. In this WSTD experiment, the repetition delay d1 is 2 s. Thus the reference spectrum is simply a regular 1-D WATERGATE spectrum with d1 = 2s. All spectra were acquired using a 700 MHz Avance spectrometer equipped with a TCI cryoprobe.

We validated the WSTD method using as model system the previously well-characterized Aβ (12-28) peptide with the sequence $VHHQ_{15}KLVFF_{20}AEDVG_{25}SNK_{28}$, which is a fragment of the full length Aβ(1-40) or Aβ(1-42) linked to Alzheimer's disease. The Aβ(12-28) peptide has been proposed to be a valuable model for the early oligomerization steps that lead to fibrillization.

5.3 Results and Discussion

5.3.1 Coupling Between the Efficiency of the Water-to-Peptide Magnetization Transfer and Peptide Self-Recognition

As we have demonstrated in the hydration chapter, the filtration with 30 kDa filter can help us approach the 'non-aggregated state' of Aβ peptide and the hydration is related to the oligomerization of Aβ peptide. The comparison of WSTD of the filtered sample (after 30 kDa cut-off filtration, 1mM Aβ (12-28), 50 mM d_3-acetate buffer, pH 4.7, 293 K) and unfiltered sample (1mM Aβ (12-28), 50 mM d_3-acetate buffer, pH 4.7, 293 K) is shown in Figure 5.2. The WSTD intensity for the unfiltered sample is significantly lower than that of the unfiltered sample for the aliphatic (~4.6 – 0.0 ppm) and the aromatic (7.2-6.6 ppm) regions. However for some of the NH protons (8.9-8.3 ppm), the filtered sample has almost the same WSTD intensity as the unfiltered sample and the filtered sample displays even higher intensity for the protons (7.5-7.2 ppm) of the NH_2 side chain of Q15 and N27 than the unfiltered sample. These NH protons (8.9-8.3 ppm)

correspond to the amide protons of H13, H14 and Q15 which are known to be in fast exchange with water in the NOE mixing time scale. Since filtration does not perturb the H/H exchange between water and the monomeric peptide the WSTD intensity for these amide protons is not expected to change upon filtration. The small negative peaks at 3 ~ 0 ppm in the spectrum for filtered sample arise from aliphatic protons. Since the aliphatic protons do not exchange with the water, possible mechanisms accounting for these negative peaks are exchange relay through flexible polar side chains and/or direct NOEs with short (< 1 ns) lived surface water molecules (please refer to the hydration chapter). An alternative explanation of the negative peaks observed for the filtered sample is based on difference artifacts caused by incoherent transfer of magnetization from water to peptide protons occurring during the radiation damping induced selective inversion of water. In order to test the presence of these possible difference artifacts, we are now in the process of testing modified WSTD pulse sequences in which water is selectively inverted before rather than during the mixing period.

5.3.2 Data analysis of WSTD data

An unfiltered Aβ (12-28) sample (1mM in 50 mM d_3-acetate buffer, pH 4.7 and 10% D_2O) was used for a 2D WSTD-TOCSY experiment. The integration of cross peaks from the 2D WSTD-TOCSY and 2D-TOCSY spectra was employed to map self-recognition at residue resolution, with the exception of H13 for which the Hα-NH cross is usually weakened by the H/H exchange with

water. The 2D-WSTD-TOCSY spectrum (Figure 5.3) shows that H14 and Q15 have strong exchange peaks on the row of water resonance, indicating that the H/H exchange are contributing to the intensities of the cross peaks of H14 and Q15 in the fingerprint region. Thus we need to calibrate the NH-CαH cross peaks of H14 and Q15. The intensities of H14 and Q15 NH-CαH cross peaks are scaled down by the ratio of intensities of hydration peaks/cross peaks. Also, we used the standard deviation of the intensities of peaks of the whole spectrum provided by the 'dpp' routing of the software XWINNMR as the error of the measured intensities. The error of the measured I_{sat}/I_{unsat} was analyzed according to the method reported by Kay [1].

Figure 5.4 (a) shows the 2D WSTD H/H-exchange corrected ratios for an unfiltered Aβ (12-28) sample (1mM, acetate buffer 50mM, pH 4.7 and 10% D2O), indicating that self-recognition by the L17-V24 fragment is detected through the WSTD experiment. Compared to the result from the methyl 2D STD (b), E22 and D23 are added to the interacting residue list, which can be easily understood because the E22 and D23 have acidic COOH groups exchanging with water. Furthermore, these results are fully consistent with the key role played by the two acidic residues E22 and D23 in the oligomer formation. The D23 has been shown to form a salt bridge with K28 by solid state NMR [2] and molecular dynamic simulation [3]. The role of E22 has been extensively investigated by mutations (*e.g.* E22G, E22Q, E22A, E22D) [4, 5] indicating that E22 affects not only the rate of protofibril formation in both the full length and 12-28 Aβ peptides, but

also the pathogenicity for the human cerebrovascular smooth muscle cells (HCHWA) [5]. The E22 mutants are also found to be related to naturally occurring familial forms of Alzheimer's disease (Figure 5.6) [4]. We therefore conclude that not only the hydrophobic effect is the driving force in the oligomer formation, but also the electrostatic interactions (*e.g.* the salt bridge) have undoubted significance in both the molecular stability and the pathogenic properties of the soluble oligomers.

The ability to reveal spectroscopically the role played by E22 and D23 in self-recognition is a unique feature of the WSTD methods. The methyl 2D STD experiment (Figure 5.4, b) detects self-recognition epitopes only for mostly hydrophobic segment K16, L17, V18, F19, F20, A21 and for V24, while the aromatic 2D STD (Figure 5.4, c) detects self-recognition epitopes only for L17, V18, F19, F20 and A21. We can understand that the residues with methyl groups will definitely have a strong signal in the methyl 2D STD, reflecting the location of the site of saturation injection. Thus, the useful information we can learn from it is that F19 and F20 are the two residues involved in self recognition. Similarly, we learned from the aromatic 2D STD that L17, V18, and A21 are important in the oligomer formation. With both methyl and aromatic STD, the so called central hydrophobic core (L17, V18, F19, F20 and A21) is proved to be important in the aggregation of Amyloid beta peptide, which is consistent with previously reported results [6]. However the methyl and aromatic STD experiments underestimate the importance of the hydrophilic residues such as E22 and D23. This apparent

limitation of the traditional STD experiments may provide a potential route to dissect the hydrophobic and polar contributions to self-recognition through the comparison of the WSTD ratios with the average of the methyl and aromatic STD ratios (Figure 5.5). However, such comparison may contain artifacts caused by different H/H exchange rates for different polar/charged residues and/or HN groups (*i.e.* H14 and Q15).

5.4 Conclusions

The WSTD method provides new opportunities to overcome the limitations caused by offset effect, partial spin diffusion and monomer contributions observed for the methyl and aromatic STD experiments. In addition, the WSTD maps self-recognition not only for hydrophobic but also for hydrophilic residues that are often missed in the self-association maps obtained by other STD approaches. For instance, the WSTD reveals that the E22 and D23 are important in the self-recognition of the Aβ peptide, indicating that both hydrophobic and electrostatic interactions are important in oligomer formation and stabilization. These results are fully consistent with the urea denaturation data (Chapter 6) showing a global and concerted disassociation that involves both hydrophobic and hydrophilic residues.

Reference

1. N.A. Farrow, R. Muhandiram, A.U. Singer, S.M. Pascal, C.M. Kay, G. Gish, S.E. Shoelson, T. Pawson, J.D. Forman-Kay and L.E. Kay, Biochemistry 33 (1994) 5984-6003
2. A.T. Petkova, Y. Ishii, J.J. Balbach, O.N. Antzutkin, R.D. Leapman, F. Delaglio, R. Tycko, Proc. Natl. Acad. Sci. 99 (2002): 16742-16747
3. B. Ma and R. Nussinov, Proc. Natl. Acad. Sci. 99 (2002): 14126-14131
4. A. Päiviö, J. Jarvet, A. Gräslund, L. Lannfelt and A. Westlind-Danielsson, J. Mol. Biol., 339 (2004) 145-159
5. J.P. Melchor, L.McVoy, and W.E. Van Nostrand, J. Neurochem., 75 (2000) 2209-2212
6. J. Jarvet, P. Damberg, K. Bodell, L.E. Göran Eriksson and Astrid Gräslund, J. Am. Chem. Soc., 122 (2000) 4261-4268

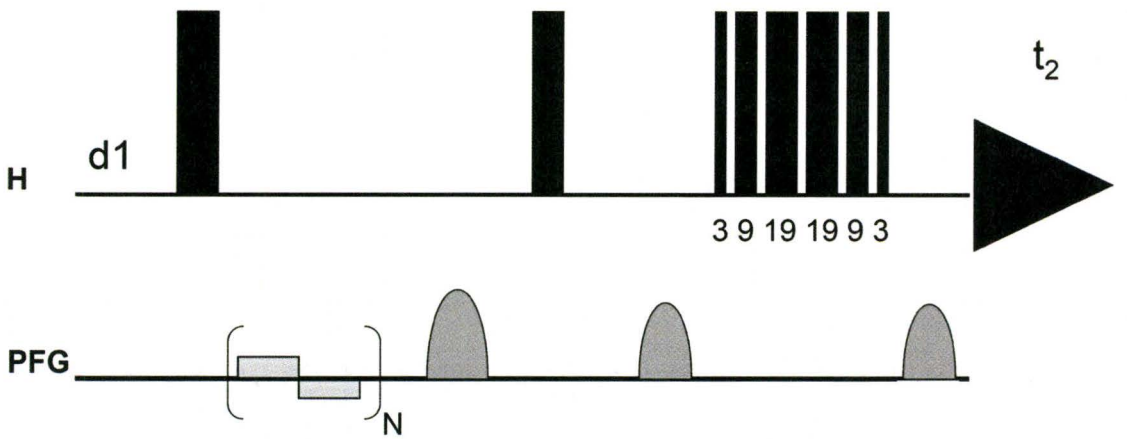

Figure 5.1: 1-D WSTD-NMR pulse sequence.

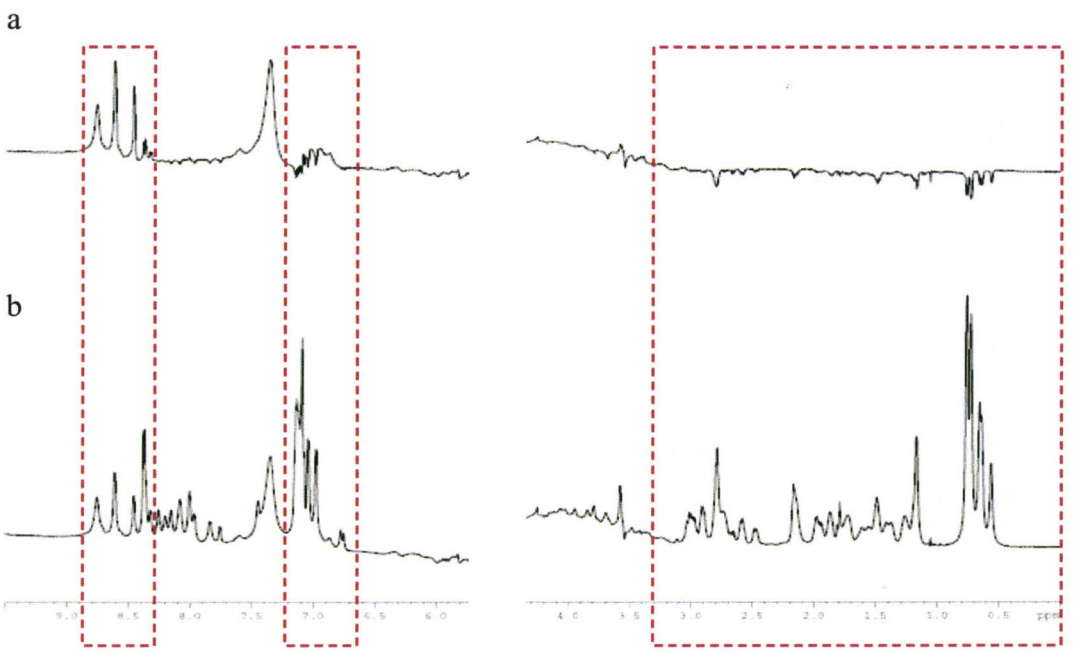

Figure 5.2: 1-D WSTD-NMR spectra of 1mM Aβ (12-28), 50 mM d_3-Acetate Buffer, pH 4.7, 293 K: (a) filtered sample (30 kDa cut-off); (b) unfiltered sample.

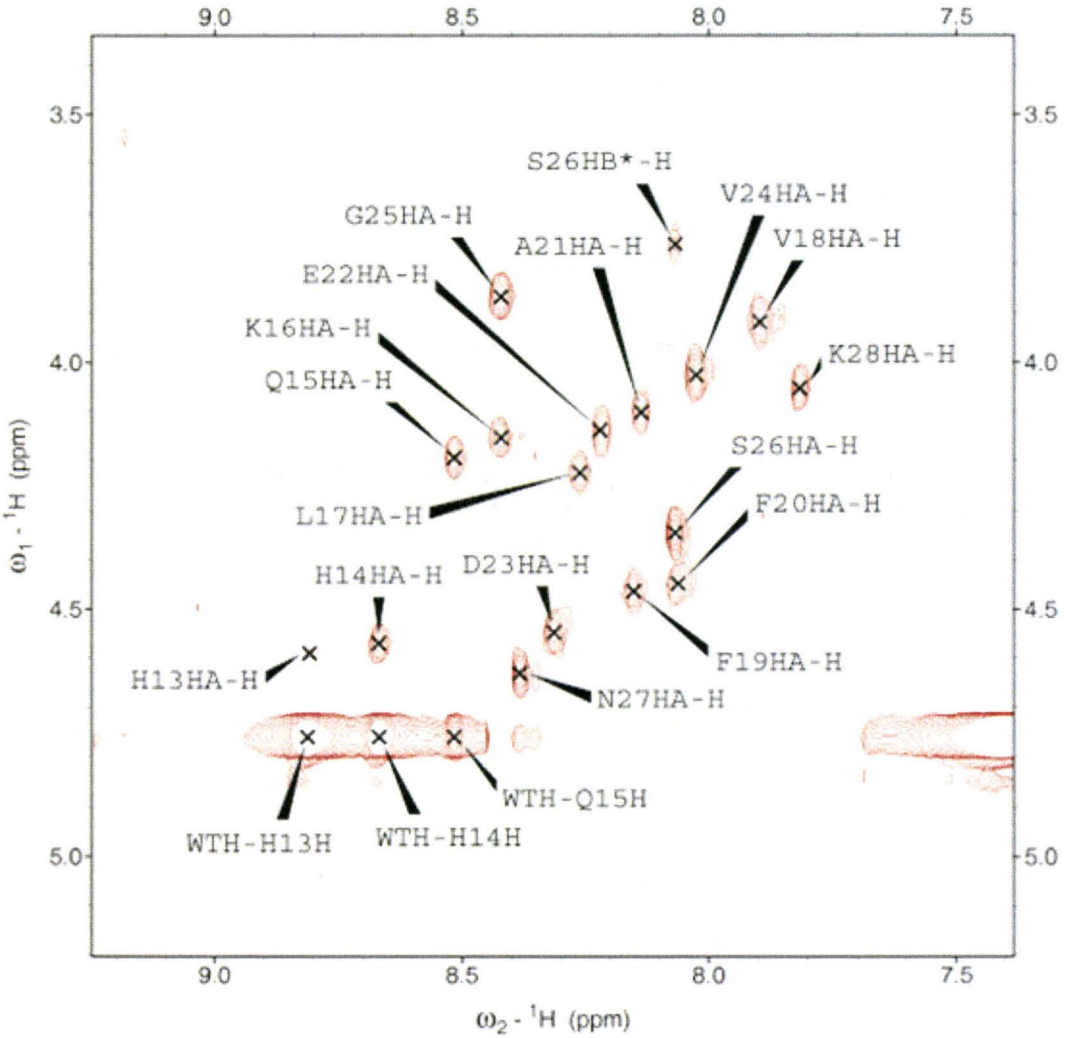

Figure 5.3: 2-D WSTD-TOCSY NMR spectrum of the Hα-NH region of 1mM Aβ (12-28), 50 mM d_3-Acetate Buffer, pH 4.7, 293 K. WTH-H13H denotes the cross peak between the water protons and amide proton (NH) of H13; H13HA-H denotes the cross peak between the Hα and amide proton (NH) of H13; S26HB*-H denotes the cross peak between the side chain Hβ protons and the amide proton (NH) of S26; and so on.

(a)

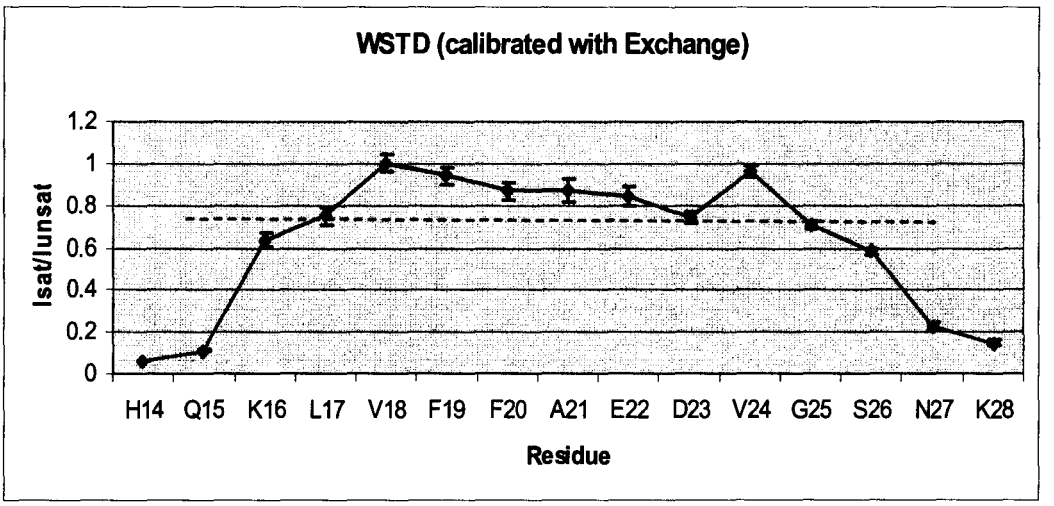
WSTD (calibrated with Exchange)
Isat/Iunsat
1.2
1
0.8
0.6
0.4
0.2
0
H14 Q15 K16 L17 V18 F19 F20 A21 E22 D23 V24 G25 S26 N27 K28
Residue

(b)

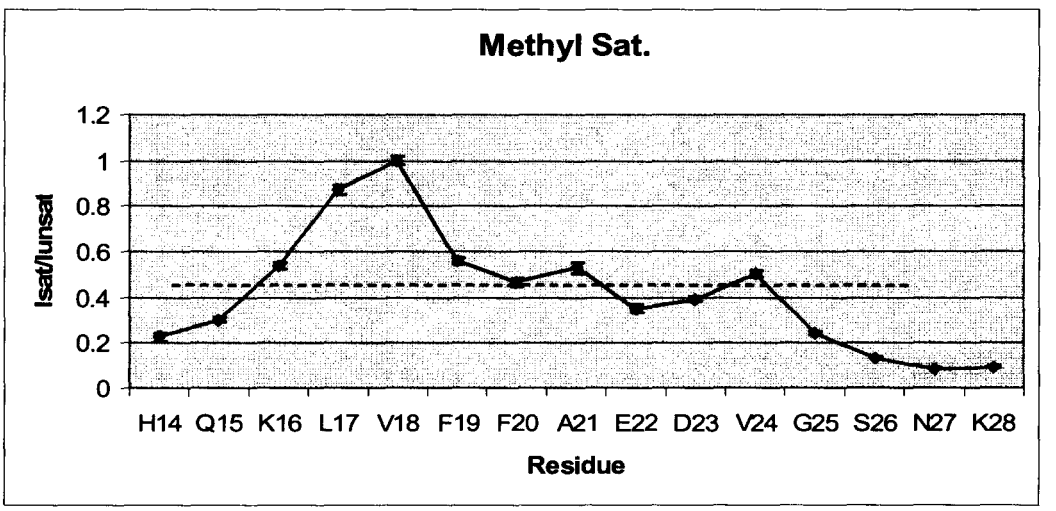
Methyl Sat.
Isat/Iunsat
1.2
1
0.8
0.6
0.4
0.2
0
H14 Q15 K16 L17 V18 F19 F20 A21 E22 D23 V24 G25 S26 N27 K28
Residue

(c)

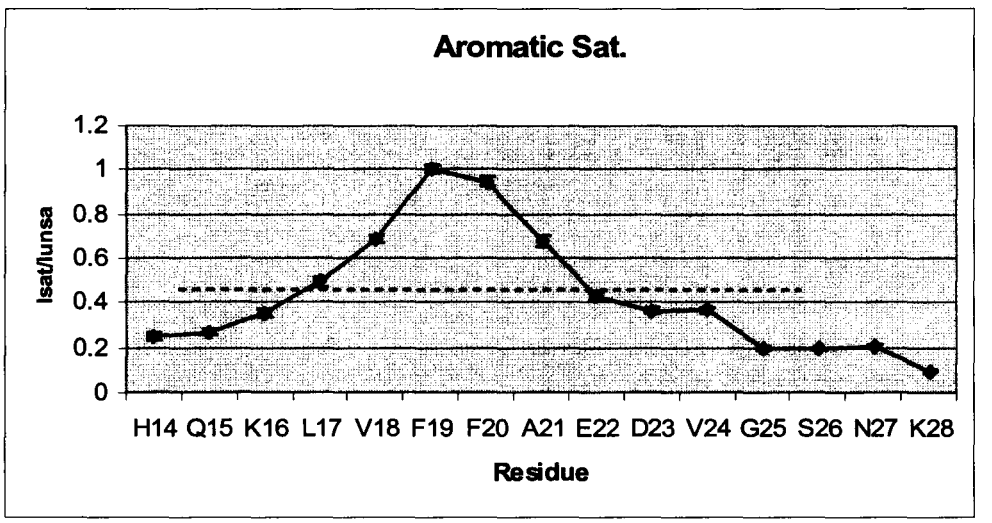

Fig. 5.4: 2D STD-TOCSY of sample "JM13" (Amyloid beta peptide 1mM, acetate buffer 50mM, pH 4.7 and 10% D2O) with water selective inversion (a), with methyl selective saturation (~0..57 ppm) (b) and with aromatic selective saturation (~7.1 ppm) (c) The dashed red line represents the peptide average value of the I_{sat}/I_{unsat} ratios. Because WSTD and the other two STD methods rely on different mechanisms, the average lines are at different values in (a), (b) and (c). The STD ratios were normalized to the highest value in each figure, which correspond to the values of V18 in (a) and (b) and F19 in (c). Vertical bars indicate the error of the measured I_{sat}/I_{unsa} ratios.

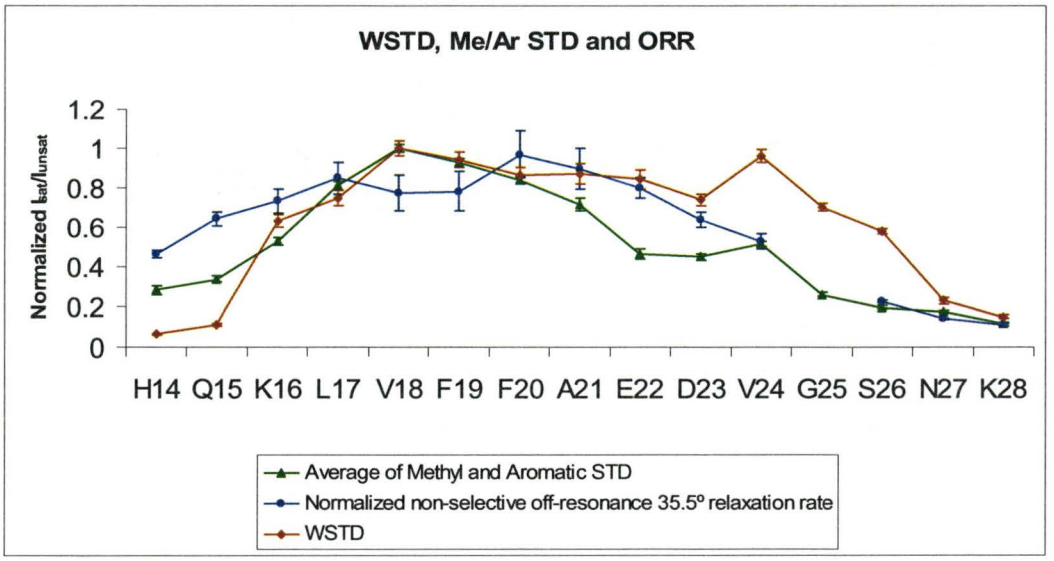

Figure 5.5: comparison of 2D WSTD, average of methyl/aromatic STD and Off-resonance relaxation rates for the sample 'JM13' (Amyloid beta peptide 1mM, acetate buffer 50mM, pH 4.7 and 10% D2O). The green curve is the normalized I_{sat}/I_{unsat} of the average of methyl and aromatic STDs,; the brown curve is the normalized I_{sat}/I_{unsat} of WSTD; the blue curve corresponds to the normalized non-selective 35.5° relaxation rates. The non-selective 35.5° relaxation rate for G25 is missing due to the additional Hα proton in glycines.

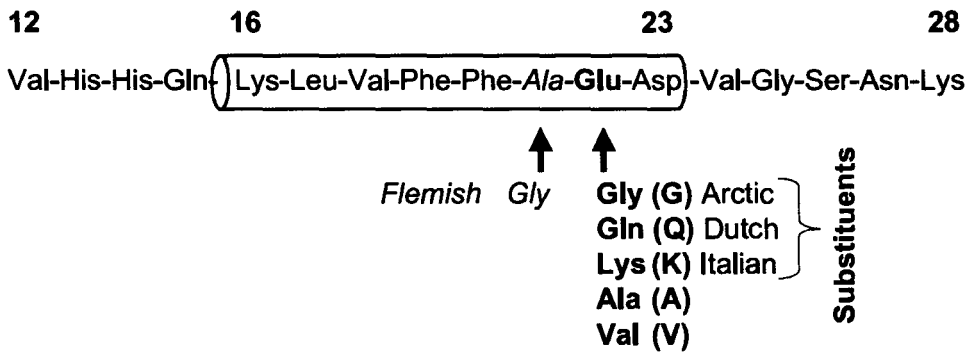

Figure 5.6: Amino acid sequence for Aβ (12–28) and important position 21 and 22 substitutions. The Aβ peptide position 21 and 22 substitutions are illustrated in the primary sequence 12–28 fragment and, where appropriate, with their relevant clinical designations. An α-helix is predicted and indicated with a schematic cylinder drawn between amino acid residues 16 and 23. [4]

Chapter 6

Urea Induced Aβ (12-28) Oligomer Unfolding Monitored by STD and ORR

6.1 Introduction

The Aβ (12-28) monomer has the capability to form oligomers, as demonstrated in the previous chapters by NMR. The structure and conformational features of full length Aβ or its fragments have also been extensively investigated by other methods, including electron microscopy [1], mass spectrometry [2], and CD [3]. However, the mechanism of this oligomerization is still not fully clear. In order to gain further insight into the molecular pathways that lead to self-association, we attempted to extended to the Aβ oligomers approaches traditionally used to investigating folding and unfolding for globular proteins [4]. For instance, oligomer unfolding can be induced by employing extremes of pH or temperature, by adding chemical denaturants or by engineering mutations in the primary sequence.

The destabilization of Aβ (16-22) oligomers induced by urea has been modeled through molecular dynamics simulations [5]. In this simulation, the urea induced β-structure and exclusion of water from the oligomer interior are reported. The major interaction between urea and the Aβ monomer is recognized as

electrostatic or polar in nature and they include the hydrogen bonds between urea and the peptide backbone. The urea-induced change in hydrophobic interactions involves the coating of the hydrophobic side chains and increases the solvent exposure of oligomers. However hydrophobic effects are considered to play only the secondary role in the destabilization of the Aβ (16-22) oligomers by urea [5]. CD and AFM have also been used to study the effect of urea on Aβ fibril [6]. The CD experiments revealed a continuous increase in the content of unstructured polypeptide chains with increasing urea concentration. Based on these previous experiments, urea is anticipated to significantly affect the stability of the Aβ (12-28) oligomers, however no high resolution experimental investigation of the effect of urea has been reported so far.

6.2 Material and Methods

Sample preparation for the urea denaturation experiments: The urea titration samples were prepared according to the following scheme. First, a 1.1 mM Aβ (12-28) solution in 50 mM d_3-acetate buffer, pH 4.7 and 10% D_2O was prepared; and then split it into two aliquots of 550 μL and 700 μL. Then 152 mg of urea (Fluka, molecular biology grade) were added into the 700μL aliquot resulting in a total mass of the solution of 847 mg. The volume of this solution is unknown since the addition of urea changed the volume. Therefore a 500 μL aliquot was taken out from this urea/peptide solution to measure its density: 1.04 mg/μL is obtained. Thus the volume of urea/peptide solution (847mg) is 847/1.04

= 814.4 μL, that is, the volume increase by 114.4 μL after adding urea, diluting the Aβ peptide from 1.1 mM to 0.9 mM. The other aliquot of the peptide solution (550 μL) is diluted by the same ratio with d_3-acetate buffer resulting in 638 μL of a 0.9 mM peptide solution. In this way, the two stock solutions have the same peptide concentration (0.9mM) and while one (solution B) contains 3M urea, the other is devoid of urea as illustrated in Figure 6.1.

With the above mentioned stock solutions A & B, urea samples were prepared by mixing A and B in different ratios (Figure 6.2). For example, the 0.4 M urea solution is the mixture of 500 μL A and 77μL B, the 0.7 M urea sample is the mixture of 500μL of the 0.4 μL urea and 65 μL B, and so on.

All spectra were acquired at 700 MHz employing a TCI cryprobe (Bruker). The 1-D WATERGATE-like (Figure 6.3) and 2-D Off-resonance relaxation [Figure 6.4] (with reburp2K for urea and water saturation) NMR experiments were employed in this study. In all of these experiments the strong urea ^1H signal limits the dynamic range and therefore was suppressed using band-selective RE-BURP double gradient spin-echos [7]. This excitation sculpting pulse sequence effective suppresses the intense urea signal at ~5.8 ppm but it also suppressed aliphatic signals above ~3.5 ppm (Figure 6.5). This limitation is effectively overcome by employing two 2D TOCSY detection blocks in which the Hα-HN fingerprint region is recorded by acquiring the amide proton signal. The methyl saturation STD is used to measure the I_{sat}/I_{unsat} ratio to get the information of the residues involving in the Aβ self recognition. The spectra are processed with

SPARKY and the integrated fit height is used to calculate the intensities of on-resonance saturation spectra (I_{sat}) and off-resonance spectra (I_{unsat}). As the methyl resonance frequencies are changing with addition of urea because urea affects the resonance frequency of water and therefore of the lock system, the saturation frequency is changing as well to make sure that the actual saturation is always at the methyl group of V18. For instance, at 0M urea, it is 401Hz, while it is 419.5Hz for at 1.6M urea. The shift of the water resonance to high field upon urea addition is appreciated by inspecting Figure 6.8. This is either a sample heating effect or a direct effect of urea (chemical exchange with water).

The OR-Relaxation experiments were acquired as previously described [8] but the relaxation period were limited to only two durations (13 ms and 88 ms, including 4 ms + 4 ms for the initial and final adiabatic ramps) thanks to the S/N gain resulting from the 700 MHz cryoprobe.

6.3 Urea Titration Results and Discussion

Effect of Urea on the Monomers: The effect of urea on the monomers can be effectively monitored by chemical shift variations. Therefore the chemical shifts of both Hα and NH spins have been measured by 2D-TOCSY experiments using a small molecule unaffected by urea as the ppm standard. In this study, the TSP (Sodium 3-(trimethylsilyl) propionate-2,2,3,3-d_4) was initially used as the chemical shift standard. However, the TSP can actually bind to Aβ oligomer [9] In Figure 6.6, the line width of TSP is getting sharper with the addition, which

suggests that the binding really exists when the urea concentration is low. Thanks to another unknown impurity in the peptide solution, the chemical shift analysis can still be conducted. The small sharp peak at 1.06 ppm was used to as chemical shift standard in the experiment without adding TSP, because the samples with TSP show that this small molecule has constant chemical shift unaffected by urea (Figure 6.6). No significant change was observed for the Hα protons ppm values (Figures 6.7 (a) and 6.8), while for the backbone NH of selected residues change significantly (Figures 6.7 (b) and 6.8). The absence of significant Hα chemical shift changes suggests that the conformational ensemble of the Aβ (12-28) monomers is unaffected by urea, consistent with its flexibility and lack of structure even at 0 M urea. The detected NH chemical changes are consistent with previously proposed interactions of urea with the peptide backbone [5]. Interestingly, the HN ppm changes induced by urea involve only non-polar amino acids (L17, V18, F20, V24 and G25) suggesting that the effect of urea on hydrophobic amino acids may be more significant than previously anticipated.

Effect of Urea on the Oligomers monitored by 1D Spectra: The ability of urea to dissociate the peptide oligomers is confirmed by the peptide peaks in 1-D spectra which become sharper and more intense at higher concentrations of urea (Figure 6.9). For example the peptide signal for the sample at 2.3M urea is about 3 times more intense than that for the sample at 0 M urea in which the peptide forms soluble oligomers (Figure 6.9). As a control to verify that urea is the main cause of the observed dramatic increase in signal intensity we compared the

spectra acquired at 0.1 mM peptide without urea with those acquired at 0.9 mM peptide with 2.3M urea. The latter has almost 8 times of the intensity of the former confirming that the peptide concentrations are in the expected range (Figure 6.10). This spectral comparison is also consistent with both samples (the sample with 0.1 mM Aβ (12-28) without urea and the sample with 1mM Aβ (12-28) with 2.3M urea) being devoid of aggregates. This conclusion was further supported by preliminary experiments showing that there is no significant difference in the 1-D spectra between 2.3 M and 5 M urea. The urea titration monitored by more advanced and more time consuming NMR experiments (2D-STD and 2D-OR-R, *vide infra*) will therefore focus on the 0 M – 2.3 M urea concentration range.

Effect of Urea on the Oligomers monitored by 2D OR-R Spectroscopy: Off-resonance relaxation experiments were also used here to map self-recognition at residue resolution and at different urea concentrations (Figure 6.11). The Aβ peptide in the 0 M urea sample has significant higher relaxation rates than at 1.3M and 1.6M urea, while the 1.3M and 1.6M urea samples have almost the same relaxation rates. This is because that the Aβ peptides in the 0 M urea sample are characterized by higher oligomer populations and these oligomers tumble slowly, thus relaxing faster. When the urea breaks the oligomers, the remaining monomer will tumble fast in solution, thus relax slowly. The central hydrophobic core (CHC) residues have higher relaxation rates because they are more directly involved in self-recognition than the flanking residues. Once the oligomers are

completely dissociated by urea, further addition of urea should not significantly change the relaxation rates explaining why the relaxation rates at 1.3 M and 1.6 M urea are not significantly different. However, our experiments also show that the OR-relaxation rates of the Aβ (12-28) peptide at 2.3M urea are higher than those at 1.6M (Figure 6.10). This observation is consistent with the formation of peptide-urea clusters stabilized by high urea concentrations through intermolecular hydrogen bond between urea and peptide. These clusters have been recently predicted [5] and their large size and possible slower tumbling as compared to fully hydrated peptides may account for the increase in OR-relaxation rates detected after 1.6 M urea (Figure 6.11). The interactions of urea with the monomeric peptide are also consistent with the HN ppm variation observed in Figure 6.7, however it should also be considered that urea is known to increase the viscosity of aqueous solutions [10] and therefore the correlation time for the effective tumbling of the peptide in solution. An alternative explanation of the OR-R rate increase after 1.6 M urea is therefore also possible simply in terms of urea-enhanced viscosity. The viscosity and specific interactions effects at high urea concentrations may be accounted for more quantitatively in future studies using small reporter molecules or extrapolating the OR-R dependence on urea concentrations above ~1.6 M when essentially only monomers are present in solution. The analysis shows that most of the residues show expected behavior if the last three points (1.6M, 1.9M, 2.3M) are used to get extrapolating simulation and then correct the OR rate with the urea titration (Figure 6.13). The H14 is

exchanging with water, thus it is excluded for this analysis. Some other residues have negative relaxation rates (L17, A21), which could be understood as the relaxation rate is 0 with negative error (Figure 6.13).

Overall the OR-R data show that ~1 M urea is already sufficient to disrupt the soluble oligomer of Aβ 12-28, and this denaturing urea concentration is significantly lower than those typically required to fully unfold a stable globular proteins indicating that the Aβ (12-28) oligomers are stabilized by relatively weak interactions. Despite the weakness of the interactions underlying self-association for the Aβ (12-28) peptide, all detected residues (14-28) undergo a similar transition between 0.7 M and 1.0 M urea suggesting a cooperative self-recognition process that involves not only the hydrophobic residues of the CHC but extends also to the charged and polar residues that flank the CHC. This conclusion is consistent with previous mutational analyses showing that non-CHC mutations also significantly affected self-association [5].

Effect of Urea on the Oligomers monitored by 2D STD Spectroscopy: The urea induced dissociation of the Aβ (12-28) oligomers was also monitored at residue resolution by 2D-STD-TOCSY experiments with methyl saturation (Figure 6.12). As expected, the 0 M urea sample is characterized by higher I_{sat}/I_{unsat} ratios than the 1.6 M urea sample for most residues in Aβ (12-28) reflecting a higher oligomer population. However, for some residues (*i.e.* V18, D23 and V24) the STD ratios do not appear to change significantly between 0 M and 1.6 M urea (Figure 6.12). This unexpected result may by an artifact caused

by intra-molecular monomer cross-relaxation which is expected to be emphasized in the more viscous 1.6 M urea solution.

6.4 Secondary Structure Analysis by NOE and ROE

Since the sequence specific assignments has been established, the secondary structure preferences of 1mM Aβ at pH 4.7 and 293K were analyzed based on the inter-residue sequential and medium range NOE patterns (Figure 6.14, 6.16). The observed sequential Hα-HN NOEs as well as the medium range NOEs (Figure 6.14, 6.16) are consistent with the presence of partially helical structures in the conformational ensemble accessible to the unfiltered Aβ (12-28) peptide under the solution conditions used. Specifically, the observed Hα–HN (i,i+2) are indicative of 3_{10} helices [13], however the NOEs measured for the unfiltered peptide sample may in principle arise either from the monomer or from the oligomers because polypeptide chains exchange between the monomeric and oligomeric states within the NOE mixing time scale [14,15] resulting in transfer of cross-relaxation (transfer NOEs) from the oligomers to the monomers. In order to separate the NOE contributions arising from the monomers from those originating from the oligomers, the NOESY experiments was repeated after 30 kDa filtration. Interestingly, after 30 kDa filtration all the medium range NOEs disappear and only the sequential NOEs are preserved (Figure 6.15, 6.17) indicating that the medium range NOEs arise predominantly from the soluble oligomers. This result is fully consistent with the helical soluble oligomers that

have been proposed as intermediates in the fibrillization pathway of the Aβ peptide [16, 17]. The overlap of the NOESY spectra of filtered and unfiltered sample shows these two spectra have the same type of NOEs and they are caused by the same interactions in the solution [Figure 6.19].

While the effect of filtration on the NOESY spectra clearly assigns the medium range NOEs observed for the unfiltered sample to the soluble oligomers, the absence of detectable medium range NOEs for the filtered sample can be caused either by the lack of well defined secondary structure in the monomers and/or by the small magnitude of laboratory frame cross-relaxation rates expected for correlation times typical for peptides of the size of Aβ (12-28). To rule out the latter possibility Off Resonance ROESY data at angle of 54.7^{o} were acquired. The analysis of the ROE patterns reveals that the conformational ensemble accessible to the monomeric polypeptide chains is still mainly unstructured (Figure 6.18).

6.5 Conclusions

The effect of urea on the pre-nuclear monomer/oligomer equilibria of Aβ (12-28) was investigated through a combined approach based on band selective TOCSY and non-selective 35.5^{o} off-resonance relaxation NMR experiments. Our analysis indicates that urea interacts with both the monomers and the oligomers of Aβ (12-28) but the nature of these two sets of interactions is markedly different. When urea interacts with the monomers, it does not perturb

significantly the conformational equilibria of the monomeric polypeptide chains consistently with the monomers being largely unstructured as shown by the inter-residue NOE analysis and by previous CD studies [11]. Conversely, when urea interacts with the oligomers, it promotes their cooperative disassembly occurring at denaturant concentrations in the 0.7-1.0 M range. These urea concentrations are significantly lower than those typically required to unfold globular proteins suggesting that the pre-nuclear oligomers formed by Aβ (12-28) are stabilized by weak interactions consistent with their mM dissociation constant. Despite the weakness of these interactions, the unfolding transition for the oligomers is cooperative and affects all the detected residues in Aβ (12-28) (*i.e.* residues 14-28) suggesting that self-recognition in the early stages of amyloid fibril formation relies on a concerted mechanism that involves both the CHC and the less hydrophobic residues flanking the CHC. This concertedness is a unique feature of the oligomers as in the monomers the stability of the CHC is independent of the flanking residues [12] and it can be explained by the conformational changes observed upon oligomerization that involve not only the CHC but also the charged and polar residues.

References

1. P.M. Gorman, A. Chakrabartty, Biopolymers (Pept Sci), 60 (2001) 381-394

2. S. L. Bernstein, T. Wyttenbach, A. Baumketner, J.-E. Shea, G. Bitan, D.B. Teplow, M.T. Bowers, J. AM. CHEM. SOC. 2005, 127, 2075-2084
3. J. Jarvet, P. Damberg, J. Danielsson, I. Johansson, L.E.G. Eriksson, A. Gräslund, FEBS letters 555 (2003) 371-374
4. C.M. Dobson, Curr. Opin. Struct. Biol. 3 (1993) 57-59
5. D.K. Klimov, J.E. Straub and D. Thirumalai, Proc. Natl. Acad. Sci. 101 (2004) 14760-14765
6. J.R. Kim, A. Muresan, K.Y. C. Lee and R.M. Murphy, Protein Science 13 (2004) 2888-2898
7. F. Schick, T. Nagele, U. Klose, O. Lutz, Magn. Reson. Imag. 13 (1995): 309-319
8. V. Esposito, R. Das, G. Melacini, J. Am. Chem. Soc., 127 (2005): 9358-9359
9. D.A. Jayawickrama and C.K. Larive, Anal. Chem. 71 (1999) 2117-2122
10. N.A. Farrow, R. Muhandiram, A.U. Singer, S.M. Pascal, C.M. Kay, G. Gish, S.E. Shoelson, T. Pawson, J.D. Forman-Kay and L.E. Kay, Biochemistry 33 (1994) 5984-6003
11. J. Jarvet, P. Damberg, K. Bodell, L.E. Göran Eriksson and Astrid Gräslund, J. Am. Chem. Soc., 122 (2000) 4261-4268
12. S. Zhang, N. Casey and J.P. Lee, Folding & Design 3 (1998) 413-422
13. H. Jane Dyson and Peter E. Wright, Current Opinion in Structural Biology, 3 (1993) 60-65

14. V. Esposito, R. Das, G. Melacini, J. Am. Chem. Soc., 127 (2005): 9358-9359

15. S. Narayanan, B. Reif, Biochemistry 44 (2005): 1444-1452

16. P. M. Gorman, A. Chakrabartty, Biopolymers 60 (2001) 381-394

17. D.M. Walsh, D.M. Hartley, Y. Kusumoto, Y. Fezoui, M.M. Condron, A. Lomakin, G.B. Benedek, D.J. Selkoe, D.B. Teplow, J. Biol. Chem. 274 (1999), 25945-25952.

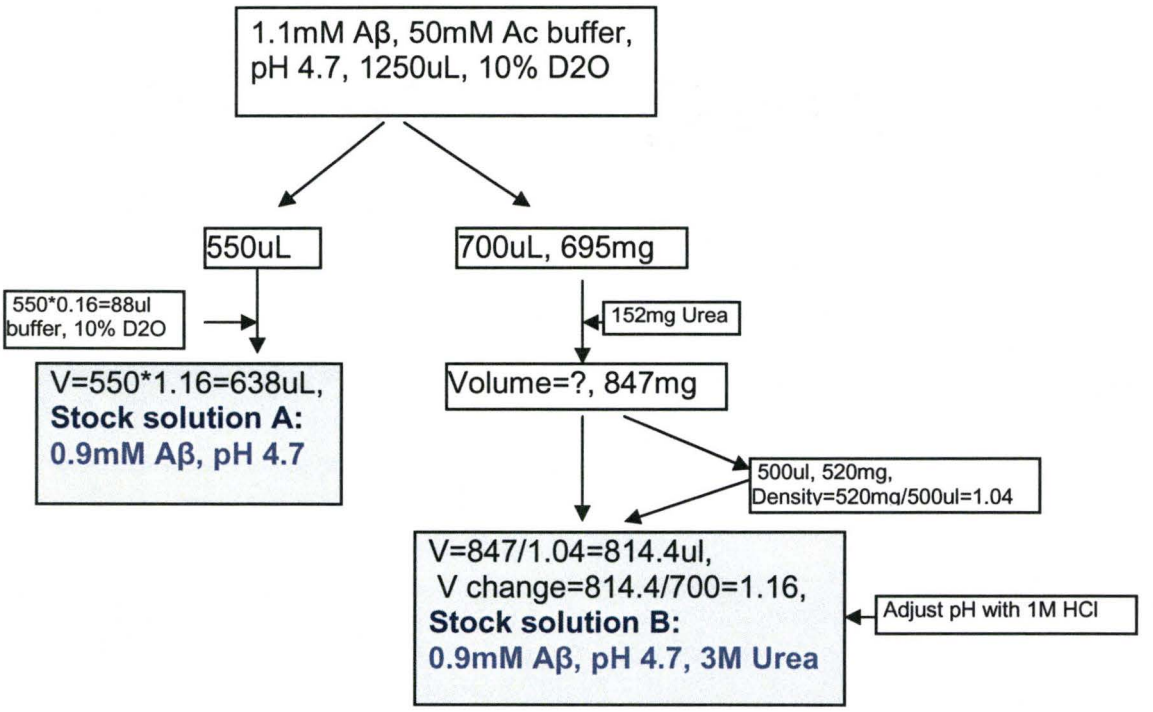

Figure 6.1: Flow chart showing the preparation of stock solutions A & B for the urea titration.

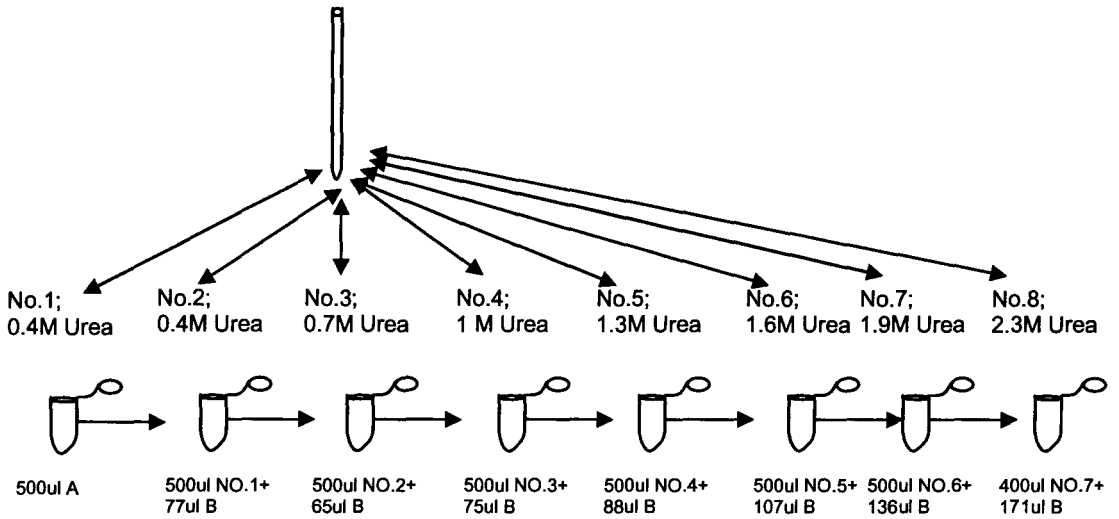

Figure 6.2: Preparation of urea titration samples with stock solutions A & B: the first sample (0.9mM Aβ and 0M Urea) is just 500μL of solution A, the second sample is the mixture of 500μL of solution No.1 and 77μL B, and so on.

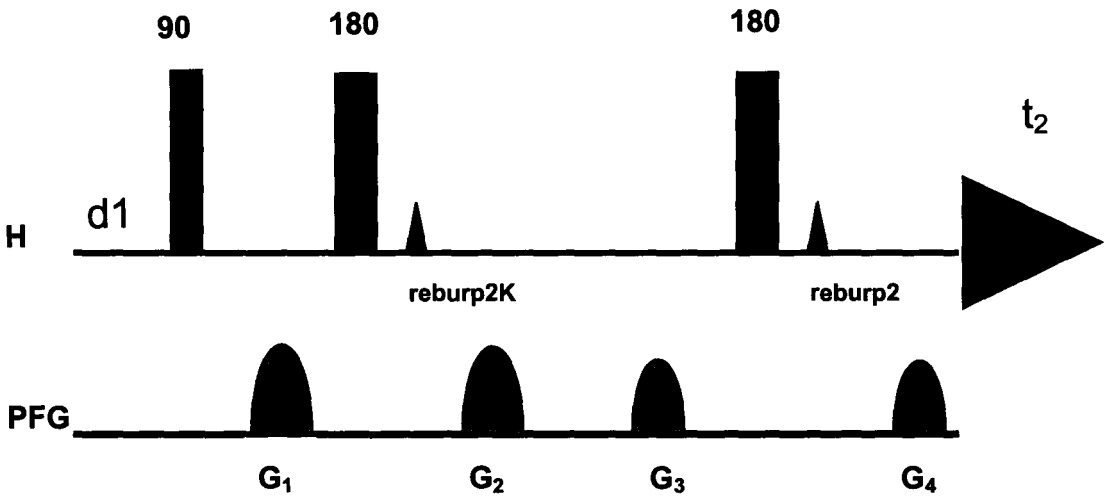

Figure 6.3: 1D NMR pulse with urea saturation. The reburp2K is used for water and urea suppression. The carrier frequency is 3303 Hz; d1=1s; acquisition time= 976.596 ms; TD = 16k. The G_1, G_2, G_3, G_4 pulsed field gradients are sine-bell shaped and have a duration of 1ms. The relative ratios for the G_1, G_2, G_3 and G_4 strengths are 21, 21, 17, 17, respectively. The reburp2K pulse is 2ms long with the strength of 107 Hz.

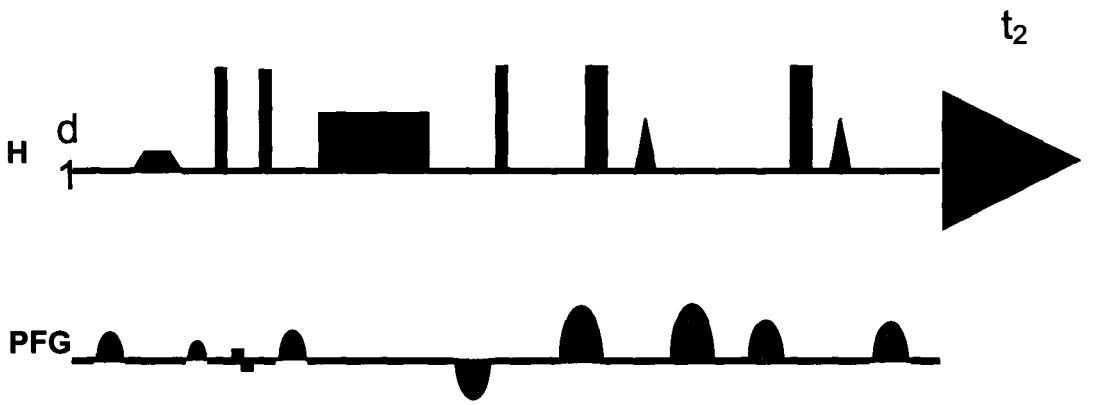

Figure 6.4: 2D Off-resonance TOCSY with urea saturation.

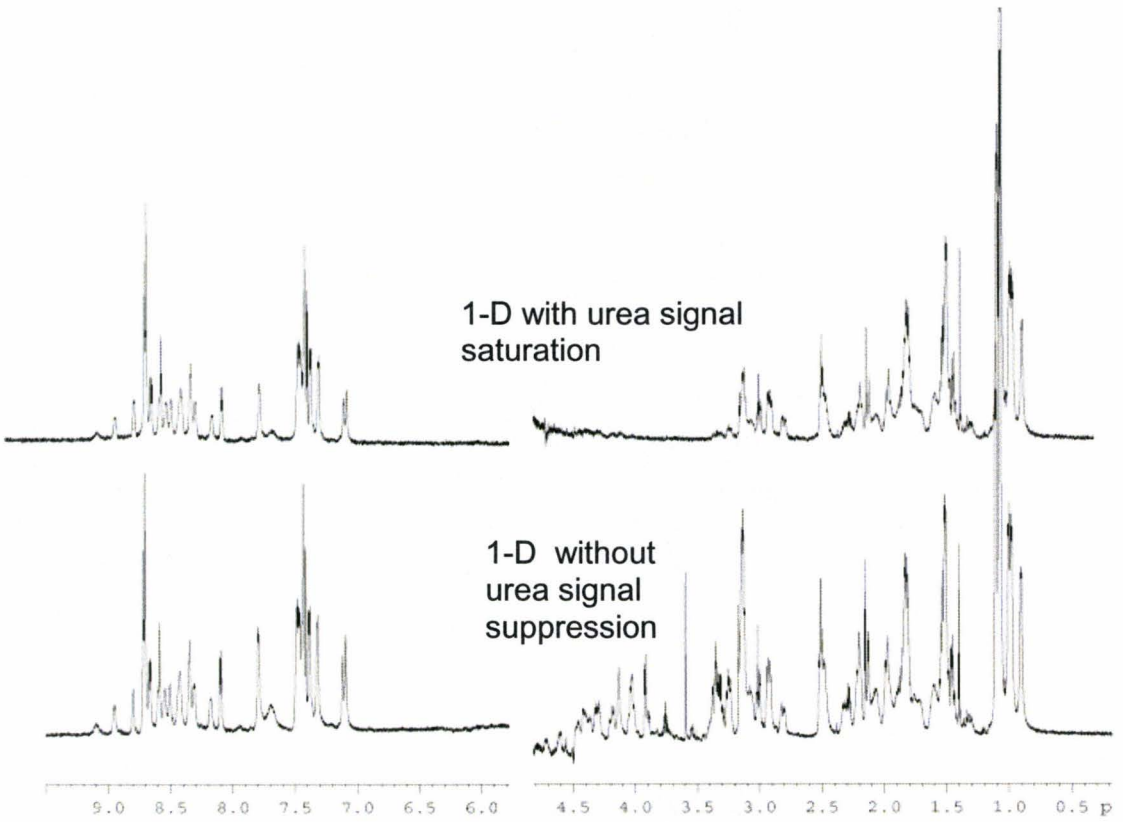

Figure 6.5: Comparison between 1-D double WG with urea suppression and 1-D double WG. The urea saturation not only makes the intensity smaller, but also erases the signal (3.5~4.5ppm) beside the urea resonance.

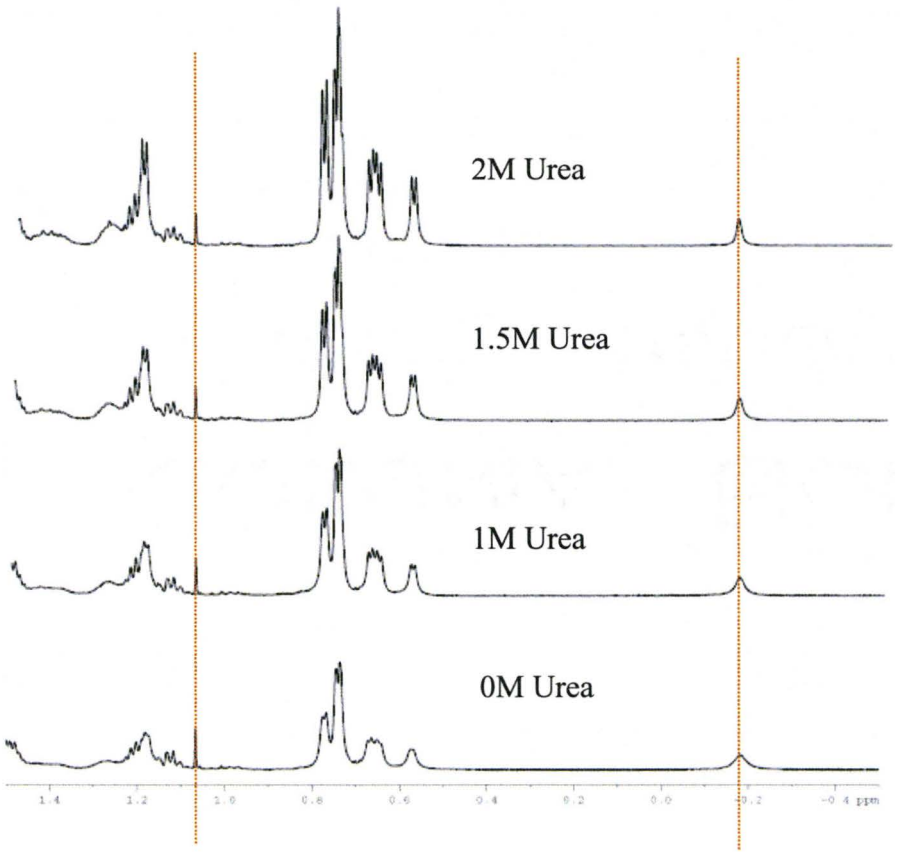

Figure 6.6: Chemical shift reference of urea titration.

a

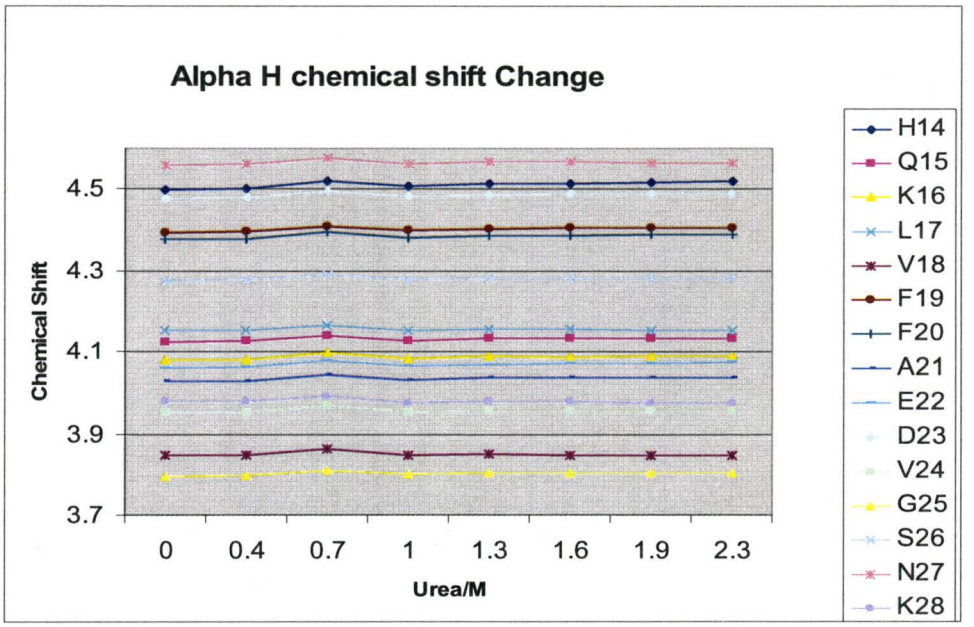

b

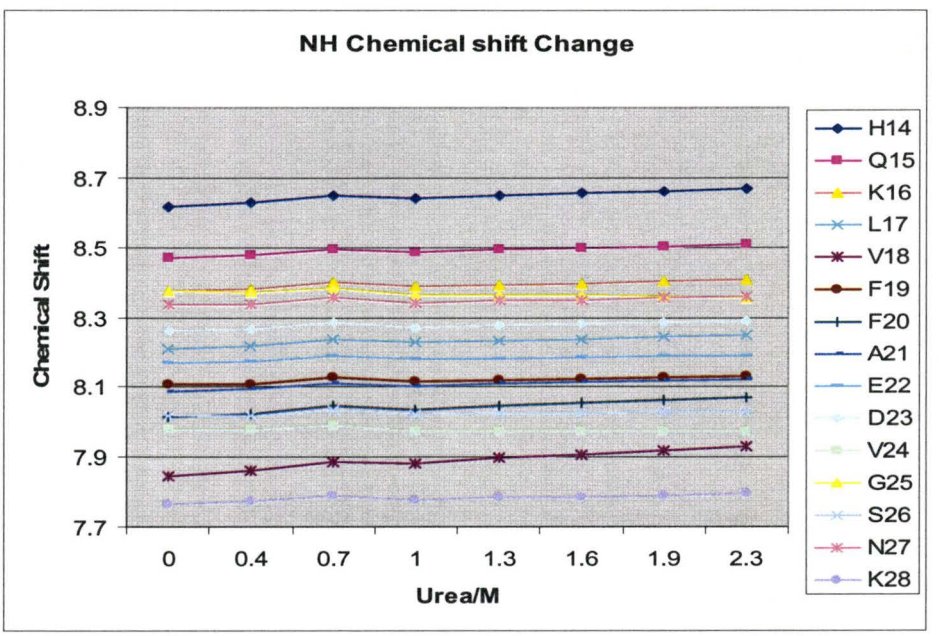

Figure 6.7: Dependence of Hα (a) and NH (b) Aβ (12-28) chemical shifts on urea concentration.

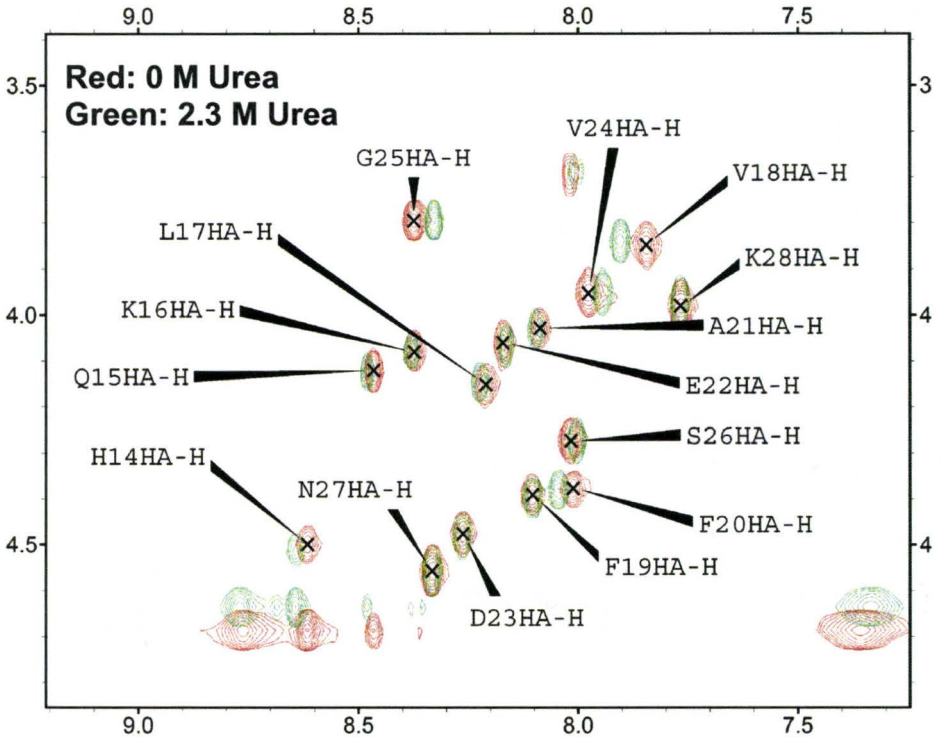

Figure 6.8: The Hα-NH region overlap of 0M urea and 2.3M urea samples: red, 0M urea; green, 2.3M urea. These spectra are not referenced according to TSP and K28 in the two spectra has been fully overlapped to highlight the major chemical shift changes in other residues.

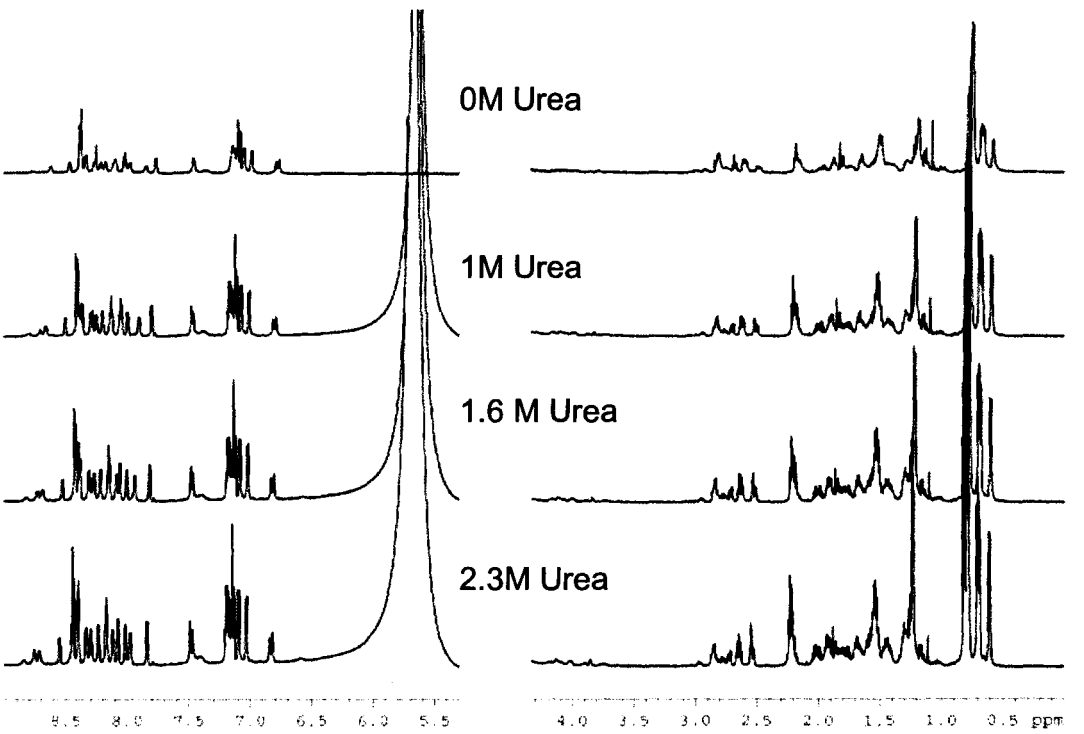

Figure 6.9: 1-D WG with urea suppression of urea titration samples. All have the peptide concentration 0.9 mM; the concentrations of urea are 0M, 1M, 1.6M and 2.3M, respectively.

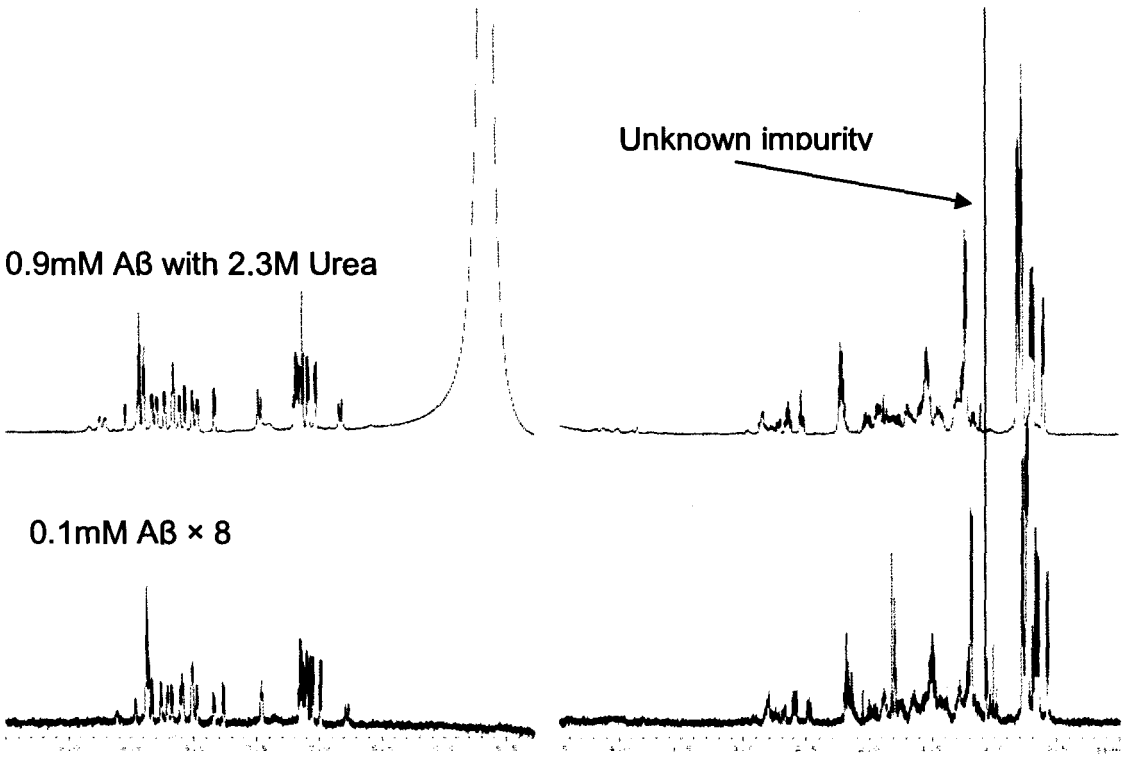

Figure 6.10: The comparison of 1-D spectra between the 0.1mM peptide without urea and 1mM with 2.3mM urea. 0.1mM Aβ without urea has almost 8 times of the intensity of 1mM Aβ with 2.3mM urea. There is an unknown impurity with super sharp peak.

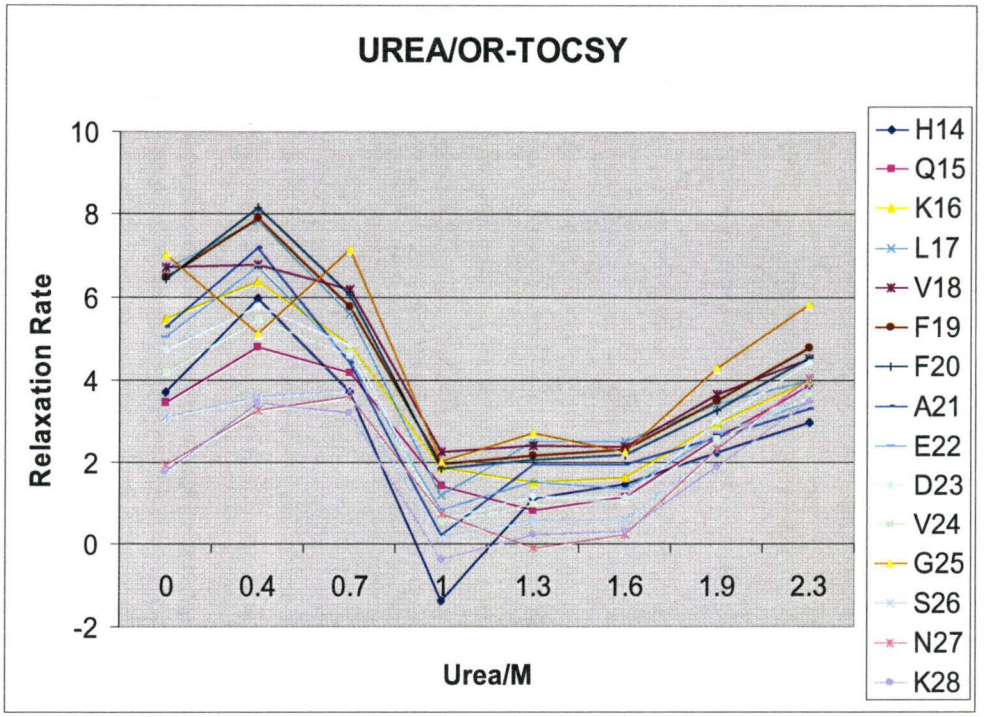

Figure 6.11: Relaxation rates of Aβ vs. urea concentration.

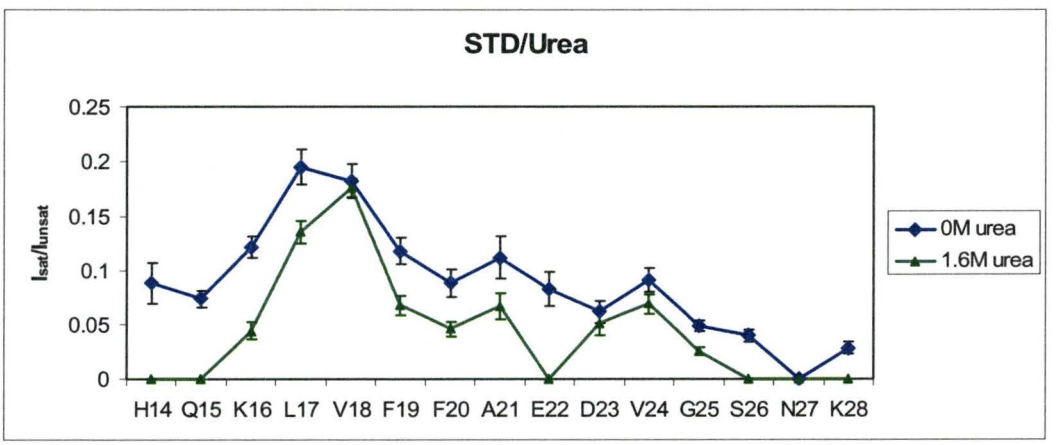

Figure 6.12: Comparison of the I_{sat}/I_{unsat} for Aβ (12-28) between 0 M urea and 1.6 M urea. Square: 0M urea; triangle: 1.6M urea.

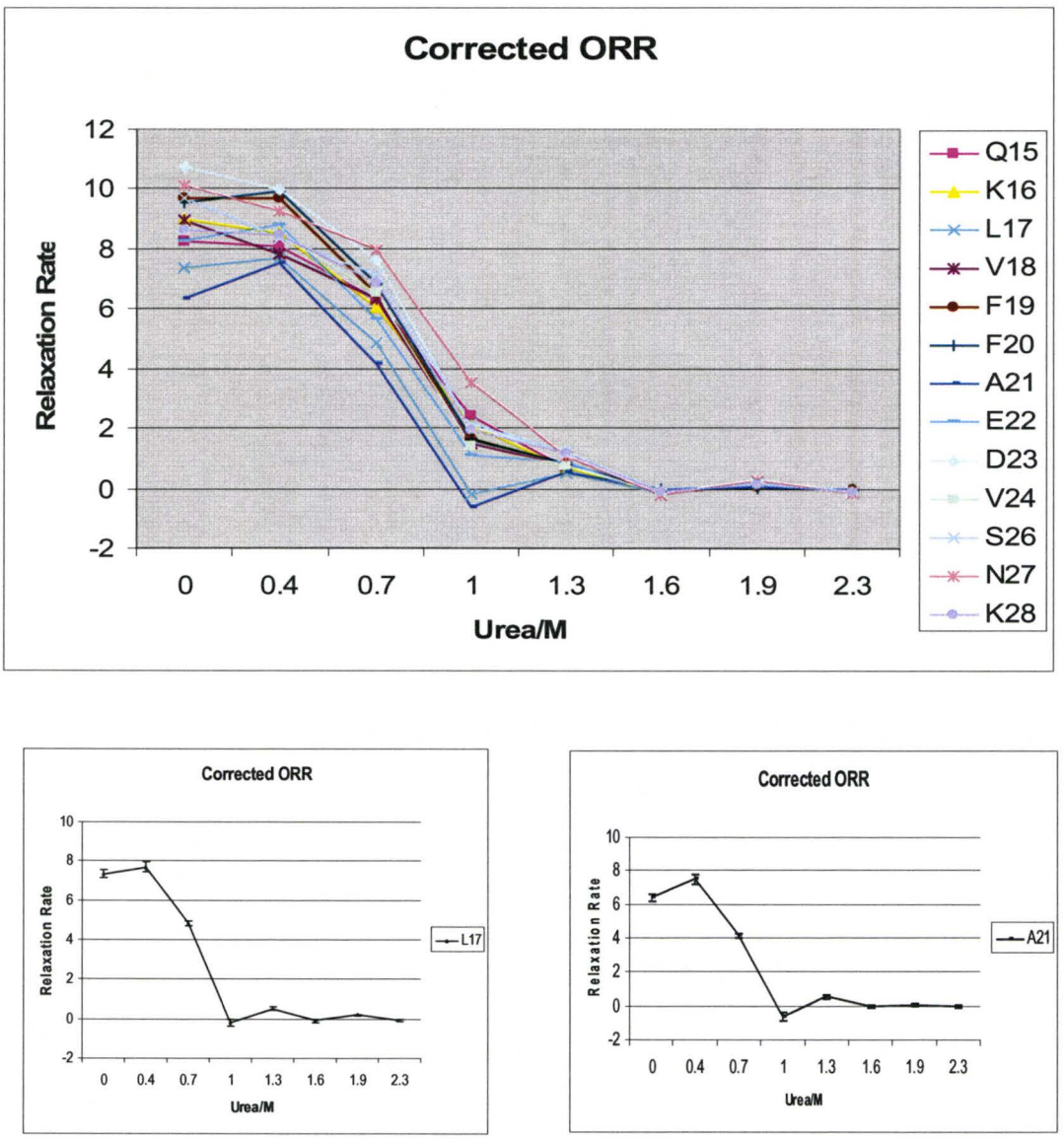

Figure 6.13: The urea titration with the last three points (1.6M, 1.9M, 2.3M) used to get extrapolating simulation and then correct the OR rate. The error analysis of 0M urea is reported here, in which the standard deviation of the spectra were used as the error of measurement [10].

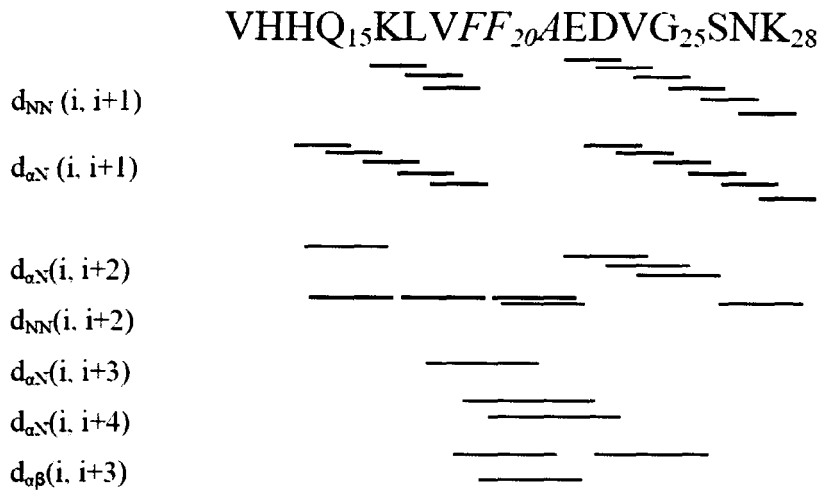

Figure 6.14: Inter-residue NOE patterns of unfiltered Aβ (12-28) 1mM, pH 4.7, 50mM d_3-acetate buffer and 10% D_2O. As the F19, F20 and A21 have very close chemical shift, some NOEs cannot be specified.

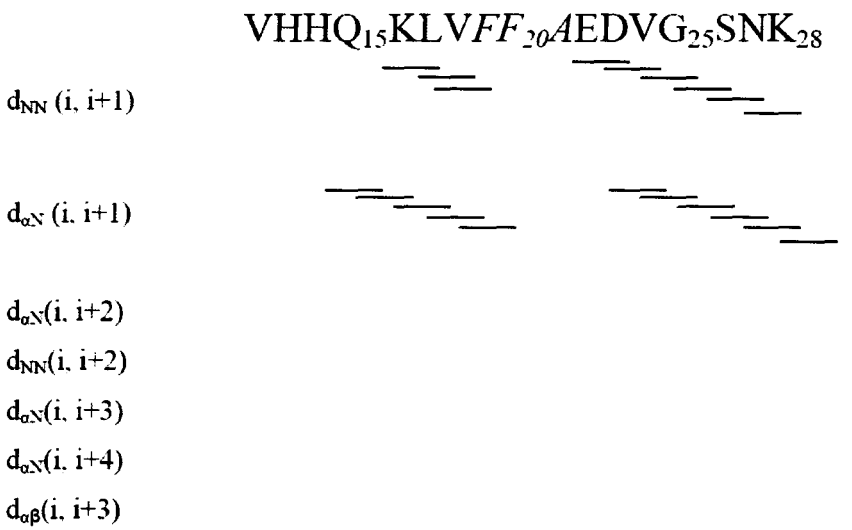

Figure 6.15: Inter-residue NOE patterns of 30 kDa cut-off filtered Aβ (12-28) 1mM, pH 4.7, 50mM d_3-acetate buffer and 10% D_2O. As the F19, F20 and A21 have very close chemical shift, some NOEs cannot be specified.

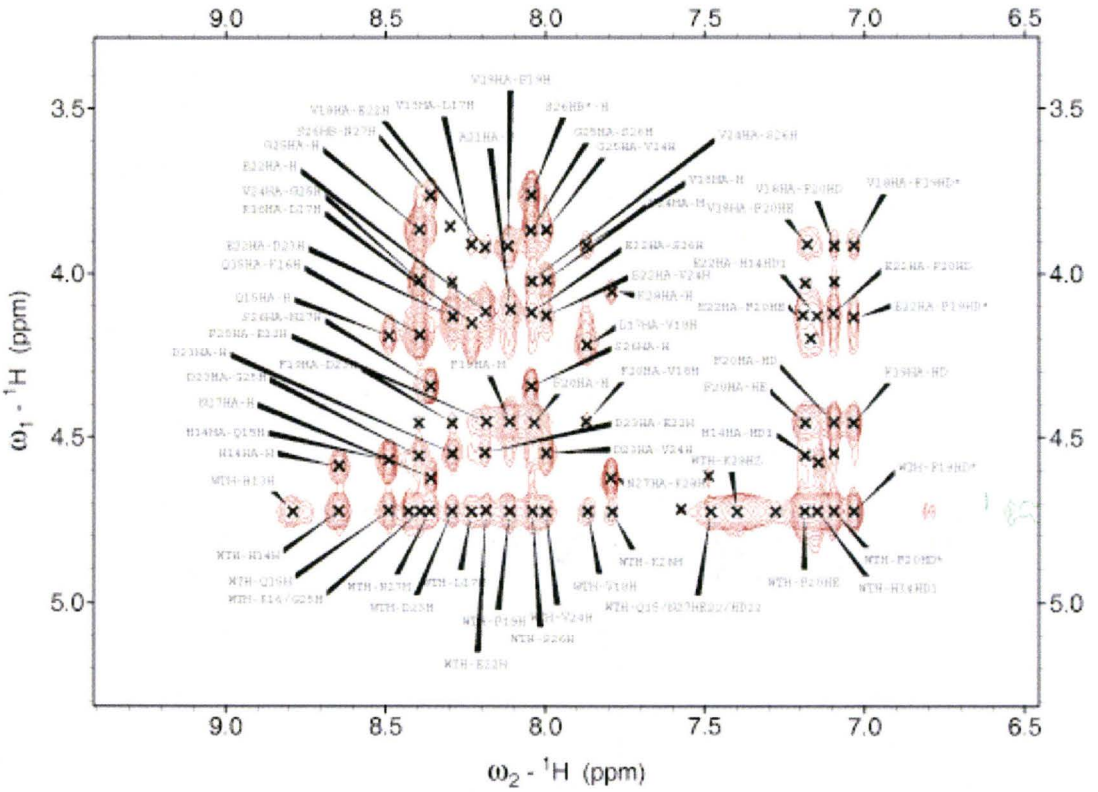

Figure 6.16: NOESY of Aβ (12-28) 1mM, pH 4.7, 50mM d_3-acetate buffer and 10% D_2O. Mixing time is 200ms.

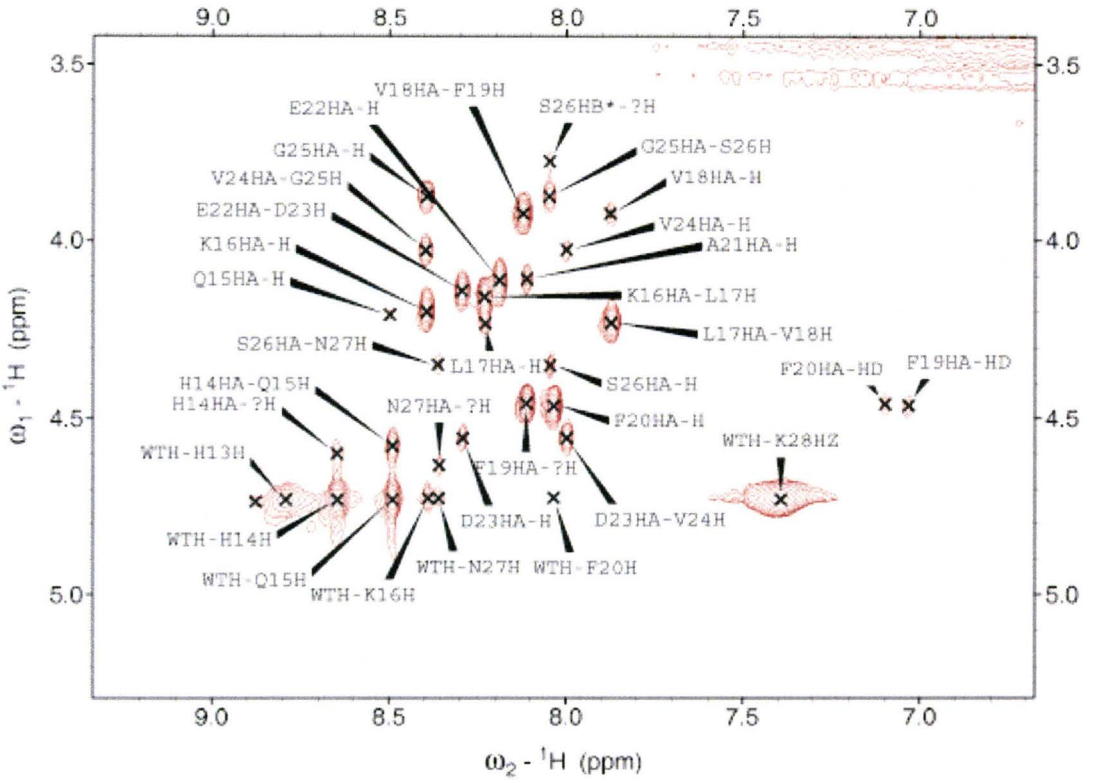

Figure 6.17: NOESY of 30 kDa cut-off filtered Aβ (12-28) 1mM, pH 4.7, 50mM d_3-acetate buffer and 10% D_2O. Mixing time is 200ms.

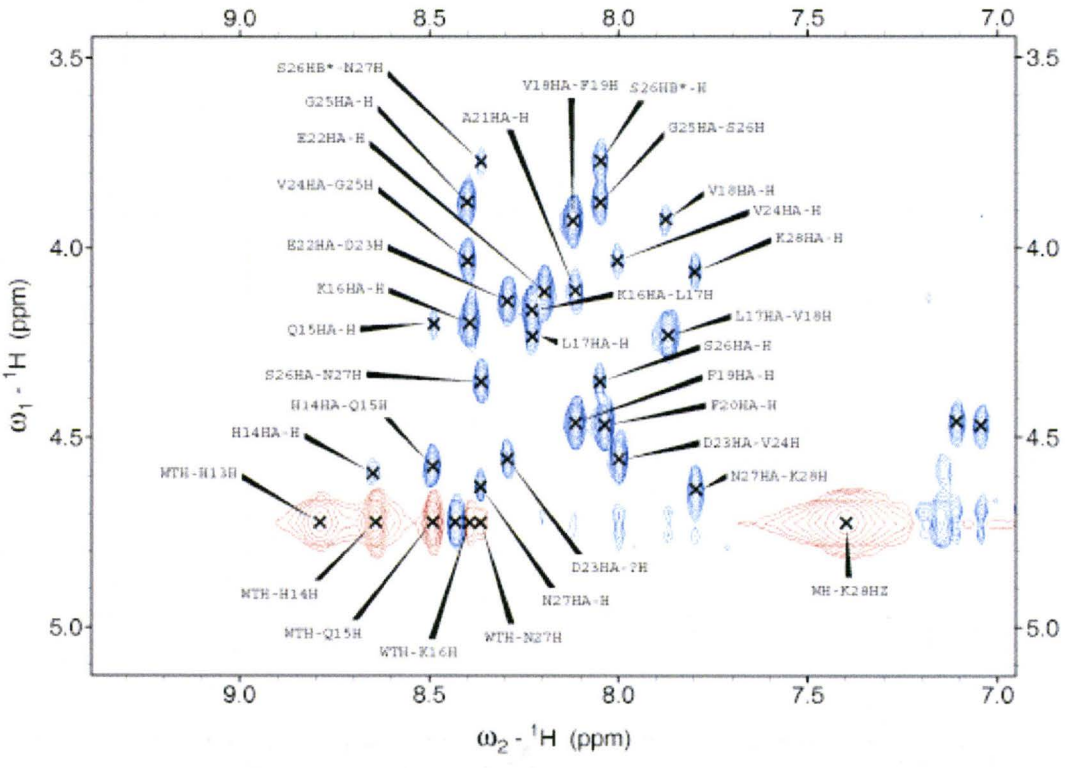

Figure 6.18: Non-selective off resonance ROESY 54.7° of 30 kDa cut-off filtered Aβ (12-28) 1mM, pH 4.7, 50mM d_3-acetate buffer and 10% D_2O. Mixing time is 150 ms. Red cross-peaks are positive, while blue cross-peaks are negative.

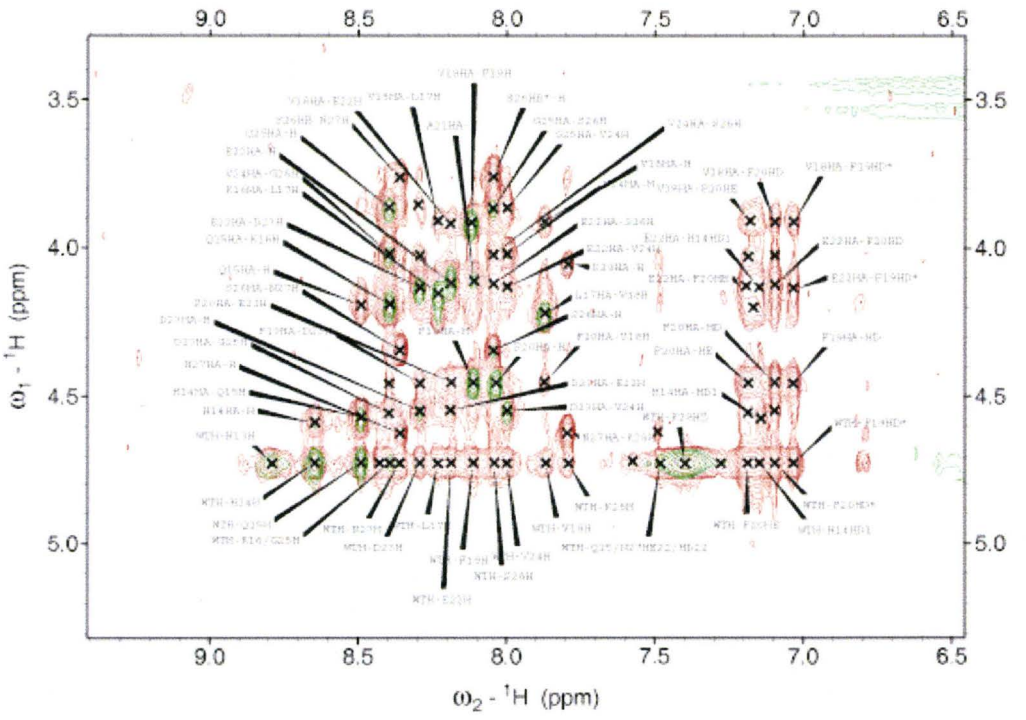

Figure 6.19: Overlap of the NOESY spectra of filtered and unfiltered samples, both spectra have been processed in the same way.

Chapter 7

Concluding Remarks

7.1 General Overview of the Thesis

The formation of soluble amyloid oligomers by polypeptide chains is the main pathogenic mechanism underlying several neurodegenerative disorders including some of the most common debilitating and aging-related illnesses such as Alzheimer's and Parkinson's diseases. However, the molecular basis of polypeptide oligomerization and amyloid formation is currently not fully understood. In this thesis the focus has been on the early steps of oligomer formation that precede the nucleation of amyloid fibrils and that are still reversible. The reversibility of these initial self-association equilibria makes them an attractive target for therapeutical intervention in the treatment of amyloid diseases. Specifically three general questions have been addressed:

(a) What are the residues within a given polypeptide chain that mediate self-recognition?
(b) What are the driving forces for self-association?
(c) Is self-recognition coupled with conformation changes?

The answers to these central questions provide a rational basis for the design of molecular therapies targeting the early reversible steps of amyloid formation. The goal of this thesis is to provide initial responses to these key questions using as prototypical system the Aβ (12-28) peptide, which has been previously proposed as a model for the initial self-association events that are linked to Alzheimer's disease. Given the flexibility of this peptide the main tool for its investigation was Nuclear Magnetic Resonance (NMR) spectroscopy.

Specifically, several NMR relaxation experiments have been used to probe the soluble oligomers through the comparative analysis of samples characterized by different monomer/oligomer distributions. The general architecture of this comparative NMR approach is outlined in Chapter 2.

The first question about the residues involved in the oligomerization can be addressed by taking advantage of non-selective off-resonance NMR relaxation measurements recently proposed by our group [1]. While this approach provides residue-resolution self-recognition maps for amyloidogenic peptides, its application is somewhat limited by the requirement of reference control data for mostly monomeric peptides, which are sometimes difficult to obtain experimentally given the high propensity of amyloidogenic peptides to oligomerize. In addition, non-selective off-resonance NMR relaxation rates provide valuable self-recognition information only for protons with similar covalent environments such as the Hα protons of non-Gly amino acids, thus hampering their application to side chain protons. A potential avenue to overcome these limitations relies on the use of saturation transfer difference (STD) experiments which have been originally developed to probe protein-ligand interaction and only very recently have been applied to self-recognition mapping [2]. In Chapter 3 therefore we extensively analyzed the strengths and limitations of the STD experiments as applied to the model system Aβ (12-28) prepared both in the monomeric and oligomeric states. The comparative analysis of the STD data presented in Chapter 3 revealed that several artifacts have to be taken into account before reliable self-recognition maps can be derived. These artifacts include significant offset-effects, monomer contributions and possibly partial spin diffusion. While an initial route to at least partially overcome these limitations relies on the acquisition of multiple STD data sets at different saturation frequencies for samples prepared in different oligomer distributions, a more robust and efficient saturation transfer methodology seems to be warranted. For this purpose we started to investigate alternative strategies to transfer

magnetization to the peptide and specifically we investigated the incoherent polarization transfer from water to Aβ (12-28) polypeptide chains.

The detailed investigation of the possible water-to-peptide magnetization transfer pathways is reported in Chapter 4 and is based on the comparative analysis of NMR hydration spectra of wt- and mutant peptides acquired for different oligomerization states. The hydration NMR studies of Chapter 4 revealed that when polarization is transferred from water to peptide protons not only the exchanging polar groups are affected but magnetization is relayed also beyond the polar groups to hydrophobic residues known to be involved in self-recognition. While it is currently not possible to separate the contributions of potential trapped water molecules and of exchange mediated-intra-molecular NOEs to the transfer of magnetization from water to peptide protons, these preliminary observations on hydration experiments suggest a possible route to overcome the limitations of the traditional STD experiments described in Chapter 3. Therefore in Chapter 5 we explored how the STD and the hydration experiments can be combined to probe more reliably self-recognition in amyloidogenic peptides. Specifically, we showed that a radiation-damping based pulse sequence, which we called WSTD, provides encouraging new results for self-association mapping by NMR overcoming at least in part the previous limitations affecting the traditional STD methods. In addition, WSTD experiments suggest that the determinants of self-recognition may extend beyond the central hydrophobic core (CHC), which is known as the primary epitope of self-association [3].

The results from the WSTD experiments point out that self-recognition in the Aβ (12-28) peptide may be more complex than the simple inter-molecular hydrophobic collapse of CHC domains. In order to further explore the driving forces of self-association (*i.e.* question (b) above) we investigated the urea induced unfolding of the Aβ (12-28) system as described in Chapter 6. The effect of urea was monitored by 2D-TOCSY and by non-selective off-resonance

relaxation measurements. Our results show that urea interacts with both monomers and oligomers but these two sets of interactions are fundamentally different. The interactions of urea with the monomers do not change detectably their secondary structure preferences and appear to be localized to non-polar residues consistently with previous molecular dynamics simulations. The interactions of urea with the oligomers cause their dissociation already at 0.7-1.0 M urea concentrations suggesting that the oligomers are stabilized by weak interactions consistent with their mM dissociation constants. Despite the weakness of these interactions the oligomer-monomer transition induced by urea appears to be concerted and to involve also residues outside the CHC, in full agreement with the WSTD results of Chapter 5. However, the urea denaturation experiment *per-se* does not show whether the non-CHC residues affected by the oligomer-monomer equilibria are directly involved in inter-molecular interactions or are linked to the CHC through conformational changes that may occur upon oligomerization (question (c) above). With the purpose of discriminating between these two possible hypotheses, we acquired NOESY/ROESY experiments for Aβ (12-28) samples prepared with different oligomeric distributions. The comparative analysis of the observed NOE/ROE patterns is consistent with a helical or partially helical structure for the soluble oligomers and with predominantly random coil and/or polyproline II conformations for the monomers. These results are fully consistent with previously hypothesized helical intermediates in the amyloid fibrilization pathway [3] and with previous CD studies [4], suggesting that indeed conformational changes are coupled to self-association providing an answer to question (c) above. These conformational changes account also for the concerted pervasive effects of self-association revealed by WSTD and urea denaturation: while the CHC drives self-recognition, stable oligomers require a conformational change towards more helical or folded structures that affect residues well outside the CHC. The conformational change occurring upon self-association thus effectively couples CHC and non-CHC

residues. This model may also explain why mutations outside the CHC (*i.e.* E22, D23) can affect significantly the kinetics of self-association [5].

7.2 Open Problems and Outline of Future Work

While the investigations outlined above have opened new perspectives for probing and understanding self-recognition in the early steps of amyloid formation, several questions remain unanswered. For instance, it will be important to refine the general comparative NMR strategy outlined in Chapter 2 with the goal of increasing our experimental control on the amount of oligomers present in each sample. So far we simply relied on the oligomers that are spontaneously formed upon peptide lyophilization, however this approach may introduce batch dependence. Improved reproducibility could be obtained by filtering all peptide solutions and then reintroducing the oligomers in a controlled manner by the addition of salt and/or by incubating the samples at high temperature. In addition, the effective cut-off size during filtration and its dependence on centrifugation duration and speed should be established using model proteins and/or diffusion experiments because accumulation of peptide oligomers on the filters may reduce the size of the pores in the filters resulting in the so called "cake effect". The optimization and standardization of these sample preparation protocols will facilitate the reliable comparisons between mutant peptides.

It will also be critical to follow up on the STD studies reported in Chapter 3 by more quantitatively estimating the extent of partial spin diffusion after subtraction of the monomer contributions. It will also be important to extend the application of the STD experiments to the side chains in order to fully appreciate the potential of this promising strategy for mapping self-recognition. As to the hydration studies of Chapter 4, the presence of long lived water molecules trapped

within the oligomers could not be unambiguously established using high-resolution ^{1}H NMR and most likely ^{17}O magnetic resonance dispersion (MRD) will be required to reach conclusive statements about the dynamics of the oligomer bound water molecules. As to WSTD experiments outlined in Chapter 5, alternative pulse sequences should be explored to avoid difference artifacts caused by the radiation damping induced selective inversion of the water magnetization. Specifically, we plan to test for this purpose selective gradient spin-echos that resemble more closely PHOGSY-type methods [6] in which radiation damping is completely suppressed.

We are also planning to extend the urea unfolding studies reported in Chapter 6 by taking into account the effect of urea-dependent viscosity increases and of urea-monomeric peptide clusters. For this purpose we plan to use the non-selective off-resonance data acquired at urea concentrations higher than 1.0M to back extrapolate the viscosity and urea clustering effects. However the viscosity effect caused by urea will depend on the size of the oligomers and therefore alternative approaches may be required to fully account for the urea-dependent viscosity changes. These additional data may include the use of "spy" molecules to probe viscosity changes and/or the use of pulsed field gradient (PFG) diffusion measurements. We are also planning to monitor the effect of urea with other methods that map self-recognition and are complementary to the non-selective off-resonance measurements outlined in Chapter 6. For instance, STD experiments devoid of the artifacts explained in Chapter 3 could be used for this purpose. In addition, the conformational changes occurring upon self-recognitions can be monitored not only by measuring NOEs/ROEs for filtered and unfiltered samples but also for samples at different urea concentrations providing valuable complementary data that may help pinpoint better the nature of the conformational transitions occurring upon oligomerization. This is a major challenge for the future because even when the contributions from monomers and oligomers to the observed cross-relaxation rates (*i.e.* NOEs and ROEs) are

separated using filtration and/or urea based approaches, the question still remains of how to de-convolute the inter- and intra-molecular NOEs arising from the oligomers. We anticipate that the inter- and intra-molecular NOEs will be assigned by using isotope filtering and editing methods which require extensive ^{15}N and ^{13}C labeling and therefore peptides produced through recombinant rather than synthetic methods. Efforts in this direction are ongoing in our laboratory and we are currently attempting to express the Aβ (12-28) peptide as a fusion construct with the soluble G-protein. An additional route to gain further insight into the conformational changes coupled to self-recognition relies on the use of an ensemble of simulated structures [5] and on their validation through NMR experiments. Last but not least, we are also planning to extend our investigation to longer peptides such as the Aβ (1-40) and to other amyloidogenic peptides linked to other diseases, such as for instance Huntinghton's.

References

1. V. Esposito, R. Das, G. Melacini, J. Am. Chem. Soc., 127 (2005): 9358-9359
2. S. Narayanan and B. Reif, Biochemistry, 44 (2005) 1444-1452
3. S.K. Maji, J.J. Amsden, K.J. Rothschild, M.M. Condron, D.B. Teplow, Biochemistry 44 (2005): 13365-13376
4. J. Jarvet, P. Damberg, K. Bodell, L.E. Göran Eriksson and Astrid Gräslund, J. Am. Chem. Soc., 122 (2000) 4261-4268
5. B. Tarus, J.E. Straub, D. Thirumalai, Journal of Molecular Biology, 345 (2005): 1141-1156
6. C. Dalvit, U. Hommel Journal Of Biomolecular NMR, 5 (1995) 306-310